

Performance Analysis of Single Neuron Adaptive PID, WNN and ANFIS Type Controller Based PMSBLDC Motor Drive

By

Md. Belal Hossen

A Thesis submitted in partial fulfillment of the requirements for the degree of Master of
Science in Engineering in the Department of Electrical and Electronic Engineering

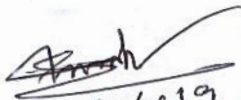


Khulna University of Engineering & Technology
Khulna-9203, Bangladesh

June 2019

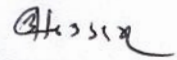
DECLARATION

This is to certify that the thesis work entitled “**Performance Analysis of Single Neuron Adaptive PID, WNN and ANFIS Type Controller Based PMBLDC Motor Drive**” has been carried out by **Md. Belal Hossen** in the Department of **Electrical and Electronic Engineering**, Khulna University of Engineering and Technology, Khulna, Bangladesh. The above thesis work or any part of this work has not been submitted anywhere for the award of any degree or diploma.



30/6/19

Signature of Supervisor

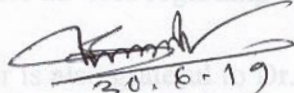
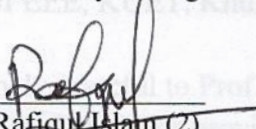

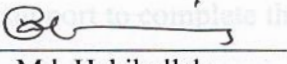
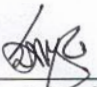


Signature of Candidate

Approval

This is to certify that the thesis work submitted by **Md. Belal Hossen**, entitled “**Performance Analysis of Single Neuron Adaptive PID, WNN and ANFIS Type Controller Based PMBLDC Motor Drive**” has been approved by the board of examiners for the partial fulfillment of the requirements for the degree of **M.Sc. Engineering** in the Department of **Electrical and Electronic Engineering**, Khulna University of Engineering & Technology, Khulna, Bangladesh in June 2019.

BOARD OF EXAMINERS

1. 
30.6.19
Dr. Bashudeb Chandra Ghosh
Professor
Department of Electrical and Electronic Engineering
Khulna University of Engineering & Technology
Chairman
(Supervisor)
2. 
Dr. Md. Rafiqul Islam (2)
Professor and Head
Department of Electrical and Electronic Engineering
Khulna University of Engineering & Technology
Member
3. 
Dr. Md. Abdur Rafiq
Professor
Department of Electrical and Electronic Engineering
Khulna University of Engineering & Technology
Member
4. 
Dr. Md. Habibullah
Associate Professor
Department of Electrical and Electronic Engineering
Khulna University of Engineering & Technology
Member
5. 
Dr. Md. Ashraful Hoque
Professor
Department of Electrical and Electronic Engineering
Islamic University of Technology (IUT), Gazipur,
Bangladesh
Member
(External)

Acknowledgement

Foremost, praise and grateful to the Almighty Creator Allah who permit me to live and complete my research work successfully.

The author would like to express his profound gratitude and indebtedness to his thesis supervisor Dr. Bashudeb Chandra Ghosh, Professor, Department of Electrical and Electronic Engineering (EEE), Khulna University of Engineering & Technology (KUET), Khulna, Bangladesh, for his guidance, constant motivation, encouragement, mental support and valuable advices regarding this thesis.

The author is also grateful to Dr. Md. Abdur Rafiq, Professor, Department of EEE, KUET, Khulna, Bangladesh for his valuable discussion.

The author would like to express special thanks to Dr. Md. Habibullah, Assistant Professor, Dept. of EEE, KUET, Khulna, Bangladesh.

The author extremely grateful to Prof. Dr. Md.Rafiqul (2) Islam, Head of the Dept. of EEE, KUET, Khulna, Bangladesh for providing all facilities to finish my research work in time. The author also thanks all the teachers in the Dept. of EEE for their valuable counseling and friendly behavior.

The author humbly acknowledges indebtedness to Engr. Arshaful Kabir, Chairman of the BCMC College of Engineering & Technology, Jashore, Bangladesh for his financial support, motivation and encouragement.

The author politely respects to his parents for their emotional love, prayers, caring and sacrifices. The author is very much thankful to his wife for her love, understanding, and continuing support to complete this research work.

Also the author would like to thank his youngest brother for motivation, continue mental support and inspiring.

June, 2019

Md. Belal Hossen

Abstract

Permanent Magnet Brushless DC (PMBLDC) Motor Drive is familiar as an innovative research for their compact size, silent operation, reliability, high efficiency, simple construction, easy to control and less maintenance requirements. Design cost of PMBLDC motor drive has been reduced drastically due to the invention of rare earth magnetic materials and advancement of power semiconductor devices. The semiconductor power devices are turned on or off sequentially using triggering and commutation circuits. Based on the rotor position the controller generates requisite signals to control the operation of the power inverter. A high performance controller is required to obtain desired performance of the drive system. It is noticed that PMBLDC Motor has a complexity to handle multi variable and nonlinear system. The motor speed control is frequently needed for controlling various drives such as robotics, copters, electric vehicles and other drives of applications. The high performance drives require very fast response, high efficiency and parameter insensitive. It is not possible to achieve desired performance with conventional PI controller. Tuning of controller parameters is necessary to achieve desired performance. To overcome these problems this study proposes the following controllers (1) Single Neuron based Adaptive (SNA) Controller, (2) Single Neuron based Adaptive PID (SNAPID) Controller, (3) Adaptive Neuro Fuzzy Inference System (ANFIS) based Controller with Radial Basis Function (RBF), (4) ANFIS Controller based on Takagi-Sugeno Model, (5) ANFIS Controller based on Line Voltage Model and (6) Wavelet Neural Network (WNN) based Controller. A PI controller with constant parameter is also designed and it is tuned by Ziegler- Nichols method. Each controller was simulated by developing software in C++ environment and performance of each controller is compared with PI controller. To get better speed, torque and current responses field orientation control method and square wave reference current input to the machine are considered with the above controllers. In this process, direct axis current is considered to zero and quadrature axis current produces useful torque. The drive performance was tested under different operating conditions such as constant starting condition, sudden load torque changes, speed variation and parameter changes. All proposed controllers perform well under speed variation and constant starting condition except fixed PI and WNN based controller. It is also observed that their speed responses are fast. For suddenly increment of load torque, motor speed is fallen by WNN based Controller, fixed PI and SNAPID

Controller but SNA Controller, ANFIS Controller based on Takagi-Sugeno Model, ANFIS controller based on Line Voltage Model and ANFIS Controller with RBF perform well with constant speed. Finally, it is seen that all controllers with PMBLDC Motor drive work effectively without any performance degradation in the increment of stator resistance hence, the proposed controllers perform as insensitive controller with the variation of stator resistance.

*This Thesis is dedicated to
my beloved parents*

Contents

	PAGE
Title Page	i
Declaration	ii
Certificate of Research	iii
Acknowledgement	iv
Abstract	v-vi
Dedication	vii
Contents	viii-x
List of Figures	xi-xiv
List of Abbreviations	xv
List of Symbols	xvi-xvii
CHAPTER I	
Introduction	1
1.1 Background	1
1.2 Motivation	3
1.3 Brief of Literature Review	4
1.4 Objectives	12
1.5 Contents of the Thesis in Brief	13
CHAPTER II	
Mathematical Model of Permanent Magnet Brushless DC Motor	15
2.1 Introduction	15
2.2 Construction	16
2.3 Principle of Operation of PM Brushless DC Motor	17
2.4 $2\pi/3$ Angles Switch on Mode	19
2.5 Current Control PWM or Voltage Control PWM	20
2.6 Review on Brushless DC Motor Modeling	20
2.7 Mathematical Model of the Machine considering Phase Voltage	20
2.8 Digital simulation of the motor	24
2.9 Conclusion	25
CHAPTER III	
Controller Designed based on Field Oriented Current Vector Control	26
3.1 Introduction	26
3.2 Field Orientation Control Technique	27
3.3 Design Fixed PI Controller	29
3.4 Construction and Operation of Hysteresis Current Controller	30
3.5 Field Oriented Rectangular Current Regulated Control	32
3.6 Simulation Results for Square Wave Reference Current	33
3.7 Sinusoidal Current Regulated Field Oriented Control	36

	3.8	Simulation Results for Sinusoidal Reference Current	37
	3.9	Conclusion	39
CHAPTER IV		Single Neuron based Adaptive Controller of PMBLDC Motor	40
	4.1	Introduction	40
	4.2	Structure of Single Neuron	40
	4.3	Single Neuron based Adaptive Controller with Adaptive Law	41
	4.4	Simulation Results	43
	4.5	Conclusion	47
CHAPTER V		Design of Single Neuron based Adaptive PID Controller and Speed Estimator for PMBLDC Motor	48
	5.1	Introduction	48
	5.2	The Basic Principle of Auto Tuning	48
	5.3	Tuning Algorithm of PID gains by SN estimator	50
	5.4	Simulation Results	51
	5.5	Conclusion	56
CHAPTER VI		ANFIS based Controller Design for PMBLDC Motor	57
	6.1	Introduction	57
	6.2	ANFIS based Controller with Radial Basis Function and Training Feature	58
	6.3	Architecture of ANFIS	58
	6.4	Training Rule of ANFIS	60
	6.5	Identification of Radial Basis Function	62
	6.6	Simulation Results for Training Feature	63
	6.7	ANFIS Controller based on Takagi-Sugeno Model	69
	6.8	Simulation Results based on Takagi-Sugeno Model	71
	6.9	Machine model of PM Brushless DC Motor based on Line Voltage	73
	6.10	Simulation Results for Line Voltage Model	74
	6.11	Conclusion	76
CHAPTER VII		Design of a Controller based on Wavelet Neural Network	77
	7.1	Introduction	77
	7.2	Structure of biological and artificial neuron	78
	7.3	Design of a Controller based on Wavelet Neural Network	79
	7.4	Gradient Descent Learning Rule	80
	7.5	Simulation Results	81
	7.6	Conclusion	84
CHAPTER VIII		Simulation Results and Performance Analysis of Proposed Controllers	85
	8.1	Introduction	85
	8.2	Performance Analysis for Constant Torque Starting	86

	Condition	
8.3	Performance Analysis for Speed Variation Condition	86
8.4	Effect on Performance due to Changing Load Torque	96
8.5	Effect on Performance due to Changing Parameter	102
8.6	Conclusion	108
CHAPTER IX	Conclusion and Future Work	110
9.1	Conclusion	110
9.2	Proposal for Future Work	113
	References	113
	Appendix A: Parameter of the PMBLDC Motor	118
	List of Publications	118

List of Figures

Fig. No	Description	Page
2.1	Cross-sectional view of a PM Brushless DC Motor	16
2.2	Basic block diagram of PM Brushless DC Motor drive	17
2.3	Sinusoidal back emf of BLDC motor	18
2.4	Three phase inverter circuit with PMBLDC Motor	18
2.5	Back-emfs, current waveforms and Hall sensors for PM Brushless DC Motor	19
2.6	Three phase Trapezoidal back EMF of PMBLDC Motor [3]	21
3.1	Structure of Hysteresis Current Controller	32
3.2	Block diagram of Field Oriented Rectangular Current Regulated Control with PM Brushless DC Motor	32
3.3	Speed characteristic is represented for field oriented rectangular current regulated control	33
3.4	Back emf variation with oriented rectangular current regulated control PMBLDC motor	34
3.5	Shows three phase voltage	34
3.6	Rotor angle variation	34
3.7	Shows (a) quadrature axis current and (b) developed torque response	35
3.8	3-Phase currents represented for field oriented (rectangular current) regulated control	35
3.9	Block diagram of sinusoidal current regulated field oriented control with PMBLDC motor	36
3.10	Speed characteristic is represented for sinusoidal current regulated field oriented control	37
3.11	Back emf variation is shown for sinusoidal current regulated field oriented control	38
3.12	Single phase back emf	38
3.13	Rotor position at starting condition	38
3.14	Quadrature axis current response	39
3.15	Developed torque response	39
3.16	Three phase Currents is showed for sinusoidal current regulated field oriented control	39
4.1	Basic structure of Single Neuron	41
4.2	Block diagram of Proposed Single Neuron based Adaptive Controller with PMBLDC Motor	42
4.3	Speed characteristic for Single Neuron based Adaptive Controller	43
4.4	Activation function	44
4.5	Response of quadrature axis current	44
4.6	Update weights are displayed for Single Neuron based Adaptive Controller	44
4.7	Update weights are displayed for Single Neuron based Adaptive	45

	Controller	
4.8	Developed torque for Single Neuron based Adaptive Controller	45
4.9	Illustration of three phase back emf with nature of trapezoidal back emf	46
4.10	3 phase current of single neuron based adaptive controller	46
4.11	Three phases voltage for Single Neuron based Adaptive Controller	47
5.1	Basic structure of an auto tuning neuron	49
5.2	Block Diagram for Tuning Algorithm of PID gains by SNE	50
5.3	Actual speed and estimated speed by SNAPID controller	52
5.4	Response of K_p , K_i and K_d gain for SNAPID controller	52
5.5	Adjustable bias of (a) saturated level and (b) slope with SNAPID controller	53
5.6	At steady state condition (a) phase current and (b) phase back emf for SNAPID controller	53
5.7	Developed torque and quadrature axis current for proposed controller	54
5.8	Illustration of three phase back emf with nature of trapezoidal back emf by SNAPID controller	55
5.9	Three phase current by SNAPID controller	55
5.10	Phase back emf with rotor angle theta for proposed technique	56
5.11	Three phase voltage for SNAPID Controller	56
6.1	Block diagram of ANFIS based controller with radial basis function and PMBLDC Motor	58
6.2	ANFIS controller with PMBLDC Motor	59
6.3	Speed response characteristic by ANFIS based controller with RBF	64
6.4	(a) Three phase current and (b) developed torque by ANFIS with RBF	64
6.5	Weight update from w_1 to w_9	65
6.6	Update consequent parameters from p_1 to p_9	66
6.7	Update consequent parameter from q_1 to q_9	67
6.8	Update consequent parameter from r_1 to r_9	68
6.9	Update premise parameters from c_1 to c_3 and b_1 to b_3	69
6.10	ANFIS Controller based on Takagi- Sugeno Model	70
6.11	Speed characteristic by ANFIS controller based on Takagi-Sugeno Model	71
6.12	Illustration of (a) three phase current and (b) developed torque	72
6.13	Three phases voltage	72
6.14	Single phase back emf	72
6.15	Speed characteristic for PMBLDC Motor based on Line Voltage Model	74
6.16	Illustration of (a) three phase current and (b) developed torque	75
6.17	Illustration of (a) Line voltage and (b) Back emf based on Line Voltage Model	75
	Model	
7.1	Structure of biological neuron	78
7.2	Structure of artificial neuron	79
7.3	Controller based on WNN with PM Brushless DC Motor	79
7.4	Motor speed response is exhibited for WNN based controller	81

7.5	Response of developed torque and I_{qr} during starting condition	82
7.6	Stator phase current is displayed at starting condition for proposed controller	82
7.7	Three phase back emf for WNN based controller	83
7.8	Illustration of (a) 3 phase voltage and (b) single phase back emf	83
8.1	(a) Speed response, (b) Single phase back emf, (c) Phase current and (d) Rotor position by fixed PI controller	87
8.2	(a) Speed response, (b) Single phase back emf, (c) Phase current and (d) Rotor position by SNA controller	88
8.3	Updated weights with SNA controller	89
8.4	(a) Speed response, (b) Back emf, (c) Phase current and (d) Rotor position for the ANFIS based controller with RBF	90
8.5	(a) Weight w_i , (b) Consequent parameter p_i , (c) Consequent parameter q_i and Consequent parameter r_i by ANFIS based controller with RBF	91
8.6	(a) Speed characteristic, (b) Back emf, (c) Phase current and (d) Rotor position by ANFIS Controller based on Takagi-Sugeno Model	92
8.7	(a) Speed characteristic, (b) Single phase back emf, (c) Phase current and (d) Rotor position by ANFIS Controller based on Line Voltage Model	93
8.8	(a) Speed characteristic, (b) Back emf, (c) Phase current and (d) Rotor position by SNAPID controller	94
8.9	Response of K_p , K_i and K_d gain by SNAPID controller	94
8.10	(a) Speed characteristic, (b) Back emf, (c) Phase current and (d) Rotor position by WNN based controller	95
8.11	(a) Speed response, (b) Back emf, (c) Phase current and (d) Torque response by fixed PI controller	96
8.12	(a) Speed characteristic, (b) Phase back emf, (c) Phase current and (d) Torque response by SNA Controller	97
8.13	Response of (a) Speed, (b) Back emf, (c) Phase current and (d) Torque by SNAPID Controller	98
8.14	(a) Speed response, (b) Back emf, (c) Phase current and (b) Torque response by ANFIS based controller with RBF	99
8.15	(a) Speed response, (b) Phase back emf, (c) Phase current and (b) Torque response by ANFIS controller based on Takagi-Sugeno Model	100
8.16	(a) Speed response, (b) Back emf, (c) Phase current and (b) Load torque with ANFIS Controller based on Line voltage Model	101
8.17	Illustration of (a) Speed response, (b) Back emf, (c) Phase current and (b) Torque response with WNN based controller	102
8.18	(a) Speed response and (b) Torque response by fixed PI controller	103
8.19	Response of phase current with fixed PI controller	103
8.20	(a) Speed characteristic and (b) Torque characteristic with Single Neuron based Adaptive (SNA) controller	104
8.21	Motor phase current with Single SNA controller	104
8.22	Response of (a) Speed and (b) Torque with Single Neuron based	104

	Adaptive PID controller	
8.23	Motor phase current with SNAPID controller	105
8.24	(a) Speed response and (b) Torque response by ANFIS based Controller with RBF	105
8.25	Motor phase current by ANFIS based Controller with RBF	106
8.26	(a) Speed characteristic, (b) Torque characteristic and (c) Phase current with ANFIS based on Takagi- Sugeno Model	106
8.27	(a) Speed response, (b) Torque response and (c) Phase current with ANFIS based on Line Voltage Model	107
8.28	(a) Speed characteristic, (b) Torque characteristic and (c) Phase current with WNN based controller	108

List of Abbreviations

ADC	Analog to Digital Converter
BLDCM	Brushless DC Motor
EMF	Electromotive Force
CC-VSI	Current Controlled Voltage Source Inverter
CNC	Computer and Numerical Control
DAC	Digital to Analog Converter
DSP	Digital Signal Processor
DTC	Direct Torque Control
d-q	Direct – Quadrature Axis
PM	Permanent Magnet
WNN	Wavelet Neural Network
ANFIS	Adaptive Neuro Fuzzy Interface System
FL	Fuzzy Logic
FOC	Field Oriented Control
ICD	In-circuit Debugger
PMBLDC	Permanent Magnet Brushless DC Motor
IGBT	Insulated Gate Bipolar Junction Transistor
PI	Proportional plus Integral
PID	Proportional Integral Derivative
PMSM	Permanent Magnet Synchronous Moto
PWM	Pulse Width Modulation
RKG	Runge-Kutta-Gill
SPM	Synchronous Permanent Magnet
SVM	Space Vector Modulation
SVPWM	Space Vector Pulse Width Modulation
SNA Controller	Single Neuron based Adaptive Controller
SNE	Single Neuron Estimator
EVs	Electric- Vehicles
ESC	Electronic Speed Control
ANN	Artificial Neural Network
PMAC	permanent magnet AC
IECV	Intelligent Electronics Controlled Vehicle
PMDC machine	Permanent Magnet DC Machine
LM	Levenberg-Marquard
LSA	Least Square Approximation
DNN	Deep Neural Network
MRAC	Model Reference Adaptive Control
IPM	Interior Permanent-Magnet
SPM	Surface Permanent-Magnet
RBF	Radial Basis Function
SNAPID	Single Neuron based Adaptive PID Controller

List of Symbols

V_{ab}, V_{bc}, V_{ca}	Line voltages
V_{as}, V_{bs}, V_{cs}	Stator phase voltages
I_a, i_b, i_c	Motor phase currents
e_a, e_b, e_c	Motor phase back emf
T_l	Load torque
T_e	Developed torque (Electro-Magnetic torque)
L_s	Stator inductance per phase
M	Mutual inductance between phases
R_s	Stator resistance per phase
I_q	Quadrature axis current
I_d	Direct axis current
I_α	Current in alpha axis
I_β	Current in beta axis
θ_r	Angular rotor position
ω_m	Angular rotor speed
λ_m	Flux linkages
K_p	Proportional constant
K_I	Integral constant
K_d	Derivative constant
$e(t)$	Speed error
J	Moment of inertia
B	Damping constant
d/dt	Derivative operator
$g_{as}(\theta_r), g_{bs}(\theta_r), g_{cs}(\theta_r)$	Trapezoidal unit functions
V_{dc}	DC source voltage
K_t	Torque constant
K_e	Back emf constant
P	Number of poles
I_{mref}	Reference current
$i_{aref}, i_{bref}, i_{cref}$	Reference currents with respect phase a, b and c.
T_{ref}	Reference torque
τ_e	Electrical time constant
τ_m	Mechanical time constant
$W_i(k)$	Update weights
$W_i'(k)$	New values of weights
$\Phi(I)$	Activation function
$\Delta w_i(k)$	Weight changed
η_i	Learning rates
$h(\cdot)$	modified hyperbolic tangent function
\hat{y}	Estimated output
Φ, a, b	Adjustable bias
\hat{e}	Estimated error
$\sigma(n)$	Sigmoid activation
$\Psi(n)$	Wavelet function

$V_j(n)$	Output of hidden layer
K_k	Sensitivity factor
$a_j(n), b_j(n)$	Translating and dilation coefficients
$\{p_m, q_m, r_m\}$	Consequent parameters
$\{c_i, b_i, C_j, B_j\}$	Premise parameters
h_j	Gaussian radial basis function

CHAPTER I

INTRODUCTION

The Chapter at a Glance

Background	Section 1.1
Motivation	Section 1.2
Brief of Literature Review	Section 1.3
Objectives	Section 1.4
Contents of the Thesis in Brief	Section 1.5

1.1 Background

A dc motor is a machine that receives electrical energy from a dc source and converts to mechanical energy. It is constructed using four main parts, say, field coil, armature circuit, commutator, and brushes. The field system of the machine is a uniform and unidirectional magnetic field that may also be produced by a permanent magnet system. Field coils are placed into the stationary field core. Armature coils are placed into the armature core which is rotating in the uniform magnetic field. A commutator is a type of rotating switch which is placed between armature coils and external circuit through brushes. Brushes supply power to commutator from DC source [1].

A synchronous motor rotates at synchronous speed and converts electrical energy from an ac source into mechanical form. This motor is also known as a constant speed motor. It has two parts such as the stator and rotor. Stator holds three-phase armature winding in the slots of the stator core and produces a revolving magnetic field by receiving power from three phase AC supply. Rotor houses exciting coils in the rotor core. For creating a constant magnetic field by the rotor, the exciting coils are connected in series through two slip rings. Direct current is injected into the coils through brushes from an external exciter mounted on the rotor shaft. Poles of the rotor are locked magnetically with opposite poles of stator and rotor rotates at synchronous speed with a revolving magnetic field of stator [1].

DC Motor may be called conduction motor as the electric power is conducted directly to the armature winding through brushes and commutator arrangement. Another category of the motor is the induction motor which is a very popular motor and is termed as the workhorse of industries. However, rotors of those motors do not receive electric power by conduction rather by electromagnetic induction. For this reason, these motors are known as induction motors. Induction motors are also familiar as rotating type transformer in the sense that stator winding acts as primary winding and rotor winding acts as secondary winding [2]

A Permanent Magnet Brushless DC (PMBLDC) Motor is an important member of Brushless DC (BLDC) Motor. It is also like Permanent Magnet Synchronous Motor (PMSM) and it has trapezoidal back emf due to its trapezoidal field flux. Its rotor is made of permanent magnet and the inverter supplies power to the motor from DC source. Three phase star connected windings are housed into stator core. A wide range of speed control is possible by using the inverter and control circuit. These motors are used as small horsepower motors due to higher efficiency, compact form, silent operation, low maintenance, and reliability. For household appliances, people are very much dependent on classic electric motors such as universal motor, capacitor –start capacitor-run, reluctance, and other single phase AC induction motors. Conventionally, these types of motors operate at desired speed with maximum possible efficiency. Now people are expecting effective electric motor for reducing acoustic noise, lower energy cost, better performance, and more convenience features. These problems can be solved by PMBLDC Motors and these motors are also gaining popularity day by day for automation, industrial control, Electric-Vehicles (EVs), constant and variable loads and position/speed control applications [3]. Permanent Magnet Brushless DC motors have fields constructed from rare earth magnetic materials like NdFeB, SmCo, etc. These motors do not require any dc excitation. The problem associated with PMBLDC Motors is the initial position sensing of rotor poles for stator excitation. Unlike induction motors speed of these motors does not depend on the number of poles. Improved magnet materials with high (B.H), the product also helps to push the BLDC motors market to tens of kW application areas with potential cost savings [5].

1.2 Motivation

The DC conduction motor enjoys a mutually perpendicular orientation of field and armature current providing simplified torque and speed control actions. However, for these motors brushes make mechanical friction with the different parts of the rotating commutator. The brush - commutator system acts as an electrical switch that causes a spark. Brush undergoes corrosion gradually, hence replacement of brushes with suitable devices is essential for commercial operation of the motor that is very difficult to attain. An alternative solution is the PMSM Motor.

In the PM Brushless DC motor, armature windings act as a stator and permanent magnet as a rotor. Hence, in this case, DC power is directly fed to the stator winding. Brush - commutator assembly is replaced by an intelligent power electronic controller and it is called commutator less or brushless motor. The power dissipated is less with reduced maintenance problems due to the lack of brush and commutator [2].

Induction motor is known as a performable motor in the electric vehicle application for their less maintenance, robust and less costly. It is noticed that the PMSM Motor has more efficiency than other motors saving fuel consumption, less pollution, and higher power to volume ratio. Hence this motor is gaining more and more popularity day by day for electric vehicle applications [4].

PMSM Motor is controlled by a microcontroller and solid state devices, so very little power is wasted. It has no friction having no brushes and commutator; hence it has less power loss, high speed, smaller size, and less noise. Heat production and bearing stress are also less because there is no winding on rotor [5].

To produce sufficient electric torque with trapezoidal field rectangular stator currents are injected to the motor. This motor has three control variables such as position, speed, and torque which are controlled with closed loop. The actual speed of the motor is measured by an optical encoder or Hall sensor. This motor can be controlled remotely with a small control signal. It has a fast speed response. Electronic Speed Control (ESC) and Computer Numeric Control (CNC) machines also use the BLDC motor [2].

A classic speed controller is needed to gain expected performance levels from the motor. Generally, the Proportional plus Integral (PI) controller is being used as a speed controller. It is widely used in the industries because of their simple control structure and easy practical implementation. This controller faces some control complexity for load disturbances, nonlinearity and parameter variations. A linear mathematical model is required for PI control. As PM Brushless DC Motor has a multi variable and nonlinear model, a conventional PI controller cannot produce high performed results. To overcome these problems Artificial Neural Network (ANN) is a good choice in this research area because it can take decisions just like human brain. ANN has high learning and nonlinear mapping essences that attracts my interest. The parallel and distributed structure of ANN can provide a nonlinear mapping between inputs and outputs of an electric drive system without the knowledge of any predetermined model. For PM Brushless DC Motor, ANN based controllers are designed which can be contributed to military and medical types of equipment, electric vehicles, and aerospace [12, 20].

The better performance of the motor and its huge future prospect attracted my interest and inspired me to work to design suitable controllers for the motor. ANN based controllers have a very good chance that encouraged me to design and test such controllers for PMSM Motor applications.

1.3 Brief of Literature Review

The application of direct torque control (DTC) to brushless ac drives has been investigated in [1]. The paper highlights the essential differences in its implementation, as regards torque estimation and the representation of the inverter voltage space vectors. A two axes model for flux and current is introduced. Simulated and experimental results are presented, and it is shown that, compared with conventional current control, DTC results in reduced torque ripple and faster dynamic response. It has been shown that DTC is capable of instantaneous torque control and, thereby, reducing torque pulsations. In paper [2] a method is proposed to drive brushless DC motor without using the complementary PWM output of the power-supply voltage and the earth voltage with simple hardware. It is shown that this method reduces power consumption by the numerical calculation and the circuit simulation when driving current was a little.

Conventionally, two types of permanent magnet electric machines are familiar such as permanent magnet AC (PMAC) machines and permanent magnet DC (PMDC) machines. DC commutator machines have two windings like one armature windings and the other one is field winding. These machines are parallel with PMDC machines but have only one difference, if field winding is replaced by a permanent magnet. Where the field of PMAC machines is produced by permanent magnet housed on the rotor. This type of machine doesn't require brushes and commutator. For this reason, this machine is simpler and cheaper than the PMDC machine. PMAC machine is known as Permanent Magnet Brushless DC (PMBLDC) Motor and has trapezoidal back emf [6]. Going back more than one hundred years; we found that the first automobiles used dc electric machines. Unfortunately, these electric machines could not hold their sustainable position due to the rapidly developing internal combustion engines and lack of research continuation for development. Currently, electric automobiles, various hybrid and other devices which are serving to transportation using brushless DC motors [7]. In the DC motors, the power losses have occurred mainly in the rotor which has a limit for the heat transfer. But in the BLDC motors, most of the power losses have practically occurred in the stator, where heat can be easily transferred through the frame or cooling systems can be used especially in large machines [8].

For solving the global warming issue in the near future world, sustainable transportation is required to minimize energy consumption and greenhouse gas emissions. In this case, hybrid and electrical vehicles are a good solution to increase safety, efficiency and controllability in the automotive industry. So, the design of the intelligent electronic controlled vehicle (IECV) can be the solution for many challenges in this field. Now a day, BLDC motor has been demanding as an in-wheel motor in electric vehicles due to sustainability and zero emission [9].

The space vector pulse width modulation (SVPWM) technique is employed with field oriented control (FOC) for BLDC motor. Motor voltages and currents can be manipulated by FOC. FOC means that three-phase reference current or voltage of stator frame is transformed into α - β axis orthogonal stationary reference frame and park transformation converts from α - β axis orthogonal into a d-q orthogonal rotating axis of rotor frame. For the current space vector, direct axis current (I_d) is considered zero because of producing

useless torque and only quadrature axis current (I_q) is used to produce useful maximum torque efficiency. PWM control is used to switch ON and OFF for varying speed of this motor [10, 11]. Motor torque depends on two variables those are back emfs and phase currents. Voltage space vector control is chosen to get better torque control and dynamic performance [11]. Brushless DC motor speed is controlled by a low-cost microcontroller. Hall sensor is a transducer that is embedded with the stator winding and it varies out voltage by sensing the rotor magnetic field. An inverter is used for electronic commutation instead of brush and commutator. Inverter switching is controlled by a logic microchip controller for speed control of the motor [5].

Adaptive Neuro-Fuzzy Inference System (ANFIS) is a combination of Artificial Neural Network (ANN) and Fuzzy Logic (FL) which is an effective method for predicting motor performance. This model is trained by the Levenberg-Marquardt (LM) training algorithm and performance is compared between ANFIS and Fuzzy PID control system. It also has compared with experimental data based on two- axis inertial stabilized platform [12].

Efficient appropriate techniques are chosen to estimate BLDC motor parameters such as motor resistance (R), motor inductance (L) and motor inertia (J). Speed control of this motor is implemented by using estimated parameters and it is compared with different estimation methods which are least square approximation (LSA), gradient search method and marquardt method. The actual value is also compared with estimated value and simulation results of LAS method shows better performance among them [13].

Fuzzy logic (FL) and PI controllers are designed to control motor speed. PI control is widely used in industrial applications due to their simple construction and easy to control but it has control complexity due to their parameter variation, load disturbance, and nonlinearity characteristic. In this case, the FL controller is used to overcome the problem and it works better than PI. The mathematical model also is described in well [3].

The two optimization methods are implemented to BLDC motor parameter identification by a deep neural network (DNN). Motor speed can be controlled with less settling time and reduced ripples. This motor widely is used in industrial automation, military appliances and aerospace [14].

Non-sinusoidal back emf is employed for direct torque control (DTC) of brushless DC motor. DTC technique is designed with speed controller using fuzzy logic control (FLC) for reducing starting current and torque ripple. It removes speed and torque overshoot. FLC is implemented with Proportional Derivative (PD) control for reducing the rise time. DTC is also called low-cost inverter due to the reduction starting current and its simple structure and robust. Now due to less sensitivity of parameter variations and faster torque response, DTC works effectively than PI control [15].

Model reference adaptive control (MRAC) is constituted of PI and ANN architecture for the BLDC motor drive. It has an auto learning capability and speed tracking performance compared to conventional PID control. MRAC and ANN controller are widely used in the control system for their non-linear and dynamic system [16]. The Brushless DC motor phase currents are estimated using different current sensors for closed-loop current control. Motor phase currents and torque fluctuate due to the variant sensitivity of current sensors. These sensors are bulky, heavy and expensive. These problems can be overcome by using a single current sensor placed in the DC link. This technique shrinks drive cost, drive size and promotes drive performances. A low-cost resistor with a current sensor is placed on the ground line [17]. The adaptive fuzzy logic speed controller is designed by a fuzzy PD and fuzzy PI controller for the BLDC motor drive. A fuzzy PI controller is employed to reduce steady-state error with improving the steady-state response and fuzzy PD is implemented to promote transient response by minimizing the rise time. Rise time, peak overshoot, settling time and steady-state error of adaptive fuzzy logic controller is better than the conventional PI controller. Also, speed does not change under constant load and load varying conditions [18].

Rotor position sensors are needed to control Brushless DC motor for starting and providing the proper commutation sequence. Especially, these sensors are Hall sensors which increase motor size and cost but it has operation limitations below about 75° C for their temperature sensitive. To avoid these sensors, a direct back emf detection technique is employed with this motor. Hence this motor is called a sensorless BLDC motor. Therefore, sensorless control has been receiving great interest for researchers [19].

The paper [20] proposes an ANFIS based controller and it consists of the combination of Artificial Neural Network (ANN) and Fuzzy Logic (FL), which uses learning techniques to control the PMBLDC motor. The performance of ANFIS depends on only two factors such as the number of parameters and shape of the membership function. ANN is a system that processes information from one neuron to another neuron-like biological neural connected human brain. PI controller is tuned by the Ziegler-Nichols method. The performance of drive systems was compared with both control systems. The motor drive system is simulated in a C++ environment in a discrete form.

In the industrial motion control applications, BLDC motors are gaining popularity day by day. PID controller is designed for keeping constant motor speed when load torque is varied. But tuning of PID parameters is complex due to their variables, nonlinearity, and uncertainty in the mathematical model. From the analysis and comparison with different control methods, PWM speed control performs best [21]. Recently, induction and DC motors are being replaced by PMBLDC Motor but it has a barrier to implement in a drive system for lack of adaptive controller. ANN based PID controller is designed to estimate disturbances from the output so that it can easily tune the parameters for minimizing the disturbances and improving the drive performance. Motor speed and torque are directly proportional to the amplitude of applied voltage and current respectively [22].

The PMSM has a sinusoidal back emf and requires sinusoidal stator currents to produce constant torque while the BLDC motor has a trapezoidal back emf and receives rectangular stator currents to produce constant torque [3]. The standard wound rotor synchronous machine is almost similar to PMSM. No damper winding and excitation is provided in PMSM but field winding is replaced by a permanent magnet. Hence the d, q model of the PMSM can be derived by avoiding the equations of the damper and field winding. As is well known, the transformation of the synchronous machine equations from the abc phase variables to the d, q variables forces all sinusoidal varying inductances in the abc frame to become constant in the d, q frame. Since the back emf of BLDC motor is non-sinusoidal, the variables and parameters do not vary sinusoidally in the abc frame and it is not wise to transform the equations to the d, q frame since the inductances will not be constant after transformation. Hence it is proposed to use the abc phase variables model for the BLDC motor [23, 3].

At present, the Permanent Magnet Brushless Direct Current (PMBLDC) Motor drive has been opened research opportunity for the development of permanent magnet materials and control technology and it also has gained a reputation, so that it could become a competitor to the DC motor [6].

A microcontroller is used to control speed for Permanent-magnet excited brushless DC motor in a closed loop control technique. The user can enter the desired speed in keypad and the motor will run at that speed. The motor speed is controlled by varying the duty cycles of pulse width modulation from the microcontroller according to the program. In general, this motor was developed from conventional brushed DC motors with the availability of solid-state power semiconductors [24].

Moreover, DC motor control is simple and does not require complex hardware. But, the lifetime of brushes is the limitation. So periodic maintenance is required. Whereas, PMBLDC Motor operates without brushes its lifetime spent can be increased and frequent maintenance can also be avoided. It has also better torque-speed characteristics than conventional DC motor [25].

PM Brushless AC motors can be classified as a surface permanent magnet (SPM) and interior permanent magnet (IPM) motors which are based on the PMs mounted on the rotor. BLDC motor has a very small inductance variation, so if the motor operates under its rated current conditions, the effect of inductance saturation is usually ignored due to the regarded current level [26]. The motor torque depends on the armature current amplitude, the number of the stator windings, the length of the rotating arm, the strength and the size of the permanent magnets, the air gap between the rotor and the stator windings and torque will also be better for increasing rotor poles number [27].

For the Permanent Magnet Brushless DC Motor Sinusoidal Current Regulated Pulse Width Modulation (CRPWM), Square Wave Current Regulated Pulse Width Modulation and Voltage Regulated Space Vector Pulse Width Modulation are proposed to control motor speed. From the results it is observed that their having good performances and first speed response under all operating conditions [28].

The paper [29] proposes a sliding mode controller (SMC) designed for a Brushless DC Motor to achieve high-performance speed control. They proposed a PWM-based controller in the inner current loop to perform a fast current control. A sliding mode speed controller is then designed in its outer control loop to enhance the speed control. Finally, the effectiveness of the proposed integrated control scheme was tested under the load disturbances and parameter uncertainties. The proposed achievement was verified by simulation results and comparison with the proportional-integral control (PIC) approach is given. Simulation studies demonstrated that the proposed SMC controller, in comparison with the PIC approach, can produce a better speed response for different speed commands, load disturbances and parameter uncertainties [29].

The paper [30] describes WNN based controller for controlling the motor speed. A wavelet neural network based controller has high applicability in the control system. Gradient descent online training method is proposed for the WNN controller. Simulation in a C++ environment with code block software is used for testing purposes. After comparison with the results obtained using a PI controller, it is observed that the control system works effectively.

A hybrid PID ANFIS controller is designed based on an identification technique for controlling BLDC motor speed. It is a summation of the output of summing PID and the ANFIS controller. Performance of hybrid PID ANFIS controller is tested with PID and ANFIS control under different operating conditions. From the observation in MATLAB simulation results, it is observed that the rise time is shorter but the overshoot has been increased [31]. A new control scheme has been proposed based on a single neural estimator for tuning the PID control gains. An auto-tuning neuron is known as a neural estimator which gives an estimated single like gradient input-output relationship. During the control process, the transient performance of the plant is more satisfactory for adjusting the gains online. Under this control strategy, it is not required to know the exact model of the controlled plant [32]. The paper [33] presents a single neuron PID controller with adaptive parameters to complete the dynamic acceleration process of a turbofan. The results illustrate that the single neuron control algorithm with gain adaptation has strong robustness; self-learning and anti-jamming capability. The performance of a turbofan

engine can be effectively improved by using the turbine expansion ratio adaptive control law.

The single neuron PID control strategy has been proposed in [34] to remove temperature turbulence problem of aircraft deicing system using artificial neuron control. The controller is applied in an aircraft deicing fluids rapid heating system. The simulation results shows that the single neuron PID control strategy perform effectively on the temperature turbulence problem of aircraft deicing fluids rapid heating system. Recent research has focused the permanent magnet synchronous motor (PMSM) and the Brushless DC motor based on PM motor drives. Both motors would become serious competitors to the induction motor for servo applications [3].

The paper [35] proposes single neuron based adaptive control with adaptation law and conventional PI controller for PMSM Motor. Both controllers control motor speed for their desire speed. But it is difficult to handle the dynamics of the motor by using a conventional PI controller due to changes in motor ratings and characteristics and tuning is necessary to achieve a desired performance. To overcome this problem, the single neuron based adaptive controller is proposed and developed. The PI controller is designed and tuned by the Ziegler-Nichols method. The performance of the drive system is studied for starting condition, speed control, load torque variation and by changing parameters of the motor using C++ simulation.

The performance of the global positioning system (GPS) is being demandable for the military as well as the civilian user. It is difficult to detect the desired quality and quantity of data for lack of base stations and other infrastructure. WNN is used to predict and correct the control system. The weights of WNN are trained and optimized by gradient descent and particle swarm optimization. The results show that the WNN-PSO method has better accuracy to design low-cost receiver [36].

Recently, control system is needed in any field. Usually, classic control is widely used but it is well-known that users need to know the system characteristics to achieve desired control. To improve control performance single neuron based PID control is proposed. The intelligent sensor is involved with control capability for a wide variety the system [37].

The motor offers a good compromise between precise control and the number of power electronic devices required to control the stator currents. A plan optimization for the motor [38] suggests that for the rotor, a greater number of poles are usually created and greater torque for the same level of current is proposed. On the other hand, by adding more magnets, a point is reached where because of the space needed between magnets, the torque no longer increases. The manufacturing cost also increases with the number of poles. As a consequence, the number of poles is a compromise between cost, torque, and volume [38]. The paper [39] has been reported on dual stator permanent magnet BLDC (PMBLDC) Motor. Dual stator topology has been widely used in motors for different applications where power segmentation and reliability are the main concern. This design considers two concentric stators having different diameters with one of the stators having a large diameter and 36 slots in the inner periphery and another stator has a smaller diameter in the outer periphery and 20 slots. The space between the two stators is occupied by a common cylindrical hollow rotor in which the surface mounted permanent magnets are pasted in the inner and outer cylindrical surfaces of the rotor.

The papers [42], [43] and [44] present ANFIS model which is trained by RBF and quantum behaved particle swarm optimization (PSO). Performance of ANFIS model depend number of fuzzy rule and membership function. Training cost is dependent on number of training parameters.

1.4 Objectives

After the discovery of high residual flux of rare earth compound materials and designing dedicated motor control microchip, the applications of these motors have been enhanced drastically. Due to high power density, the motors are smaller in dimension and have a low inertia rotor that results in faster speed response. As the cost of power semiconductor switching devices has been reducing with time. Application area of PM Brushless DC Motors has been enhanced day by day. Due to high power density, smaller dimension and light weight of the controller, the drive system encourages us to select this motor for servo and drive control applications. There appears a fewer number of commercial simulation packages for the design of a controller for such PMBLDC Motor drives.

ANNs are universal controllers and estimators having wide applications. A simple single neuron controller is proposed in this research that can be used for state estimation. The main objective of this research is to study the performance of this PMBLDC Motor under field orientation control. The vector control system is complex and requires several transformations. Secondly this research proposes a plan and applies a single ANN controller with online training for substituting traditional PID controller and also develop a control system based on a wavelet neural network. For training purpose, gradient descent technique is proposed. Artificial Neuro-Fuzzy Inference System has also been used very recently as a controller and estimator. An endeavor has been taken to design ANFIS based control system for the FO PMBLDC Motor drive. Finally, the research is motivated to evaluate the performance of these drive control systems and compare the performance with the conventional PI control system.

In this study the proposed controllers were designed based on Artificial Neural Networks which are (1) Single Neuron based Adaptive (SNA) Controller, (2) Single Neuron based Adaptive PID (SNAPID) Controller, (3) Adaptive Neuro Fuzzy Inference System (ANFIS) based Controller with Radial Basis Function (RBF), (4) ANFIS Controller based on Takagi-Sugeno Model, (5) ANFIS Controller based on Line Voltage Model and (6) Wavelet Neural Network (WNN) based Controller. It is evident that the above controllers work effectively than a fixed PI controller.

1.5 Contents of the Report in Brief

The contents of this thesis are described in nine chapters with a description of the modeling and control technique of a PMBLDC Motor. A brief for these contents is as follows

Chapter I focuses a brief of literature review, objective, and motivation for this thesis.

Chapter II presents operation of PMBLDC Motor with an inverter that is operated in 120 degree phase displacement. The operation of PWM voltage and current are also described. A brief description of position sensors and mathematical modeling of a machine in state space form are also included in this chapter.

Chapter III describes the Field Oriented Control with Hysteresis Current Controller. We have proposed fixed PI controller based on Field Oriented Rectangular Current Regulated Control and Sinusoidal Current Regulated Field Oriented Control for PMBLDC Motor. For these techniques a detail discussion is also delivered.

Chapter IV describes Single Neuron based Adaptive Controller with Adaptive Law. A detail discussion is also given for this method.

Chapter V reveals a principle of Auto tuning and Tuning Algorithm of PID gains by SN estimator for the PM Brushless DC Motor.

Chapter VI displays a description of ANFIS architecture with Radial Basis Function. We have proposed ANFIS based controller that is trained by Radial Basis Function. A detail description of ANFIS based controller by Takagi- Sugeno Model and Line Voltage Model is given in this chapter.

Chapter VII provides a comparison of artificial and biological neuron. We have proposed a controller based on Wavelet Neural Network with Gradient Descent Learning Rule. A detail discussion is also given for this method.

Chapter VIII presents simulation results and discussion under different dynamic operating condition for the proposed controller of PMBLDC Motor.

Chapter IX presents the conclusion of the speed control strategies of the Permanent Magnet Brushless DC Motor and proposal for future work.

CHAPTER II

MATHEMATICAL MODEL OF PERMANENT MAGNET BRUSHLESS DC MOTOR

The Chapter at a Glance

Introduction	Section 2.1
Construction	Section 2.2
Principle of Operation of PM Brushless DC Motor	Section 2.3
$2\pi/3$ Angles Switch on Mode	Section 2.4
Current control PWM or Voltage control PWM	Section 2.5
Review on Brushless DC Motor Modeling	Section 2.6
Mathematical Model of the Machine Considering phase voltage	Section 2.7
Digital simulation of the motor	Section 2.8
Conclusion	Section 2.9

2.1 Introduction

PMBLDC Motors are gaining interest in application areas due to availability of high retentive rare earth magnetic materials. These motors are free from any dc excitation. Due to high power density, the motors are smaller in dimension and low inertia rotor resulting faster speed response. The motor stator has 3-ph balanced star connected windings. The electronic switches replace the mechanical commutator and brushes. For proper operation and control, accurate rotor position information is required. For this purpose maintaining proper commutation sequence to turn on the power electronic devices in the inverter bridge is very crucial. Normally Hall or optical position sensors are employed for exact rotor position information. In closed loop speed control systems, instantaneous speed information is also required. For complex control systems such as CNC machines absolute position information is required. The commutator and brush-system in dc machines is replaced by a set of electrical switches in PMBLDC Motor, controlling firing sequence, such that electrical-power always flows through the armature-coil closest to the stationary stator (PM). On the contrary, in a PMBLDC Motor, the electromagnets [3] do not rotate;

instead, the permanent magnets rotate and the armature remains static. The static armature excitation controlled by inverter solves the dc motor problem.

2.2 Construction

A brushless dc motor is a dc motor with inverted construction, so that the field is on the rotor and the armature is on the stator. The brushless dc motor is actually a permanent magnet ac motor whose torque producing current is identical to the dc motor. The rotor is made of permanent magnet and normally varies from two to eight pole pairs with alternate north and south poles [3]. NdFeB material is used for permanent magnet construction. Instead of commutating the armature current using brushes in a dc motor, electronic commutation is used in a PMBLDC Motor. This eliminates the problems associated with the brush and commutator arrangement, for example, sparking and wearing out of the commutator-brush arrangement, thereby, making a BLDC motor more rugged as compared to a dc motor. Putting the armature on the stator makes it easy to conduct heat away from the windings. Hence cooling arrangement of this armature will be much easier as compared to a dc motor [3, 5]. Cross-sectional view of a permanent magnet Brushless DC Motor is shown below in Fig.2.1.

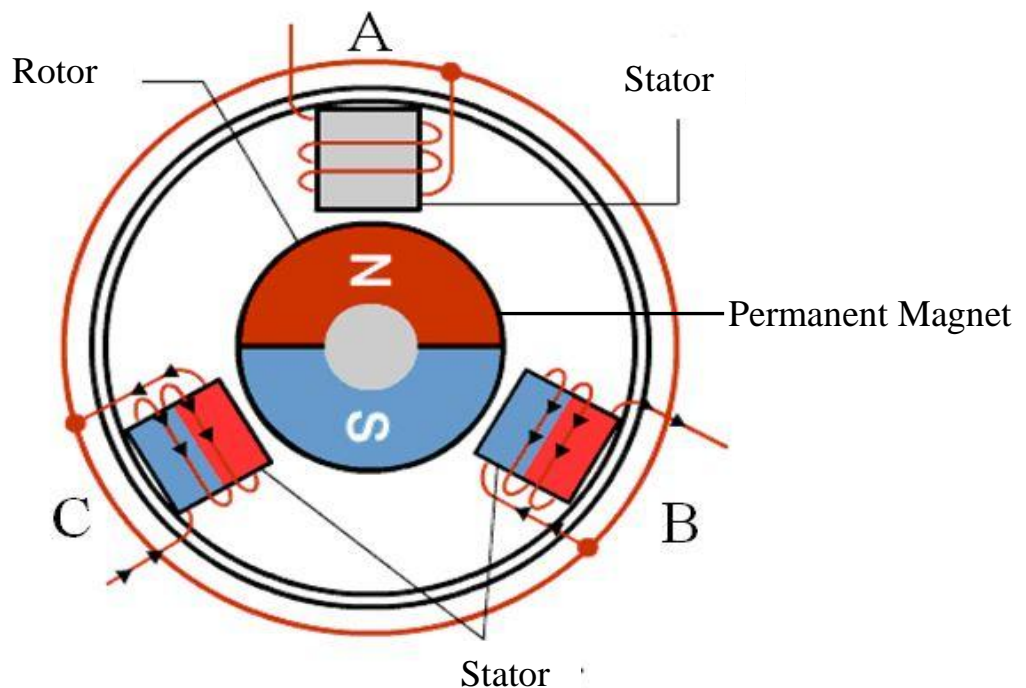


Fig 2.1: Cross-sectional view of a PM Brushless DC Motor

The “commutation region” of the back emf of a BLDC motor should be as small as possible, while at the same time it should not be so narrow as to make it difficult to commutate a phase of that motor when driven by a Current Source Inverter [5]. The flat constant portion of the back emf should be 120° for a smooth torque production. The position of the rotor can be sensed by using an optical position sensor and its associated pulse conditioning circuit. Optical position sensors consist of phototransistors (sensitive to light), revolving shutters, and a light source. The output of an optical position sensor is usually a Logical signal.

2.3 Principle of Operation of PM Brushless DC Motor

Brushless DC motor is a permanent magnet synchronous machine with rotor position feedback. The motor output variables are generally controlled using a three phase power semiconductor bridge inverter. The basic block diagram of Brushless Dc motor drive is shown in Fig.2.2. Four main parts involved in PM Brushless DC motor control are inverter, PMBLDC Motor, sensors, and control algorithm. The inverter transforms power from the source to the PMBLDC Motor [3].

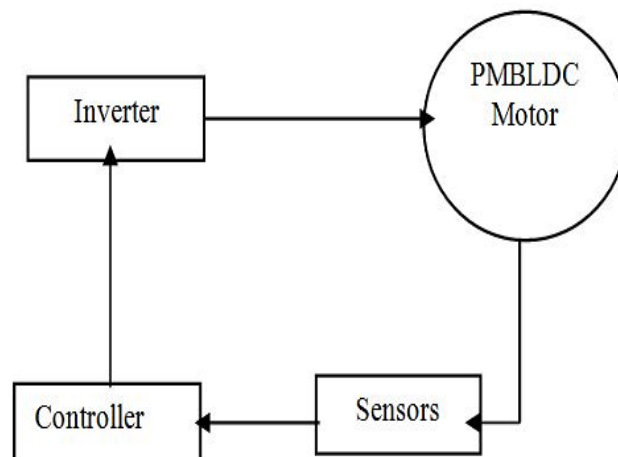


Fig.2.2: Basic block diagram of PM Brushless DC Motor drive

Command signals to the system may be a torque command or speed command. The control algorithms determine the gate signal to each semiconductor switch of the power electronic inverter. The structure of the control algorithms determines the type of the PMBLDC Motor drive of which there are two main classes: the voltage source based drives and the current source based drives [3]. Both voltage source and current source based drives are used with permanent magnet synchronous machine with either sinusoidal or non-sinusoidal

back emf in waveform. Machines with non-sinusoidal back emf as shown in Fig.2.6 may be controlled in such a way to achieve nearly constant torque. However, machine with a sinusoidal back emf in Fig.2.3 offer reduces inverter sizes and reduces losses for the same power level [28, 3].

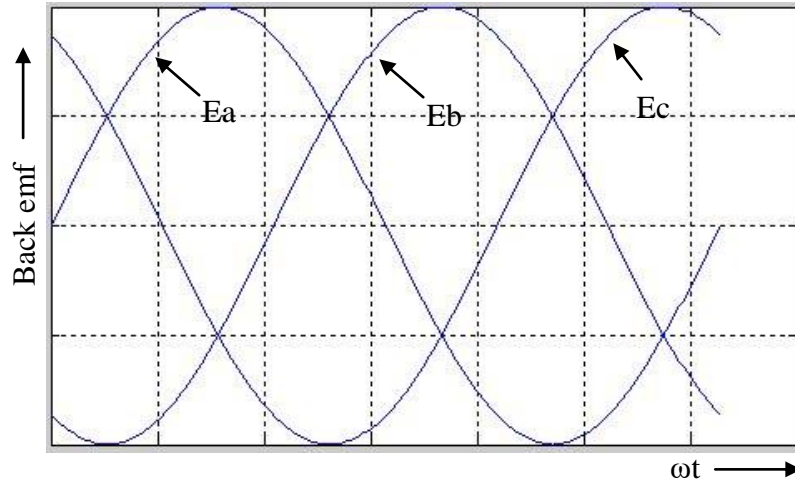


Fig.2.3: Sinusoidal back emf of BLDC motor

Basically it is an electronic motor and requires a three-phase inverter in the front end as shown in Fig. 2.4. In self control mode the inverter acts like an electronic commutator that receives the switching logical pulse from the absolute position sensors.

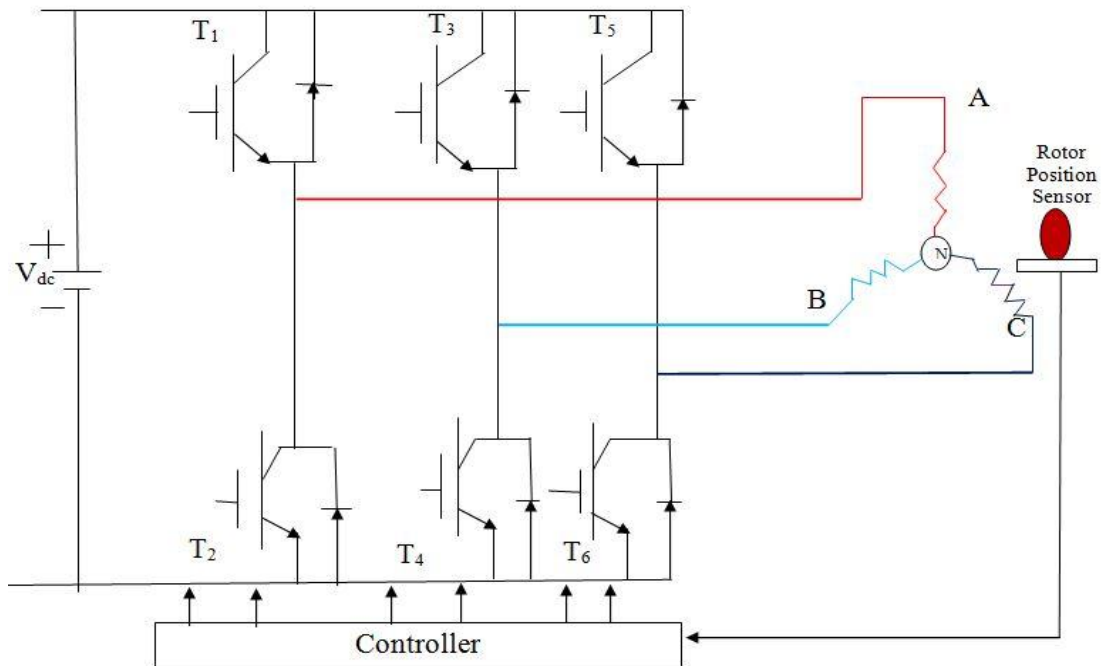


Fig.2.4: Three phases inverter circuit with PMBLDC Motor

The drive is also known as an electronic commutated motor. The inverter can operate in two modes like $2\pi/3$ angle switch on mode and Current control PWM or Voltage control PWM mode [3].

2.4 $2\pi/3$ Angles Switch On Mode

As shown in Figure (2.5), there are (T_1 - T_6) six switches of inverter. In angle switch on mode [28], they operate to take the input DC current I_{dc} symmetrical for $2\pi/3$ angles in the middle of each phase voltage wave. The α is the angle of current with respect to voltage. In any instant, two switches are on (one in the upper group and another one in the lower group). For any moment of time t_1 , the T_1 and T_6 are on; then the supply voltage V_{dc} and I_{dc} are put across the line ab (phase A, phase B in series), to make I_{dc} positive in phase a; but negative in phase b, after $\pi/3$ interval (middle of phase A). After that T_6 is turned off and T_2 is turned on, but T_1 continues to conduct current during the full $2\pi/3$ angle. This switching commutates negative I_{dc} from phase b to phase c while phase a draws positive I_{dc} , the conduction changes for every $\pi/3$ angles representing the switching modes in a full cycle [3].

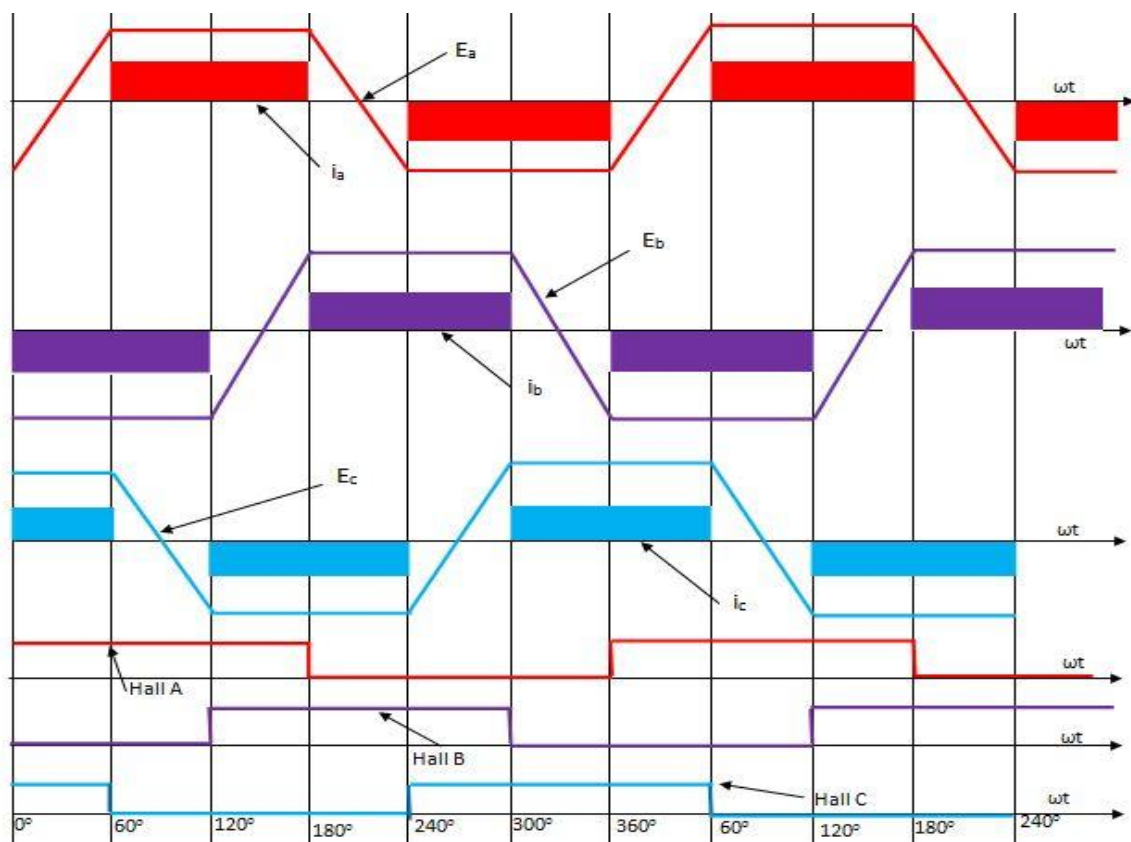


Fig.2.5: Back-emfs, current waveforms and Hall sensors for PM Brushless DC Motor

2.5 Current control PWM or Voltage control PWM

The PWM technique is the chopping frequency having fixed parameter; hence, acoustic and electromagnetic noises are relatively easy to filter [28]. We can control the switches with Pulse Width Modulation and 'Chopping' to control the voltage and current continuously at motor terminal [3]. There are two 'Chopping' modes for current controlled operation of the inverter, (1) feedback (FB) mode and (2) freewheeling mode. In these modes devices are turned 'on' and 'off' on duty cycle basis for controlling current average I_{av} and voltage average V_{av} .

2.6 Review on Brushless DC Motor Modeling

The PMSM has a sinusoidal back emf and requires sinusoidal stator currents to produce, while the BLDC motor has a trapezoidal back emf and 120° rectangular stator currents are injected to produce constant torque. Conversion of the abc phase variables to the d, q variables transforms the synchronous machine varying inductances to become constant. In the PMBLDC Motor, since the back emf is non sinusoidal, the inductances do not vary sinusoidally in the abc frame, so it does not seem advantageous to transform the equations to the dq frame. For this reason, it is proposed to use the machine model using abc phase variables. Moreover, this approach in the modeling of the motor allows a detailed examination of the machine's torque behavior if any simplifying assumptions were made. The abc phase variable model has been used to examine the behavior of a PMBLDCM speed servo drive [3, 28] instead of dq variable model of PM synchronous machines.

2.7 Mathematical Model of the Machine considering Phase Voltage

PM Brushless DC Motor consists of three stator windings and a permanent magnet rotor. Induced currents in the rotor are neglected because of high resistance in both magnets and steel core. Damper windings are also neglected in the equation of the windings where phase variables are calculated. This motor is constructed by the modification of permanent magnet synchronous motor as well as motor induced voltage is trapezoidal back emf due to field flux as shown in Fig.2.6. Back emf depends on rotor position and actual motor speed. The back emf functions are expressed mathematically as [3, 28]

$$g_{as}(\theta_r) = \begin{cases} \theta_r \frac{6}{\pi} & 0 \leq \theta_r \leq \frac{\pi}{6} \\ 1 & \frac{\pi}{6} \leq \theta_r \leq 5\frac{\pi}{6} \\ (\pi - \theta_r) \frac{6}{\pi} & 5\frac{\pi}{6} \leq \theta_r \leq 7\frac{\pi}{6} \\ -1 & 7\frac{\pi}{6} \leq \theta_r \leq 11\frac{\pi}{6} \\ (\theta_r - 2\pi) \frac{6}{\pi} & 11\frac{\pi}{6} \leq \theta_r \leq 2\pi \end{cases} \quad (2.1)$$

$$g_{bs}(\theta_r) = \begin{cases} -1 & 0 \leq \theta_r \leq \frac{\pi}{2} \\ \left(-\frac{2\pi}{2} + \theta_r\right) \frac{6}{\pi} & \frac{\pi}{2} \leq \theta_r \leq 5\frac{\pi}{6} \\ 1 & 5\frac{\pi}{6} \leq \theta_r \leq 3\frac{\pi}{2} \\ \left(-5\frac{\pi}{3} + \theta_r\right) \frac{6}{\pi} & 3\frac{\pi}{2} \leq \theta_r \leq 11\frac{\pi}{6} \\ -1 & 11\frac{\pi}{6} \leq \theta_r \leq 2\pi \end{cases} \quad (2.2)$$

$$g_{cs}(\theta_r) = \begin{cases} 1 & 0 \leq \theta_r \leq \frac{\pi}{6} \\ \left(\frac{\pi}{3} - \theta_r\right) \frac{6}{\pi} & \frac{\pi}{6} \leq \theta_r \leq \frac{\pi}{2} \\ -1 & \frac{\pi}{2} \leq \theta_r \leq 7\frac{\pi}{2} \\ \left(-4\frac{\pi}{3} + \theta_r\right) \frac{6}{\pi} & 7\frac{\pi}{2} \leq \theta_r \leq 3\frac{\pi}{2} \\ 1 & 3\frac{\pi}{2} \leq \theta_r \leq 2\pi \end{cases} \quad (2.3)$$

Where $g_{as}(\theta_r)$, $g_{bs}(\theta_r)$ and $g_{cs}(\theta_r)$ are unit function generator corresponding to the trapezoidal representation of induced emfs of PMBLDCM as a function of θ_r . The $g_{bs}(\theta_r)$, $g_{cs}(\theta_r)$ is similar to $g_{as}(\theta_r)$ but with a phase displacement of 120° [3, 28].

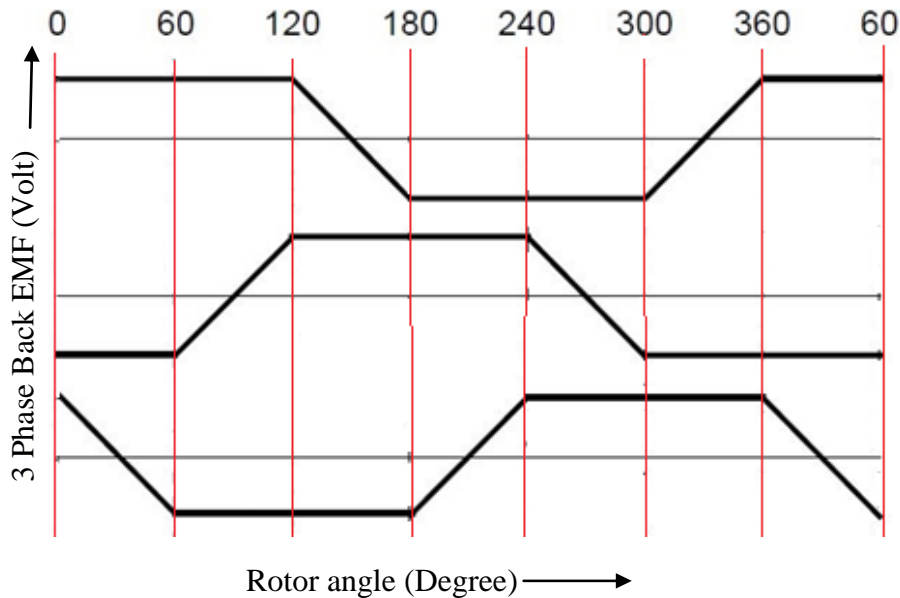


Fig.2.6: Three phase Trapezoidal back EMF of PMBLDC Motor [3]

Trapezoidal back emfs are

$$\begin{bmatrix} e_a \\ e_b \\ e_c \end{bmatrix} = \omega_m \lambda_m \begin{bmatrix} g_{as}(\theta_r) \\ g_{bs}(\theta_r) \\ g_{cs}(\theta_r) \end{bmatrix} \quad (2.4)$$

Where angular rotor speed = ω_m (Radians per second), Flux linkage = λ_m , Rotor position = θ_r (Radian). Resistances of all the phase windings are assumed to be equal to R_s . The phase currents of stator are considered to be balanced. Phase back electromotive forces = e_a , e_b and e_c [3, 28].

There are no sharp corners in the induced emfs due to their trapezoidal nature. The functions $g_{as}(\theta_r)$, $g_{bs}(\theta_r)$ and $g_{cs}(\theta_r)$ have the same shape as e_a , e_b and e_c with a maximum magnitude of ± 1 . The flux linkages are continuous function. The emfs comes from the flux linkages derivatives. The Flux density function becomes smooth without sudden edges because of fringing.

V_{as} , V_{bs} and V_{cs} are phase voltage with respect to a, b and c phase. In the similar way i_a , i_b and i_c are stator phase current with respect to a, b and c phase. Self-inductances of a, b and c phase are L_{aa} , L_{bb} and L_{cc} respectively. Mutual inductances between the phases a, b and c are L_{ab} , L_{bc} and L_{ac} , respectively. The three phase voltage equations in abc phase variables in matrix form is given as [3, 28].

$$\begin{bmatrix} V_{as} \\ V_{bs} \\ V_{cs} \end{bmatrix} = \begin{bmatrix} R_s & 0 & 0 \\ 0 & R_s & 0 \\ 0 & 0 & R_s \end{bmatrix} \begin{bmatrix} i_a \\ i_b \\ i_c \end{bmatrix} + \frac{d}{dt} \begin{bmatrix} L_{aa} & L_{ab} & L_{ac} \\ L_{ba} & L_{bb} & L_{bc} \\ L_{ca} & L_{cb} & L_{cc} \end{bmatrix} \begin{bmatrix} i_a \\ i_b \\ i_c \end{bmatrix} + \begin{bmatrix} e_a \\ e_b \\ e_c \end{bmatrix} \quad (2.5)$$

It is also assumed that if the rotor reluctance does not change with angle due to a non-salient nature of rotor. So simplification can be expressed as

$$L_{aa} = L_{bb} = L_{cc} = L \quad (2.6)$$

$$L_{ab} = L_{ba} = L_{ac} = L_{ca} = L_{bc} = L_{cb} = M \quad (2.7)$$

From this expression, equation (2.5) can be rewritten as [3, 28]

$$\begin{bmatrix} V_{as} \\ V_{bs} \\ V_{cs} \end{bmatrix} = \begin{bmatrix} R_s & 0 & 0 \\ 0 & R_s & 0 \\ 0 & 0 & R_s \end{bmatrix} \begin{bmatrix} i_a \\ i_b \\ i_c \end{bmatrix} + \frac{d}{dt} \begin{bmatrix} L & M & M \\ M & L & M \\ M & M & L \end{bmatrix} \begin{bmatrix} i_a \\ i_b \\ i_c \end{bmatrix} + \begin{bmatrix} e_a \\ e_b \\ e_c \end{bmatrix} \quad (2.8)$$

Where V_{as} , V_{bs} and V_{cs} are indicated as phase voltage and can be expressed as

$$V_{as} = V_{ao} - V_{no} \quad (2.9)$$

$$V_{bs} = V_{bo} - V_{no} \quad (2.10)$$

$$V_{cs} = V_{co} - V_{no} \quad (2.11)$$

Where V_{ao} , V_{bo} , V_{co} and V_{no} are marked as three phase and neutral voltage with respect to zero potential. To make balance stator phase currents can be written as [3, 28].

$$i_a + i_b + i_c = 0 \quad (2.12)$$

Simplification of equation (2.12) is given by

$$Mi_b + Mi_c = -Mi_a \quad (2.13)$$

Machine equation is indicated as

$$\begin{bmatrix} V_{as} \\ V_{bs} \\ V_{cs} \end{bmatrix} = \begin{bmatrix} R_s & 0 & 0 \\ 0 & R_s & 0 \\ 0 & 0 & R_s \end{bmatrix} \begin{bmatrix} i_a \\ i_b \\ i_c \end{bmatrix} + \frac{d}{dt} \begin{bmatrix} L - M & 0 & 0 \\ 0 & L - M & 0 \\ 0 & 0 & L - M \end{bmatrix} \begin{bmatrix} i_a \\ i_b \\ i_c \end{bmatrix} + \begin{bmatrix} e_a \\ e_b \\ e_c \end{bmatrix} \quad (2.14)$$

Electromagnetic torque developed is considered as

$$T_e = \frac{(e_a i_a + e_b i_b + e_c i_c)}{\omega_m} \text{ N-m} \quad (2.15)$$

Total moment of inertia of the drive system is summation of inertias of motor and load can be expressed as

$$J = J_m + J_l \quad (2.16)$$

If inertia is J , friction coefficient is B , and load torque is T_l then the motion system equation can be defined as

$$J \frac{d\omega_m}{dt} + B\omega_m = T_e - T_l \quad (2.17)$$

Relation of electrical and mechanical speed is described as [3, 28]

$$\frac{d\theta_r}{dt} = \frac{p}{2} \omega_m \quad (2.18)$$

Here B is the damping co-efficient, which is usually small and is neglected. The rotor position θ_r repeats every 2π angle. Potential of the neutral point with respect to the zero potential V_{no} is considered restrain imbalance in the applied voltage. Substituting values of V_{as} , V_{bs} and V_{cs} into equation (2.14) and then adding it [3, 28].

$$V_{as} + V_{bs} + V_{cs} - 3V_{no} = R_s(i_a + i_b + i_c) + p(L - M)(i_a + i_b + i_c) + (e_a + e_b + e_c) \quad (2.19)$$

Simplification of equation (2.12) and (2.19) [3, 28].

$$V_{as} + V_{bs} + V_{cs} - 3V_{no} = e_a + e_b + e_c$$

$$\text{Thus } V_{no} = \frac{(V_{as} + V_{bs} + V_{cs}) - (e_a + e_b + e_c)}{3} \quad (2.20)$$

The differential equations define the developed model in terms of the variables i_a , i_b , i_c , ω_m and θ_r with time as an independent variable. Then the system in state-space form [3, 28] is

$$\dot{X} = AX + Bu + Ce \quad (2.21)$$

$$x = [i_a \ i_b \ i_c]^T \quad (2.22)$$

$$A = \begin{bmatrix} -\frac{R_s}{L-M} & 0 & 0 \\ 0 & -\frac{R_s}{L-M} & 0 \\ 0 & 0 & -\frac{R_s}{L-M} \end{bmatrix} \quad (2.23)$$

$$B = \begin{bmatrix} \frac{1}{L-M} & 0 & 0 \\ 0 & \frac{1}{L-M} & 0 \\ 0 & 0 & \frac{1}{L-M} \end{bmatrix} \quad (2.24)$$

$$C = \begin{bmatrix} -\frac{1}{L-M} & 0 & 0 \\ 0 & -\frac{1}{L-M} & 0 \\ 0 & 0 & -\frac{1}{L-M} \end{bmatrix} \quad (2.25)$$

$$u = [V_{as} \ V_{bs} \ V_{cs}]^T \quad (2.26)$$

$$e = [e_a \ e_b \ e_c]^T \quad (2.27)$$

Main model of PM Brushless DC motor is represented the following equation as (2.4), (2.14), (2.17) and (2.18).

2.8 Digital simulation of the drive system

For digital simulation of the motor drive system a computer program in C++ is to be written. The state equations are solved using the Runge-Kutta-Gill 4th order method. The equations in 2.12, 2.15 and 2.16 along with related equations of 2.9 are solved simultaneously. The four coefficients are evaluated according to the following rule.

The basic technique is to start with a known value of $y(t)$ and then approximate the next interval value $y(t+h)$ using a finite difference approximation to the derivative $\frac{dy}{dt}$. For a first order finite difference [28]

$$\frac{dy}{dt} \approx \frac{y^{(n+1)} - y^n}{h} = f(y^*, t^*) \Rightarrow y^{(n+1)} = y^n + h \cdot f(y^*, t^*) \quad (2.28)$$

Where $y^{(n)}$ refers to the value of y from the numerical scheme at the n -th time step. The trick is to find some appropriate values for h and $f(y^*, t^*)$ that lead to high accuracy and stability without requiring an unmanageable number function evaluations and time steps.

The techniques that we look at will also be applicable to systems no linear 1st order differential equation [28]

$$\frac{dy_i}{dt} = f_i(y_1, y_2, \dots, y_n), \text{ for } i=1, 2, \dots, N \quad (2.29)$$

Or in vector notation:

$$\frac{dy}{dt} = f(y) \quad (2.30)$$

Where y refers to the set of variables $[y_1, y_2, \dots, y_N]^T$ and f refers to the set of defining functions $[f_1, f_2, \dots, f_N]^T$. Note that a dependency on time can always be included by defining a new variable.

The most widely used fourth order method with constants developed by Gill. The method [28] is

$$y^{(n+1)} = y^{(n)} + \frac{1}{6}k_1 + \frac{b}{3}k_2 + \frac{d}{3}k_3 + \frac{1}{6}k_4 \quad (2.31)$$

$$k_1 = h \cdot f(t^{(n)}, y^{(n)}) \quad (2.32)$$

$$k_2 = h \cdot f\left(t^{(n)} + \frac{1}{2}h, y^{(n)} + \frac{1}{2}k_1\right) \quad (2.33)$$

$$k_3 = h \cdot f\left(t^{(n)} + \frac{1}{2}h, y^{(n)} + ak_1 + bk_2\right) \quad (2.34)$$

$$k_4 = h \cdot f\left(t^{(n)} + h, y^{(n)} + ck_2 + dk_3\right) \quad (2.35)$$

Where the coefficients in RKG method [28] are

$$a = \frac{\sqrt{2}-1}{2}, \quad b = \frac{2-\sqrt{2}}{2}, \quad c = -\frac{\sqrt{2}}{2}, \quad d = \frac{2+\sqrt{2}}{2} \quad (2.36)$$

It is reported that Runge-Kutta-Gill method is stable for $h \leq 2.8/\lambda$.

2.9 Conclusion

In this chapter construction, operation and mathematical model of a PMBLDC Motor are described. The mathematical model is simultaneous differential equations. The equations may be solved using RKG method in a digital computer environment. The time step is taken as 25 microsecond to have solution closer to analog system.

CHAPTER III

CONTROLLER DESIGNED BASED ON FIELD ORIENTED CURRENT VECTOR CONTROL

The Chapter at a Glance

Introduction	Section 3.1
Field Orientation Control Technique	Section 3.2
Design Fixed PI Controller	Section 3.3
Construction and Operation of Hysteresis Current Controller	Section 3.4
Field Oriented Rectangular Current Regulated Control	Section 3.5
Simulation Results for Square Wave Reference Current	Section 3.6
Sinusoidal Current Regulated Field Oriented Control	Section 3.7
Simulation Results for Sinusoidal Reference Current	Section 3.8
Conclusion	Section 3.9

3.1 Introduction

Recently, PM Brushless DC (PMBLDC) Motor drives have been introduced in Hybrid Electric Vehicles (HEVs) technology and it is gaining popularity. A Permanent Magnet Brushless DC motor is a low inertia motor and shall work effectively in high performance drives. The motor speed and torque are frequently controlled for controlling operation of various drives such as robotics, copter, hybrid-electric vehicles and similar other applications [30]. In a current fed vector controlled drive, current magnitude and their switching position should be controlled. For this purpose the applied voltages must be switched properly using the inverter switches. There may be two loops, the speed control loop and the current control loop for high performance control systems.

For vector control, Field Orientated Current (FOC) Vector Control technique is proposed in this chapter. Fixed Proportional plus Integral (PI) controller is designed based on FOC

vector control technique and parameters of PI is tuned by Ziegler- Nichols method. The effectiveness of the control scheme is tested using C++ program simulation environment.

3.2 Field Orientation Control Technique

Field Oriented Control is a high performance form of vector control. In this control system motor flux is maintained constant for nominal range of operation. The control action is implemented with the current variables and voltages are manipulated in the d-q reference frame. This requires that the measured motor currents must be mathematically transformed from the three-phase stator fixed static reference frame to the two axis synchronously rotating d-q reference frame. Then the comparators produce error from the speed loop variables and then processed by the PI controllers to generate reference current. Similarly, the voltages to be applied to the motor are transformed from the synchronously rotating d-q frame to the three phase static reference frame of the stator [11].

In Field Oriented Control, the direct and quadrature axis currents i_d and i_q are controlled to achieve the demanded torque. In a DC motor, field and torque component currents can be independently controlled by adjusting field and armature currents and the motor is controlled like a separately excited DC motor [11, 28]. In FOC three phase stator currents are identified as two orthogonal 'dq' components, where direct axis component defines magnetic flux and quadrature axis component defines torque. Field flux linkage and armature flux linkage created by respected field current and armature current (torque component) are orthogonally aligned, such that when torque is controlled, the field flux linkage is not affected. So, it gives dynamic torque response. FOC is capable to generate full torque at zero speed and has faster speed response, fast acceleration and fast deceleration [11, 28].

The direct axis component of motor current has negligible role on torque production and it needs to be maintained zero to reach maximum torque per ampere. So in field oriented controlled drives direct axis reference current component is considered zero and therefore, forces the input current vector in the quadrature axis direction. For Permanent Magnet BLDC Motor the direct axis reference current is considered zero to maximize the torque efficiency of the system [11] and in this study we consider this principle. In the proposed method rectangular shape current and sinusoidal wave current are regulated as three phase

reference current. Sinusoidal reference currents are generated by inverse Park and inverse Clarke transformation. Rectangular current shape is generated by each 60⁰ electrical commutation sequence. 60⁰ electrical commutation sequence means it's like square shape

The required [11] transformation is written as follows

1. Clarke's Transformation: (3.1)

$$i_{\alpha} = i_a$$

$$i_{\beta} = \frac{1}{\sqrt{3}}i_a + \frac{2}{\sqrt{3}}i_b$$

2. Park's Transformation: (3.2)

$$i_d = i_{\alpha} \cos \theta + i_{\beta} \sin \theta$$

$$i_q = i_{\beta} \cos \theta - i_{\alpha} \sin \theta$$

3. Inverse Park's Transformation: (3.3)

$$i_{\alpha} = i_d \cos \theta - i_q \sin \theta$$

$$i_{\beta} = i_d \sin \theta + i_q \cos \theta$$

4. Inverse Clarke's Transformation: (3.4)

$$i_a = i_{\alpha}$$

$$i_b = -\frac{1}{2}i_{\alpha} + \frac{\sqrt{3}}{2}i_{\beta}$$

$$i_c = -\frac{1}{2}i_{\alpha} - \frac{\sqrt{3}}{2}i_{\beta}$$

The magnitude of reference currents are written as

$$I_{mref} = \sqrt{i_{qref}^2 + i_{dref}^2} \quad (3.5)$$

The reference phase currents are regulated according to the following [3] equations

$$\text{When } 0 < \theta < \pi/6 \quad \begin{cases} i_{aref} = 0 \\ i_{bref} = -I_{mref} \\ i_{cref} = I_{mref} \end{cases} \quad (3.6)$$

$$\text{When } \pi/6 < \theta < \pi/2 \quad \begin{cases} i_{aref} = I_{mref} \\ i_{bref} = -I_{mref} \\ i_{cref} = 0 \end{cases} \quad (3.7)$$

$$\text{When } \pi/2 < \theta < 5\pi/6 \quad \begin{cases} i_{aref} = I_{mref} \\ i_{bref} = 0 \\ i_{cref} = -I_{mref} \end{cases} \quad (3.8)$$

$$\text{When } 5\pi/6 < \theta < 7\pi/6 \quad \begin{cases} i_{aref} = 0 \\ i_{bref} = I_{mref} \\ i_{cref} = -I_{mref} \end{cases} \quad (3.9)$$

$$\text{When } 7\pi/6 < \theta < 9\pi/6 \quad \begin{cases} i_{aref} = -I_{mref} \\ i_{bref} = I_{mref} \\ i_{cref} = 0 \end{cases} \quad (3.10)$$

$$\text{When } 9\pi/6 < \theta < 11\pi/6 \quad \begin{cases} i_{aref} = -I_{mref} \\ i_{bref} = 0 \\ i_{cref} = I_{mref} \end{cases} \quad (3.11)$$

$$\text{When } 11\pi/6 < \theta < 2\pi \quad \begin{cases} i_{aref} = 0 \\ i_{bref} = -I_{mref} \\ i_{cref} = I_{mref} \end{cases} \quad (3.12)$$

3.3 Design Fixed PI Controller

For a PMSM Motor the outer control loop is speed or position. Optical encoder or synchronous resolver is used for measuring the actual speed of the motor in an experimental set up. In complex control systems, separate position sensors may be used to get absolute position information. Computer Numeric Controlled (CNC) machines are a good example of such a control system.

In industries PI controller is widely used due to its simple structure and easy to implement nature. A PI controller tries to correct the error between a measured process variable and a desired reference point by calculating and giving corrective action to adjust the process as desired [3]. In this study the PI controller is used to process speed error in a feedback control loop with proportional and integral components processors [28]. The calculation of Fixed PI controller output is done in two separate modes the proportional mode and the integral mode. The proportional mode minimizes the settling time to gain reference speed. The integral mode reduces system oscillation. The proportional mode determines the analysis of current error and the integral mode determines the analysis based on history of error. Sum of these two modes output, gives corrective action into control section. We can implement algorithm of PI controller as [3, 28]. A limiter is put on the speed controller output depending on permissible maximum winding current.

$$e_o(t) = k_p e_i(t) + k_i \int_0^t e_i(t) dt \quad (3.13)$$

Where, K_p and K_i are the proportional and integral gains of the PI controller respectively.

$e_i(t) = \text{Desired set reference value} - \text{actual calculated value.}$

$$i_{qref} = \frac{T_{ref}}{k_t} \quad (3.14)$$

Where, T_{ref} is the reference torque and K_t is the torque constant. Since only the quadrature current produces useful torque. The P-I controller operates on quadrature current control and takes the requested torque as input. This causes the quadrature component of current to track the requested torque, as desired. So, the actual speed of the PMBLDC Motor is compared with its reference speed and the speed error is processed through PI controller to estimate reference quadrature axis current I_{qref} [3].

$$e(t) = \omega_{mref} - \omega_m \quad (3.15)$$

$$i_{qref}(t) = i_{qref}(t-1) + k_p[e(t) - e(t-1)] + k_i(t)dt \quad (3.16)$$

Where, the gains of PI speed controller K_p and K_i are needed to be tuned for obtaining the desired performance. The model of PMBLDC Motor is designed based on electrical components and mechanical elements. For symmetrical arrangement, mechanical and electrical time constant equations are written by

$$\tau_m = \sum \frac{RJ}{K_e K_t} = \frac{J \sum R}{K_e K_t} \quad (3.17)$$

$$\tau_e = \sum \frac{L}{R} = \frac{L}{\sum R} \quad (3.18)$$

Where R and L are resistance and inductance per phase, K_e and K_t are back emf and torque constant, J is rotor inertia. Therefore, the transfer function of the PMBLDC Motor is

$$G(s) = \frac{\frac{1}{K_e}}{\tau_m \tau_e s^2 + \tau_m s + 1} \quad (3.19)$$

Using the Ziegler and Nichols technique the controller constants are evaluated as [40] $k_p=2.7$; $k_i=16.2$.

3.4 Construction and Operation of Hysteresis Current Controller

In the hysteresis-type current regulator, the power transistors are switched off and on according to whether the current is greater or less than a reference current within the defined window [38]. The error is used directly to control the states of the power transistors. The hysteresis controller is used to limit the phase current within a preset hysteresis band. As the supply voltage is fixed, the result is that the switching frequency varies as the current error varies. Since the width of the tolerance band is a design parameter, this mode allows current control to be as precise as desired, but acoustic and electromagnetic noise are difficult to filter because of the varying switching frequency

[38]. The current input to the motor is controlled by delta modulation technique. The main aim of any modulation technique is to obtain variable output having a maximum fundamental component with minimum harmonics. In Delta modulated current control, the PWM is used for the switching of voltage source inverter. This hysteresis-band PWM is basically an instantaneous feedback current control method of PWM where the actual current continually tracks the reference current. When the current exceeds upper band limit, then the upper switch has to be off and lower switch has to be on. Similarly when the current exceeds lower band limit, upper switch is on and lower switch is off. Switch No 1, 3, 5 are considered as upper switches and Switch No 4, 6, 2 are considered as lower switches respectively of the inverter [38, 28].

The switching logic which is operated based on the following conditions [3].

$$\text{If } i_a < (i_{aref} - h_b)$$

Then switch 1 is ON and switch 4 is OFF ($S_A = 1$)

$$\text{If } i_a > (i_{aref} + h_b)$$

Then switch 1 is OFF and switch 4 is ON ($S_A = 0$)

$$\text{If } i_b < (i_{bref} - h_b)$$

Then switch 3 is ON and switch 6 is OFF ($S_B = 1$)

$$\text{If } i_b > (i_{bref} + h_b)$$

Then switch 3 is OFF and switch 6 is ON ($S_B = 0$)

$$\text{If } i_c < (i_{cref} - h_b)$$

Then switch 5 is ON and switch 2 is OFF ($S_C = 1$)

$$\text{If } i_c > (i_{cref} + h_b)$$

Then switch 5 is OFF and switch 2 is ON ($S_C = 0$)

Here, h_b is the hysteresis band around reference current. The inverter output voltage according to the above switching conditions are given [3] below,

$$V_a = \frac{1}{3} [2S_A - S_B - S_C]$$

$$V_b = \frac{1}{3} [-S_A + 2S_B - S_C]$$

$$V_c = \frac{1}{3} [-S_A - S_B + 2S_C]$$

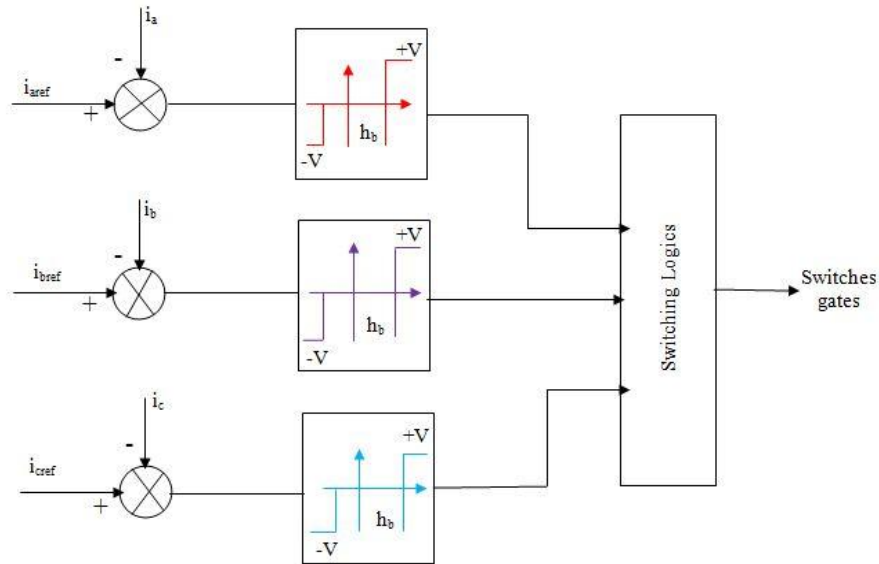


Fig.3.1: Structure of Hysteresis Current Controller

3.5 Field Oriented Rectangular Current Regulated Control

The proposed Field Oriented Rectangular Current Regulated (FORCR) Control consists of following elements: PM Brushless DC Motor, delta modulated pulse width modulated current controller, IGBT based current controlled voltage source inverter (CC-VSI), Fixed PI speed controller and square wave reference current generator. The block diagram of Field Oriented Rectangular Current Regulated Control of PM Brushless DC Motor is shown in Fig.3.2.

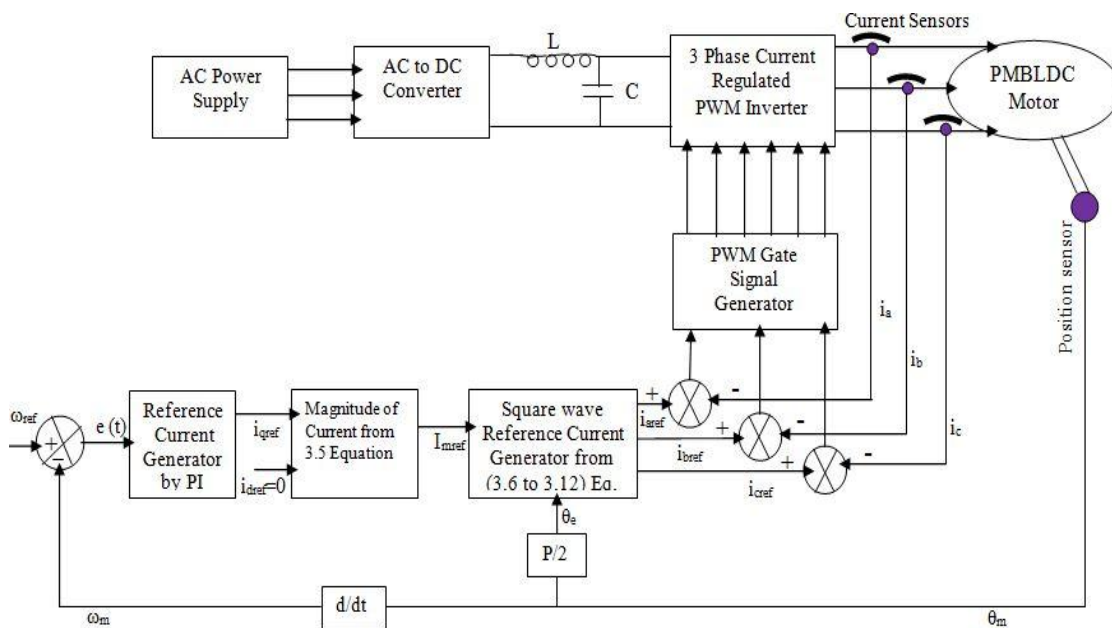


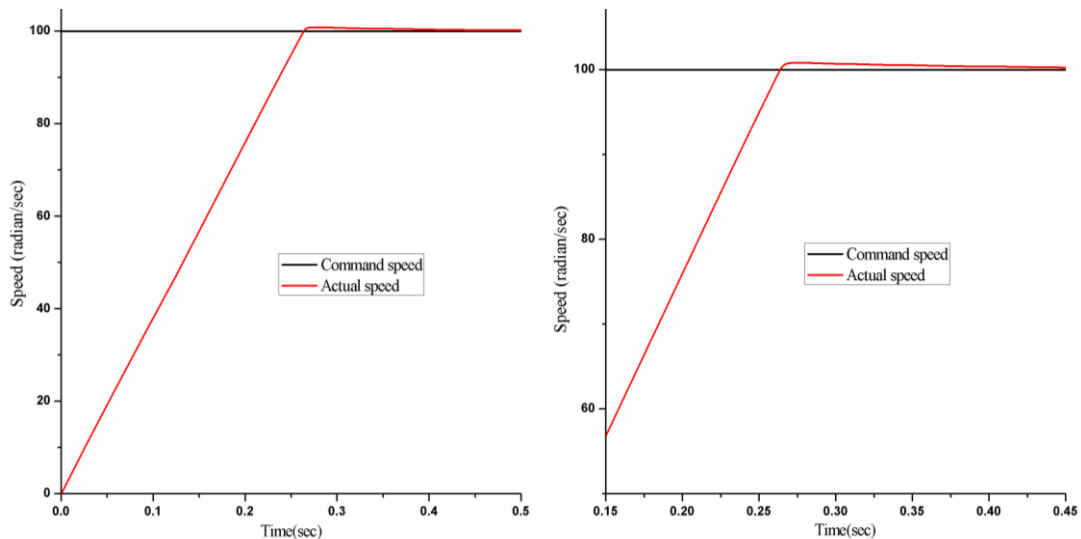
Fig.3.2: Block diagram of Field Oriented Rectangular Current Regulated Control with PM Brushless DC Motor

The reference direct axis current i_{dref} is assumed zero to generate maximum torque efficiency. The reference quadrature axis current i_{qref} is determined according to the requested load torque through the constant PI controller from speed error using Equation (3.16). The magnitude of reference currents are obtained using Equation (3.5). The square wave shape of reference currents are generated using Equation (3.6-3.12). Three phase reference currents are compared with the actual currents for voltage vector generation using delta modulation and the inverter switches are turned off or on according to a hysteresis controller which is discussed in the previous section.

3.6 Simulation Results for Square Wave Reference Current

For fixed PI control system field oriented controlled current fed PMLD motor drive has been simulated in C++ program. The sampling time used for this simulation is 0.0000025 second. The specifications of motor parameters are given in Appendix A.

The drive system was started from rest condition with load torque 1.0 N-m and command speed 100 radian per sec. Speed characteristic is shown in Fig.3.3. It is observed that motor reaches its set speed within 0.26 sec. But it has 1.3% over shoot and actual speed catch up command speed near about 0.35 sec. The back emf variations at starting and steady state conditions are given in Fig.3.4.

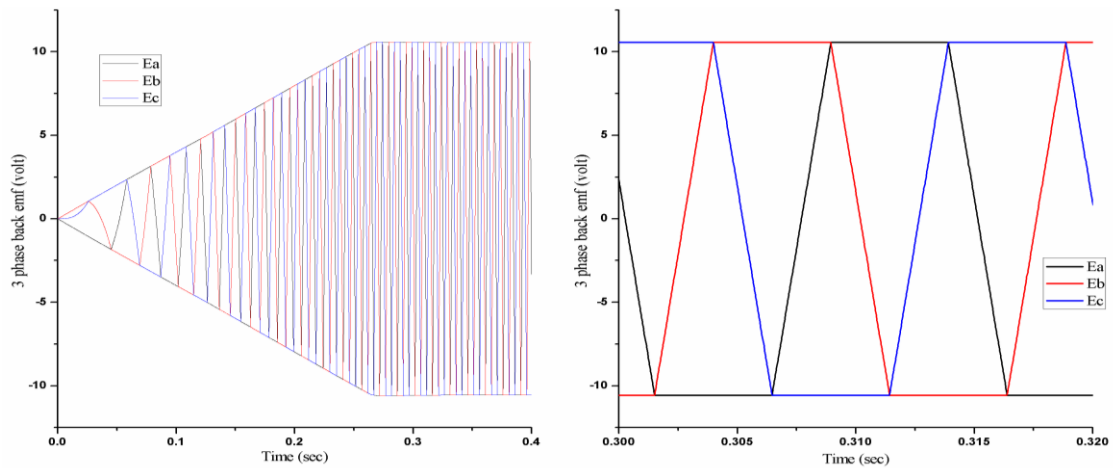


(a) Speed characteristic at starting

(b) Zoomed Speed response

Fig.3.3: Speed characteristic is represented for field oriented rectangular current regulated control

It is seen that initial back emfs are zero because at starting actual speed is zero. Gradually, back emfs are increased with the increment of speed. When actual speed reaches to command speed, actual speed remains constant and back emfs also remain constant. As field pattern of PMSM motor is trapezoidal shape, motor induced back emfs will be trapezoidal shape. It is shown in Fig.3.4 for starting condition.



(a) Back emfs at starting

(b) Back emfs zoomed in steady state condition

Fig.3.4: Back emf variation with field oriented rectangular current regulated control PMSM motor

At steady state condition, three phase voltage is plotted in Fig.3.5 and it is seen that phase voltage is changed as smoothly. Rotor angle varies from 0 to 6.28 radian in Fig.3.6. As the initial speed is very low, it takes more time to reach 2π radian. Near about after 0.26 sec, rotor angle variation is changed frequently.

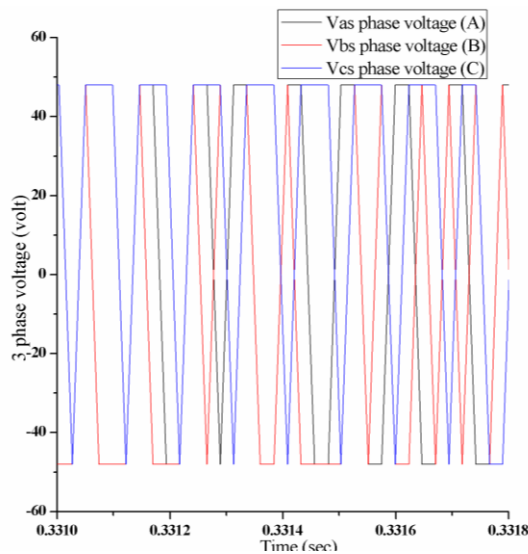


Fig.3.5: Shows three phase voltage

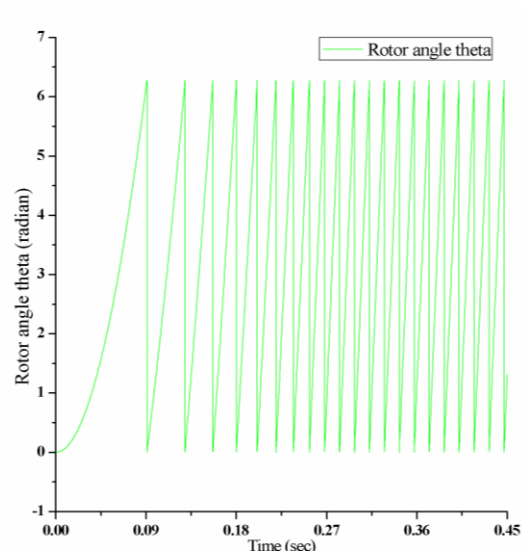


Fig.3.6: Rotor angle variation

During starting condition, motor draws rated current before reaching desired speed. At desired speed, current level decreases according to demand load torque. In field oriented control this current is defined reference quadrature axis current. Developed torque follows load torque when motor reaches the command speed. Quadrature axis current and developed torque are depicted in Fig.3.7 (a) and Fig.3.7 (b).

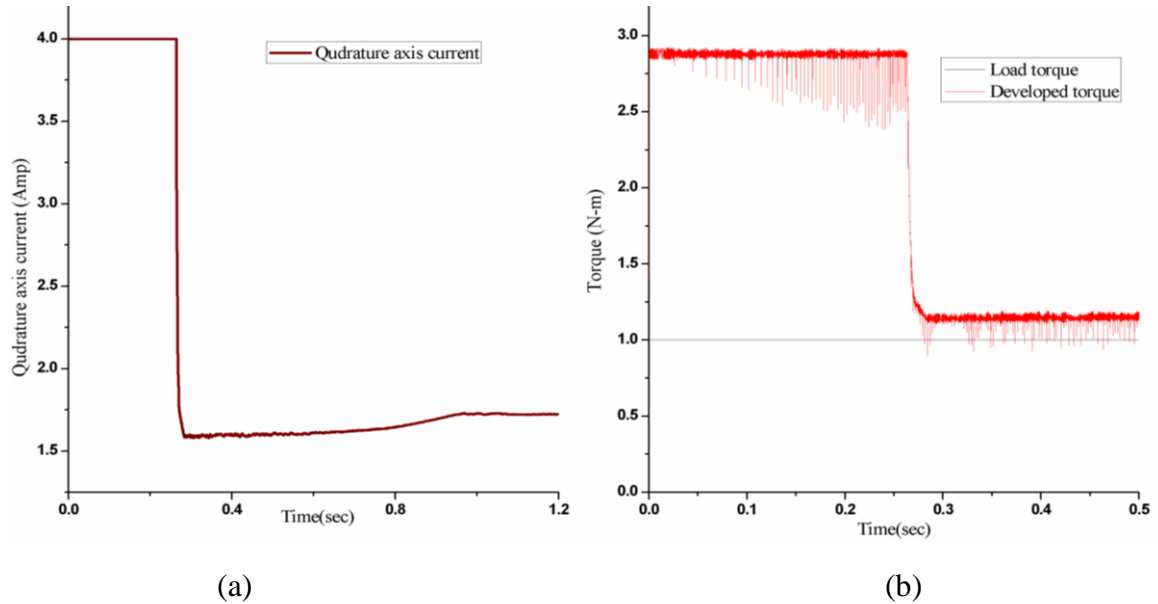


Fig.3.7: Shows (a) quadrature axis current and (b) developed torque response

During starting condition when speed is raising maximum current flows but it does not exceed 4 Amp due to current limiter. After 0.26 second when motor reaches the desired speed, level of current decreases as shown in Fig.3.8.

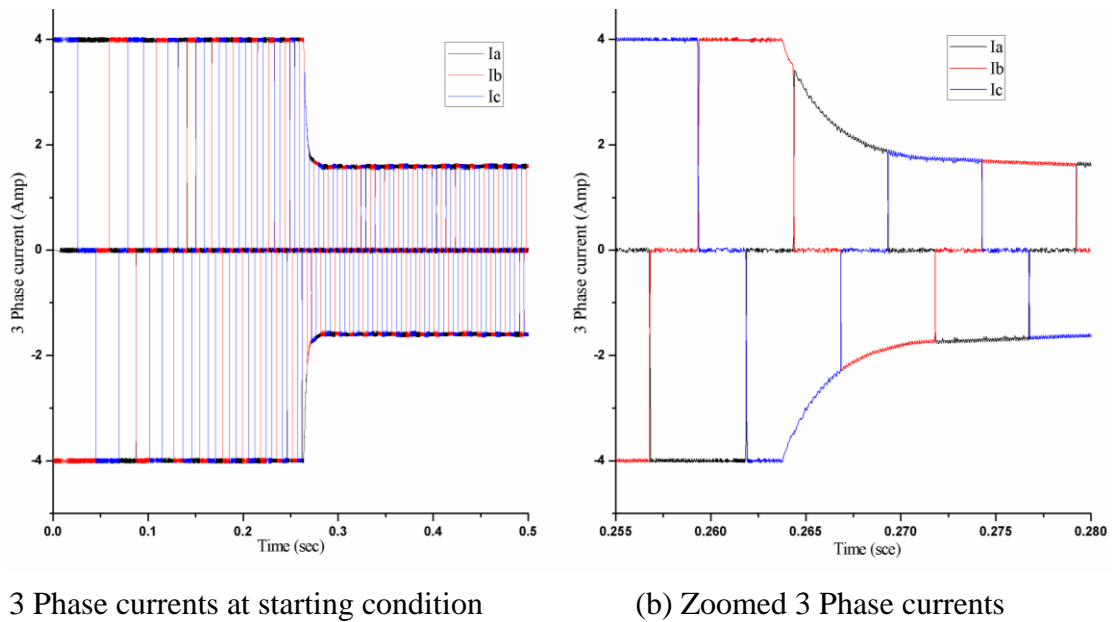


Fig.3.8: 3-Phase currents represented for field oriented (rectangular current) regulated control

3.7 Sinusoidal Current Regulated Field Oriented Control

The proposed method has following elements: PM Brushless DC Motor, delta modulated pulse width modulated current controller, IGBT based current controlled voltage source inverter (CC-VSI), Fixed PI speed controller and sinusoidal reference current generator. The current vector is adjusted by generating the reference current vector from torque component current from speed error and rotor position information. The reference phase currents are assumed to be sinusoidal and obtained from inverse Park and inverse Clarke transformation. Reference three phase currents are compared with the actual currents for voltage vector generation using delta modulation and the inverter switches are turned off or on according to a hysteresis controller.

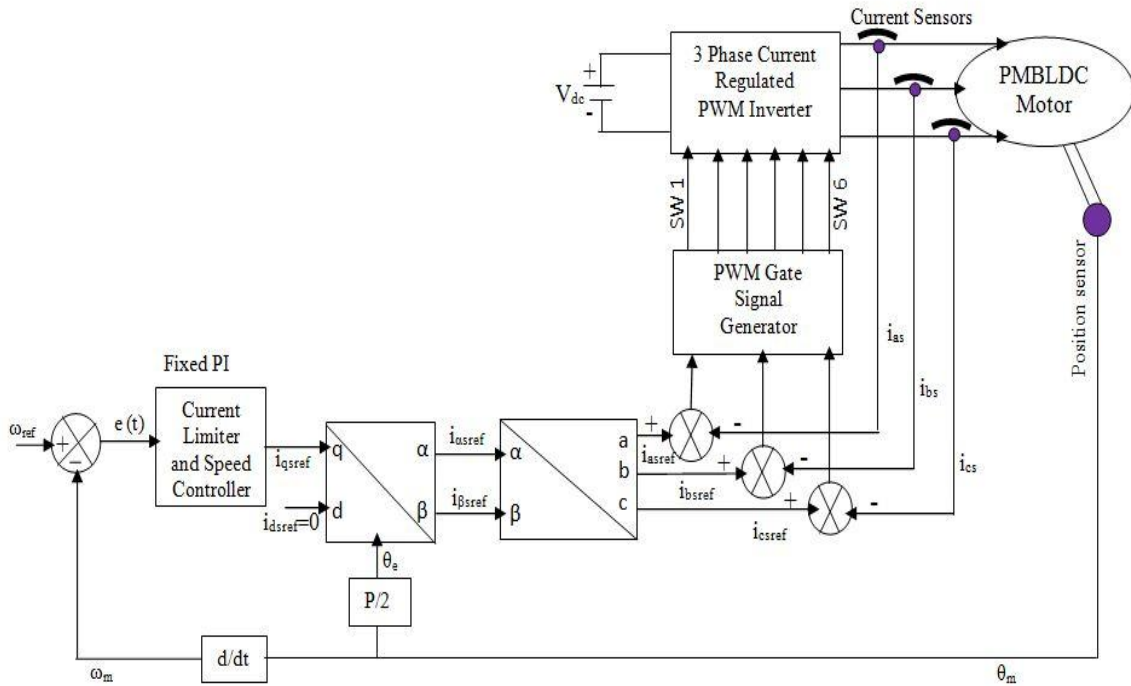


Fig.3.9: Block diagram of sinusoidal current regulated field oriented control with PMBLDC motor

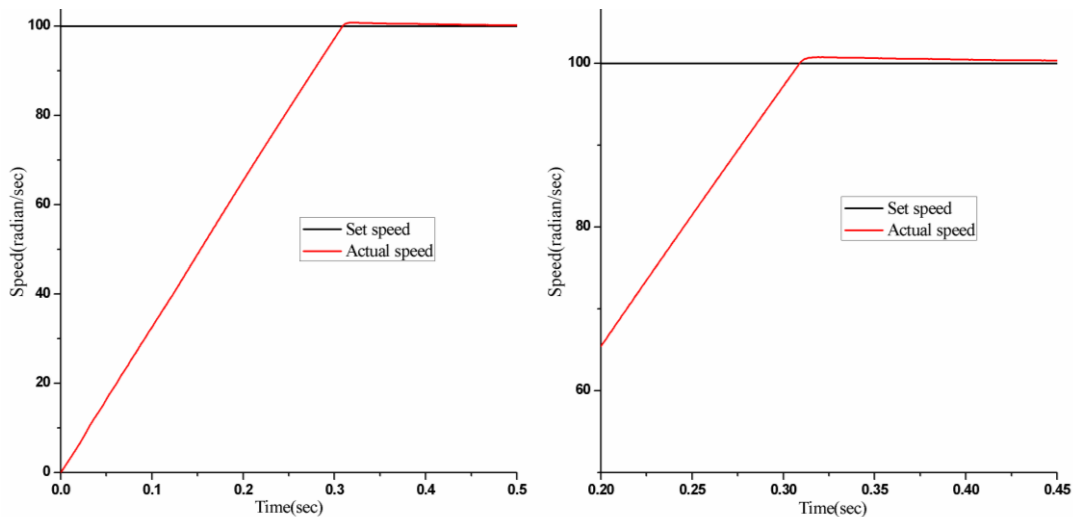
The block diagram of sinusoidal current regulated field oriented control of PMBLDC Motor is showed in Fig.3.9 In proposed control systems, three phase reference currents are generated by considering reference direct axis current $i_{dref} = 0$ and by calculating value of reference quadrature axis current i_{qref} according to the requested load torque through the fixed PI controller from speed error using Equation (3.16). At first, the currents in rotating

d-q reference frame are transformed to two-axis orthogonal stationary α - β reference frame by using Inverse Park transformation using Equation (3.3). Then Inverse Clarke transformation is applied to generate three phase reference current in 'abc' frame using Equation (3.4).

3.8 Simulation Results for Sinusoidal Reference Current

A C++ program code is written for sinusoidal current regulated field oriented based fixed PI control system. The performance of the drive system is studied based on computer simulation. Motor parameters are given in Appendix A.

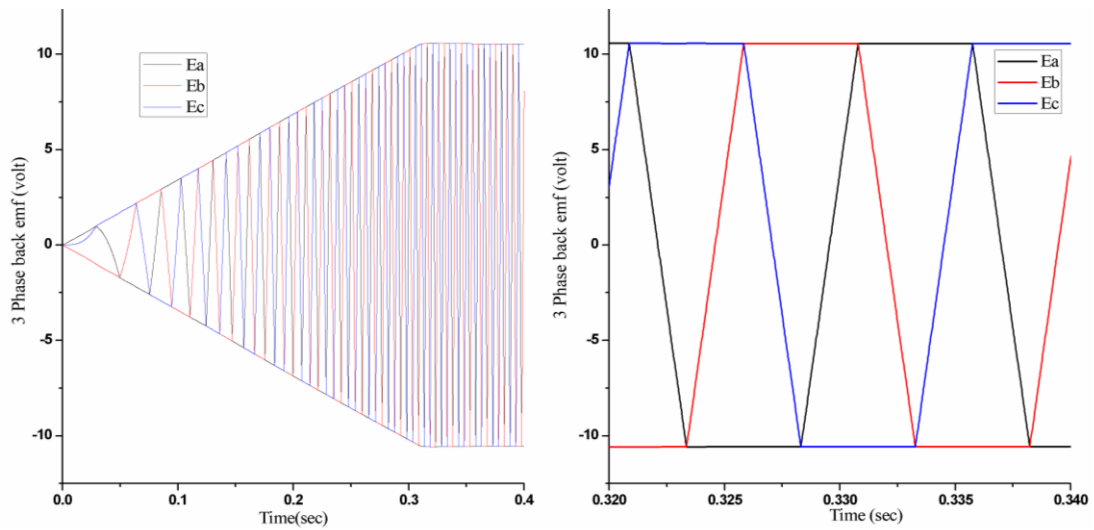
Starting speed characteristics i.e. time taken by the motor to reach its set speed 100 radian per second with its initial torque 1.0 Nm for the propose technique of PMBLDC motor drives is shown in Fig. 3.10 From this graph, it is seen that, PMBLDC field oriented control drive takes 0.31 seconds to gain set speed. But it has 1.3% over shoot and actual speed catch up set speed near about 0.40 sec. At starting back EMF is zero caused initial motor speed is zero that is shown in Fig. 3.11 (a). But when motor reaches set speed, back EMF becomes trapezoidal shape as shown in Fig. 3.11 (b).



(a) Speed characteristic in transient time

(b) Zoomed Speed characteristic

Fig.3.10: Speed characteristic is represented for sinusoidal current regulated field oriented control



(a) Three phase back emfs at starting condition (b) 3 phase back emf zoomed
 Fig.3.11: Back emf variation is shown for sinusoidal current regulated field oriented control

Single phase back emf is illustrated in Fig.3.12. Rotor position varies from 0 to 6.28 radian in Fig.3.13. As the initial speed is very low it takes more time to reach 2π radian. Near about 0.31 sec later, rotor position is changed frequently according to set speed.

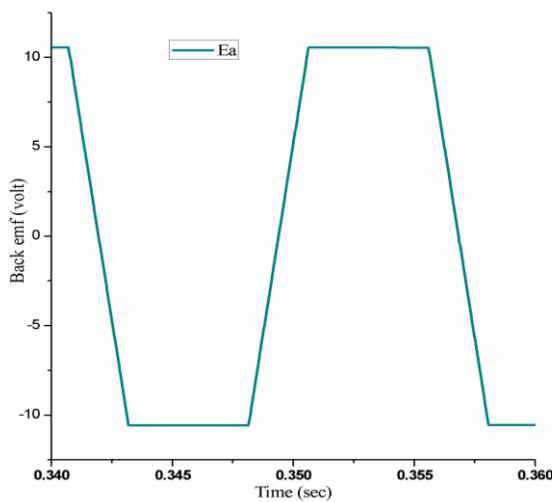


Fig.3.12: Single phase back emf

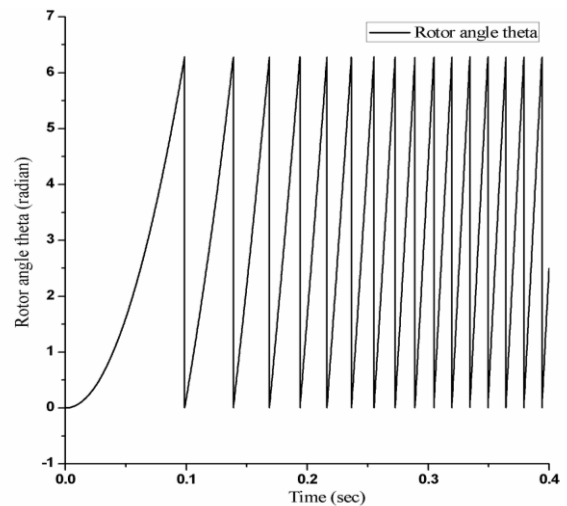


Fig.3.13: Rotor position at starting condition

Fig.3.14 and Fig.3.15 show quadrature axis current and torque response curve respectively. Here by proposed controller the quadrature axis current and the developed torque are controlled almost 0.31 sec. Developed torque and I_{qr} show maximum when motor speed is behind the set speed. I_{qr} and developed torque are decreased having oscillation when motor reaches the set speed

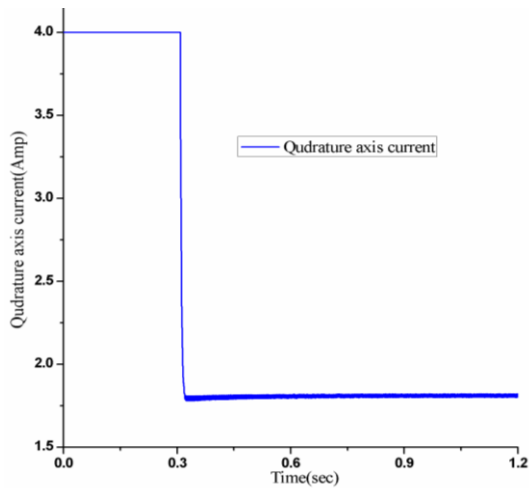


Fig.3.14: Quadrature axis current response

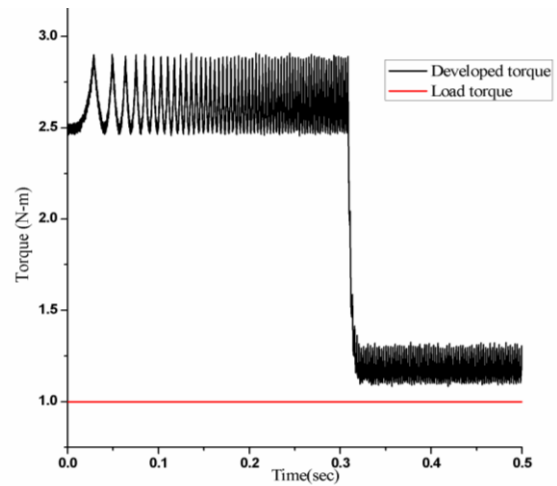


Fig.3.15: Developed torque response

Phase current of PM Brushless DC Motor at the time of starting for sinusoidal current regulated field oriented control is depicted in Fig. 3.16. It shows that the amplitude of 3-phase current is 4 Amp (rated current of the motor) at the transient time. Started current is limited through the current limiter. Fig. 3.16 also describes that after gaining set speed i.e. at stable condition motor takes 1.8 Amp current when $I_{dr}=0.0$.

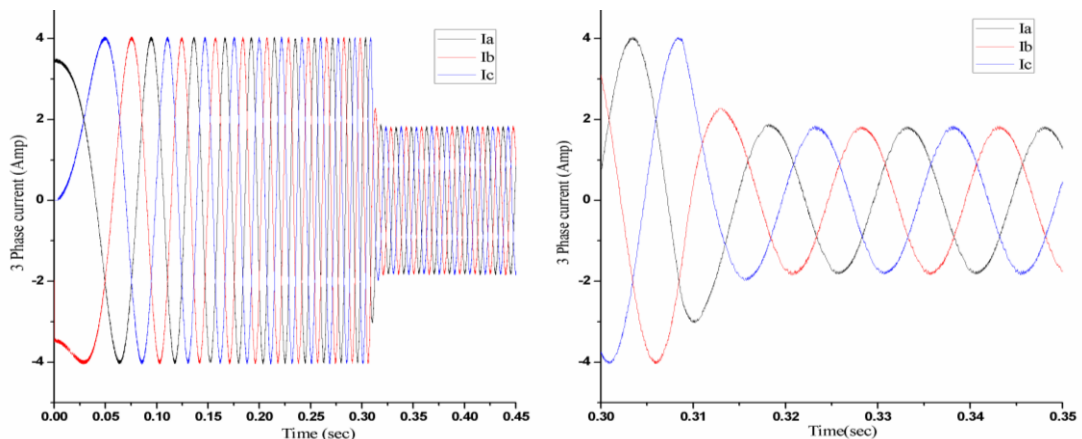


Fig. 3.16: Three phase Currents is showed for sinusoidal current regulated field oriented control

3.9 Conclusion

In this chapter current regulated based filed oriented controlled PM Brushless DC Motor is proposed .It is noticed that drive systems work effectively. The performance is better in rectangular current regulated FO control as it can reach desired speed firstly than Sinusoidal Current Regulated Control considering same fixed PI controller. So, the rectangular Current Regulated FO control has better speed response. It is also seen that it has better torque control capability.

CHAPTER IV

SINGLE NEURON BASED ADAPTIVE CONTROLLER OF PMSBLDC MOTOR

The Chapter at a Glance

Introduction	Section 4.1
Structure of Single Neuron	Section 4.2
Single Neuron based Adaptive Controller with Adaptive Law	Section 4.3
Simulation Results	Section 4.4
Conclusion	Section 4.5

4.1 Introduction

In this chapter, single neuron based adaptive controller is proposed replacement of conventional PI or PID controller because of their intelligence, non linearity and multi variables nature. PI or PID controller works effectively based on linear control theory in industrial plant, hence this controller is easy to implement. If plant parameters are changed due to any disturbance the controller parameters require to be retuned to gain desired performance. But single neuron based controller can provide satisfactory performance under any fault and this controller works based on neural network control theory. Recently, a lot of research work is going on artificial neural network for the advancement of ANN. The adaptation rule is implemented using artificial neural network theory [37].

Fed field oriented control of PMSBLDC Motor drive is a convenient technique for the motor control. A hysteresis type current controller is also proposed and implemented in previous chapter. This study proposes a mathematical model of single neuron based adaptive controller that is simulated in a C++ environment.

4.2 Structure of Single Neuron

A basic unit of neuron network is known as single neuron and this structure is illustrated in Fig.4.1. Here are three basic element of a neuron such as weights, summing function and activation function. Interconnected weights are marked as w_1 , w_2 and w_n . Input signals are

specified as z_1, z_2 and z_n . In this section output and threshold are considered as y and b respectively

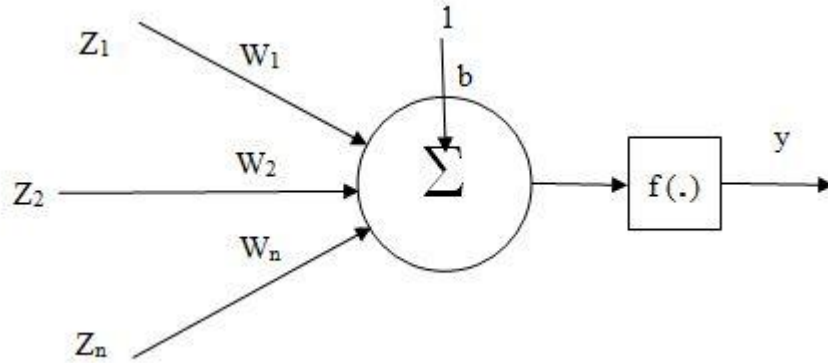


Fig.4.1: Basic structure of Single Neuron

4.3 Single Neuron based Adaptive Controller with Adaptive Law

In this section we will introduce a single neuron based controller for controlling the PMBLDC Motor. The controller is more versatile and robust [37]. It uses nonlinear excitation function for the neuron. The single neuron based adaptive controller with PMBLDC Motor is shown in Fig.4.2. The controller can be used for systems with unknown parameters. Here, [37] the inputs of the controller are

$$X_1(k) = e(k) - e(k - 1) \quad (4.1)$$

$$X_2(k) = e(k) \quad (4.2)$$

$$X_3(k) = e(k) - 2e(k - 1) + e(k - 2) \quad (4.3)$$

Where, $e(k) = \omega_{mref} - \omega_m$

These variables are multiplied by the corresponding weights to produce summation function I as [37]

$$I = \sum_{i=1}^3 X_i(k)w_i(k) \quad (4.4)$$

Using the Hebbian rule, the weights are changed by a value Δw_i as follows

$$\Delta w_i(k) = \eta_i X_i(k)e(k)u(k) \quad (4.5)$$

Where η is learning rate and $i=1, 2, 3$

The new values of the weights are obtained using the following equations [37].

$$w_i'(k) = w_i(k) + \Delta w_i(k) \quad (4.6)$$

The updated weights are obtained now normalizing the values

$$w_i(k) = \frac{w_i'(k)}{\|\sum_{i=1}^3 w_i(k)\|} \quad (4.7)$$

The activation function is hyperbolic tangent and is written as

$$\phi(I) = A_{max} \frac{1-e^{-I}}{1+e^{-I}} \quad (4.8)$$

The output of the single neuron controller is given by [37]

$$u(k) = u(k-1) + \phi(I) \quad (4.9)$$

For $k=1, 2, 3 \dots$ Output of this controller is equal to i_{qref} which is input to the PMBLDC Motor.

The proposed controller can be summarized as follows assuming initial values of $\eta_1=1.4$, $\eta_2=10.4$, $\eta_3=5.12$, $w'_1=0.1$, $w'_2=0.1$, $w'_3=0.1$ and $A_{max}=4.0$. Error $e(k)$ is computed as the difference between set speed and actual motor speed. The values of $x_1(k)$, $x_2(k)$, $x_3(k)$ are obtained from equations 4.1 to 4.3. Output of controller is computed by $u(k-1)$ plus equation 4.8. New values of w'_1 , w'_2 , w'_3 are obtained by using equations 4.5 to 4.7.

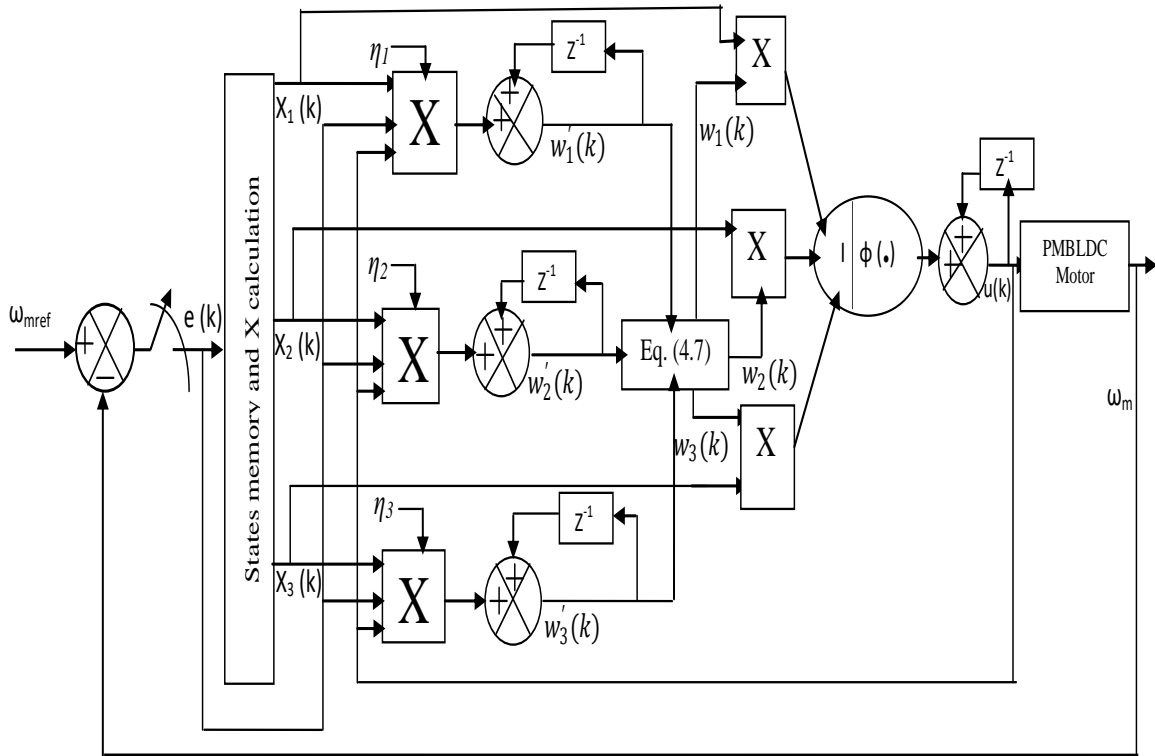


Fig.4.2: Block diagram of Proposed Single Neuron based Adaptive Controller with PMBLDC Motor

The reference direct axis current $i_{d\ ref}$ is considered zero for field oriented control. The reference quadrature axis current $i_{q\ ref}$ is calculated according to the demanded load torque through the single neuron based adaptive controller from using Equation 4.9. The magnitude of reference currents are obtained using Equation 3.5. The square wave shapes

of reference currents are generated using Equation (3.6-3.12). For rectangular type reference three phase currents are compared with the actual currents for proper voltage vector generation using delta modulation and the inverter switches are turned off or on according to a hysteresis controller as discussed in chapter. The construction and operation of hysteresis controller are discussed before in chapter three.

4.4 Simulation Results

A C++ program code is developed for Single Neuron based Adaptive Controller of PM Brushless DC Motor for computer simulation. Effectiveness of the drive system is studied. Name plate data of PM Brushless DC Motor is given in Appendix A.

At the time starting, the initial load torque on the PM Brushless DC motor is 1.0 Nm. From Fig. 4.3, it is seen that, PMBLDC Motor takes 0.26 second for the proposed single neuron based adaptive controller drive to gain desired speed 100 radian per second. No appreciable overshoot or undershoot is noticed in the actual motor speed. Fig. 4.4 shows how the value of the activation function is decreased from 4.0 to near about zero values to adjust speed. Before reaching desired speed, reference quadrature axis current (I_{qr}) is obtained rated current of 4.0 Amp in Fig.4.5. I_{qr} is controlled at 0.26 second having spikes and oscillation for the load torque 1.0 N-m. Fig.4.6 shows response of updated weights for Single Neuron based Adaptive Controller. It is observed that three weights are updated in order to adjust motor speed.

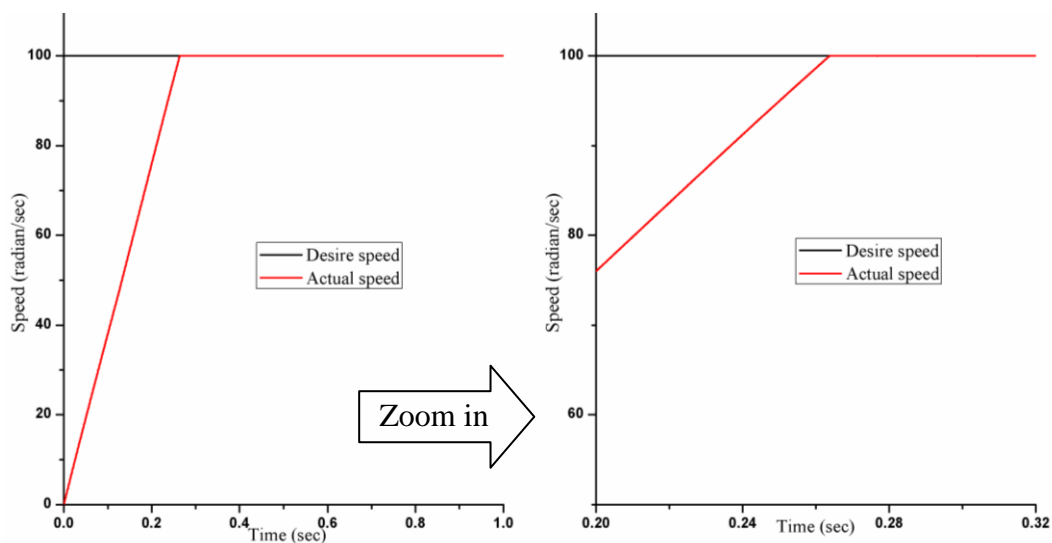


Fig.4.3: Speed characteristic for Single Neuron based Adaptive Controller

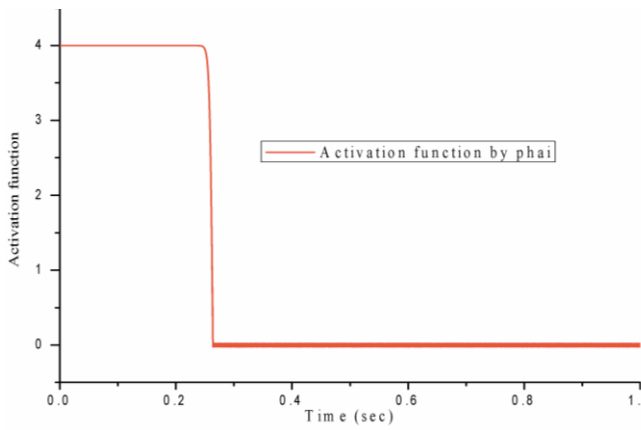


Fig.4.4: Activation function

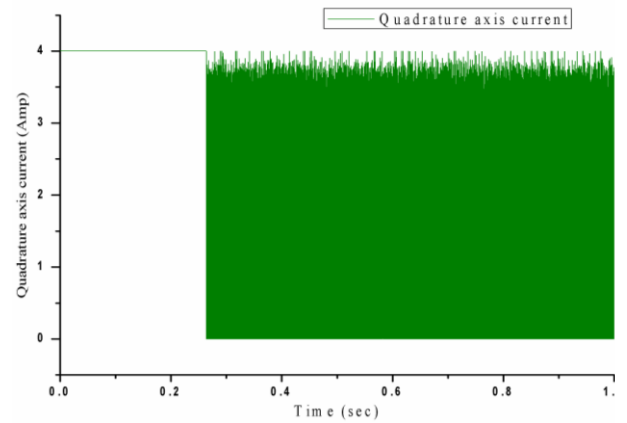
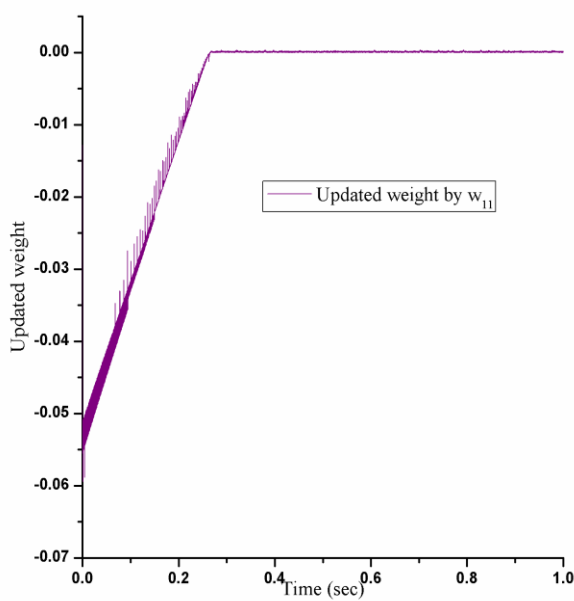
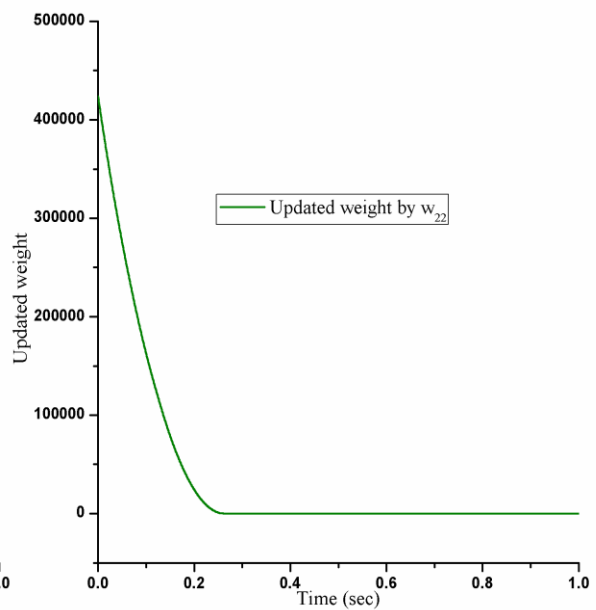


Fig.4.5: Response of quadrature axis current

The weight of w_{11} is increased from -0.055 to 0.00 in Fig.4.6 (a) and weight of w_{22} is decreased from 425000 to 0.0 in Fig.4.6 (b) at the time 0.26 sec when speed error is minimized and motor settles to constant speed of 100 rad/sec. Initially weight of w_{33} varies between 0.020 and -0.020 in Fig.4.7 when speed error is large. Gradually variation of weight is decreases to 0.0 values to minimize speed error when motor reaches desire speed.



(a)



(b)

Fig.4.6: Update weights are displayed for Single Neuron based Adaptive Controller

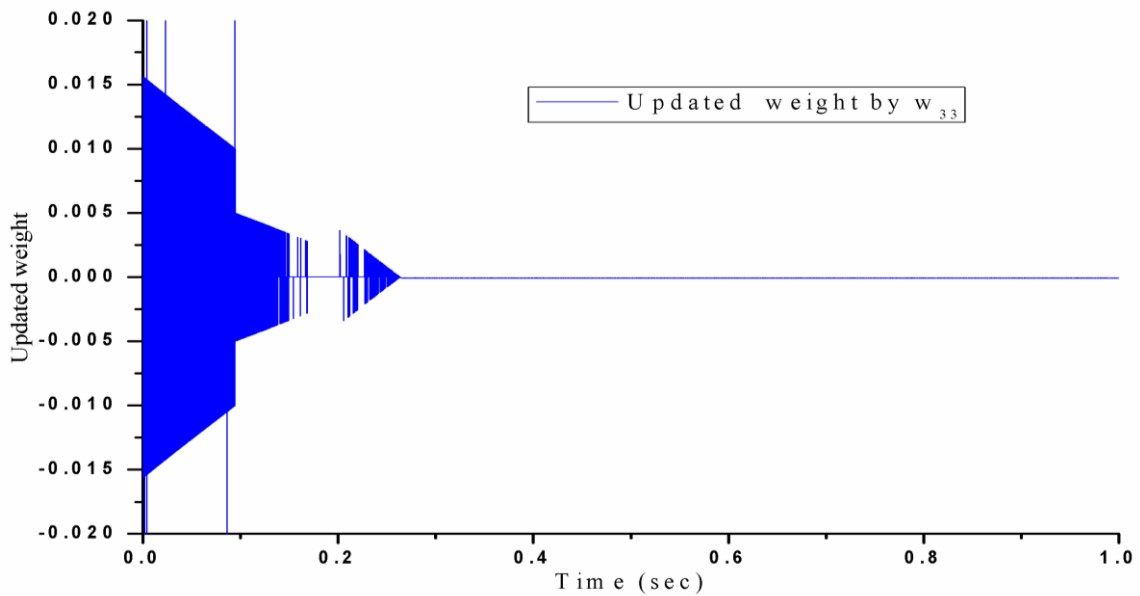


Fig.4.7: Update weights are displayed for Single Neuron based Adaptive Controller

The developed torque is depicted in Fig.4.8 for load torque 1.0 N-m at starting condition. From this figure, it is noticed that developed torque is maximum when actual motor speed is less than the reference speed as the motor is started from standstill condition. When the motor reaches the desired speed developed torque is decreased to 2.7 N-m. Developed torque is controlled as well the motor reaches to set speed is the indication of fastness of the controller.

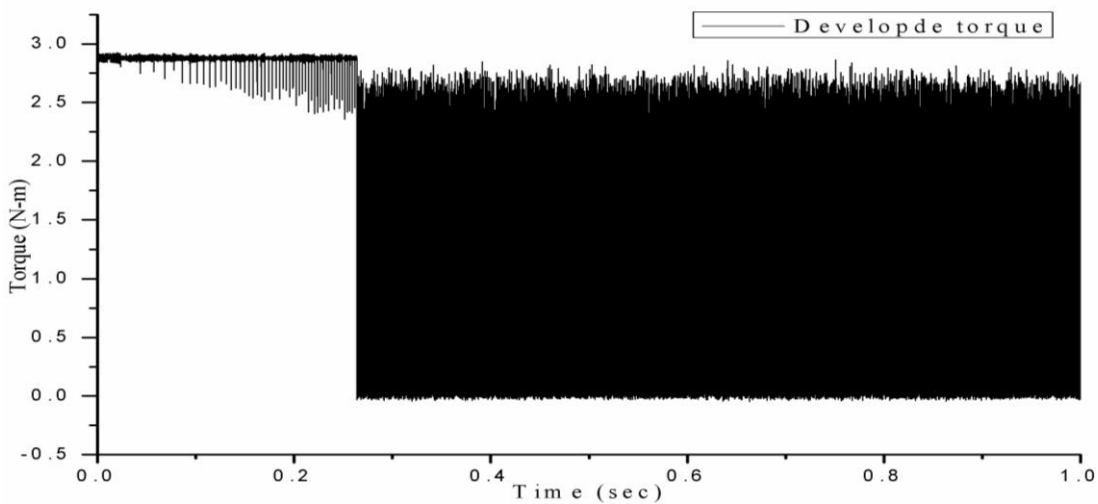


Fig.4.8: Developed torque for Single Neuron based Adaptive Controller

It is seen that initially induce back emf is zero as shown in Fig.4.9 (a) when motor speed behind the desire speed. When motor reaches desire speed back emf is set as remain constant. Trapezoidal back emf is illustrated in Fig.4.9 (b).

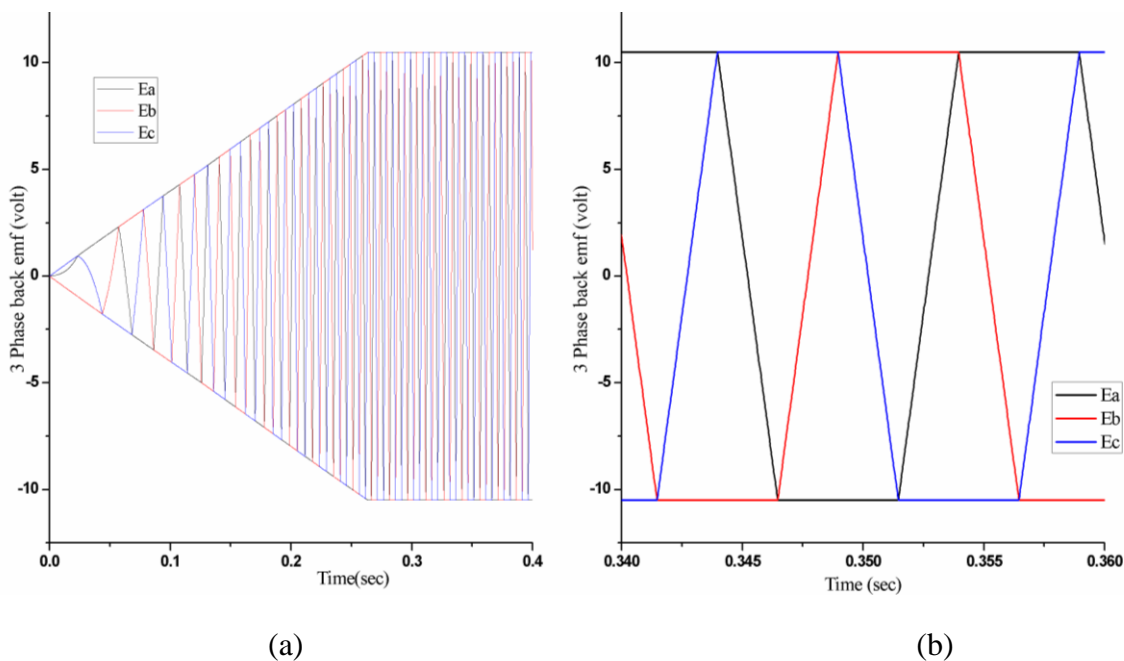


Fig.4.9: Illustration of three phase back emf with nature of trapezoidal back emf

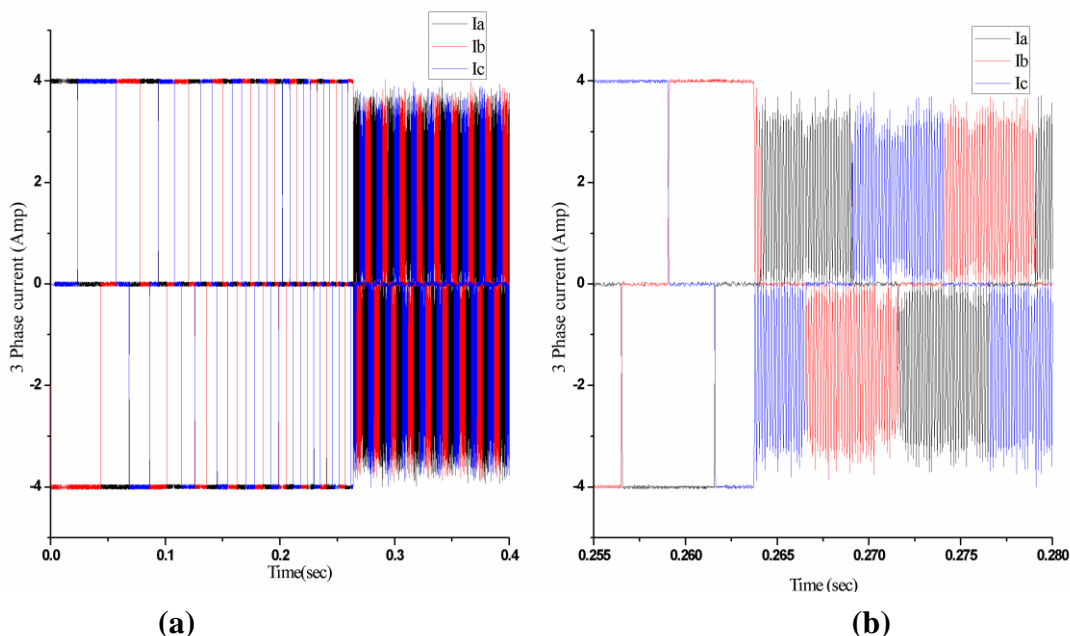


Fig.4.10: 3 phase current of single neuron based adaptive controller

Fig.4.10 (a) displays three phase current and this current is zooming in Fig.4.10 (b). But phase current is controlled according to load torque by single neuron based controller.

At starting condition three phase voltage are depicted in Fig.4.11. From this Figure, it is seen that controller output voltages are controlled as well according to dc input voltage of 48 volt.

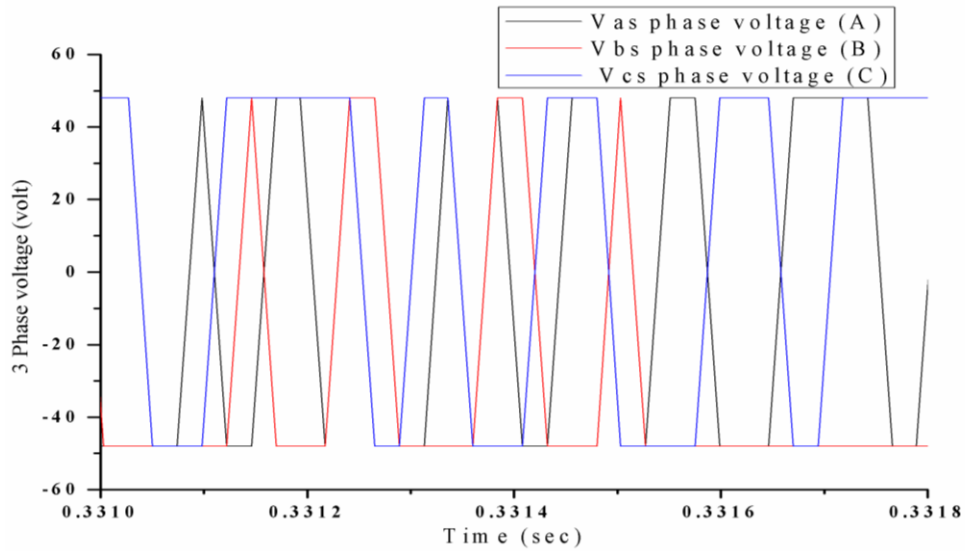


Fig.4.11: Three phases voltage for Single Neuron based Adaptive Controller

4.5 Conclusion

In this chapter a single neuron based adaptive controller was designed and its performance was tested through simulations. From this simulation it is seen that all weights are updated precisely according to desired speed and requested load torque. In this study no appreciable overshoot or undershoot is noticed in the actual motor speed and having fast speed response.

CHAPTER V

DESIGN OF SINGLE NEURON BASED ADAPTIVE PID CONTROLLER AND SPEED ESTIMATOR FOR PMBLDC MOTOR

The Chapter at a Glance

Introduction	Section 5.1
The Basic Principle of Auto tuning	Section 5.2
Tuning Algorithm of PID gains by SN estimator	Section 5.3
Simulation Results	Section 5.4
Conclusion	Section 5.5

5.1 Introduction

From the previous chapter it is evident that single neuron can be used for PID controller design. In general, PID controllers are designed on the basis of Ziegler-Nichols or Cohen-Coon methods. However, these controller constants need to be tuned for parameter or environment changes. In recent years, neural networks or Fuzzy logic systems are used to adjust the constants of PID controller. Neural networks have powerful learning and adaptation capabilities. Gradient of input-output changes behavior is essential for adaptation by neural networks. But it is very difficult to evaluate the value in all cases. Sometimes estimates of the partial derivatives are considered. In this chapter we will propose to apply single neuron based auto-tuned controller and speed estimator for a PMBLDC Motor drive system.

5.2 The Basic Principle of Auto-tuning

The basic structure of an auto-tuning neuron is shown in Fig.5.1. In it I is the external input and ϕ is the adjustable bias then [32].

$$net = I - \phi \quad (5.1)$$

Output of the system can be defined as

$$O = h(net) = \frac{a[1 - \exp(-b.net)]}{[1 + \exp(-b.net)]} \quad (5.2)$$

Where, $h(\cdot)$ is modified hyperbolic tangent function. a is saturated level and b is slope of this function.

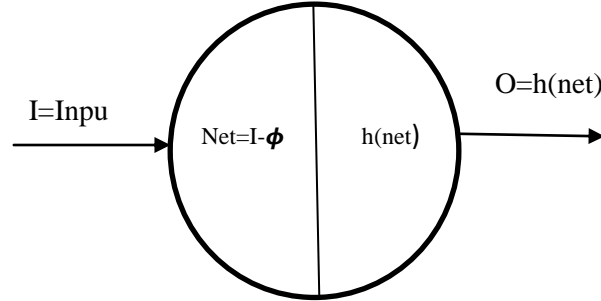


Fig. 5.1: Basic structure of an auto tuning neuron

The errors in speed to be processed by controllers are given below [32] in the Fig. 5.2.

$$X_1(k) = \omega_{mref}(k) - \omega_m(k) \quad (5.3)$$

$$X_2(k) = X_2(k-1) + X_1(k)dt \quad (5.4)$$

$$X_3(k) = \{X_1(k) - X_1(k-1)\}/dt \quad (5.5)$$

For this system in Fig 5.2, if u is external input to SNE and ϕ is adjustable bias, now we can write the following equation from eq. (5.1) $net=u-\phi$ (5.6)

The estimated output of this system is obtained as follows according to equation (5.2) [32]

$$\hat{y} = h(net) = \frac{a[1-\exp(-b.net)]}{[1+\exp(-b.net)]} \quad (5.7)$$

Model reference adaptive system works based on MIT rule to update control parameters and adjustable parameters of SNE. For MIT rule, the cost function is defined as

$$E(\theta) = \frac{e^2}{2} \quad (5.8)$$

Where, θ is vector of adjustable parameters and e is error signal. In order to make e small, according to MIT rule is to update θ in the negative gradient direction of E which is given below [32].

$$\theta' = -\eta \frac{\partial E}{\partial \theta} = -\eta e \frac{\partial e}{\partial \theta} \quad (5.9)$$

Here, $\eta > 0$ is called as the tuning rate and $\partial e / \partial \theta$ is sensitivity factor. If the desired output is y_d and actual output of motor is y then the error signal is written as $e = y_d - y$ (5.10)

If estimated output is \hat{y} then estimated error can be written, $\hat{e} = y - \hat{y}$ (5.11)

We consider another cost function for estimated error [32]

$$\hat{E}(\hat{\theta}) = 2^{-1}(y - \hat{y})^2 = 2^{-1}(\hat{e})^2 \quad (5.12)$$

Here, $\hat{\theta}$ is updated by MIT rule, so that \hat{E} is minimized, $\dot{\hat{\theta}} = -\hat{\eta} \frac{\partial \hat{E}}{\partial \hat{\theta}} = -\hat{\eta} \hat{e} \frac{\partial \hat{e}}{\partial \hat{\theta}}$ (5.13)

In this study y_d is reference speed, y is actual speed and \hat{y} is estimated speed of the motor. For the single neuron estimator, let $\hat{\theta}_i = [K_p, K_i, K_d]^T = [\theta_1, \theta_2, \theta_3]^T$ is the vector of three PID control gains and $\hat{\theta}_i = [\phi, a, b]^T$ is the vector of three adjustable parameters of SNE. The control structure of the proposed system is shown below in Fig. 5.2 [32].

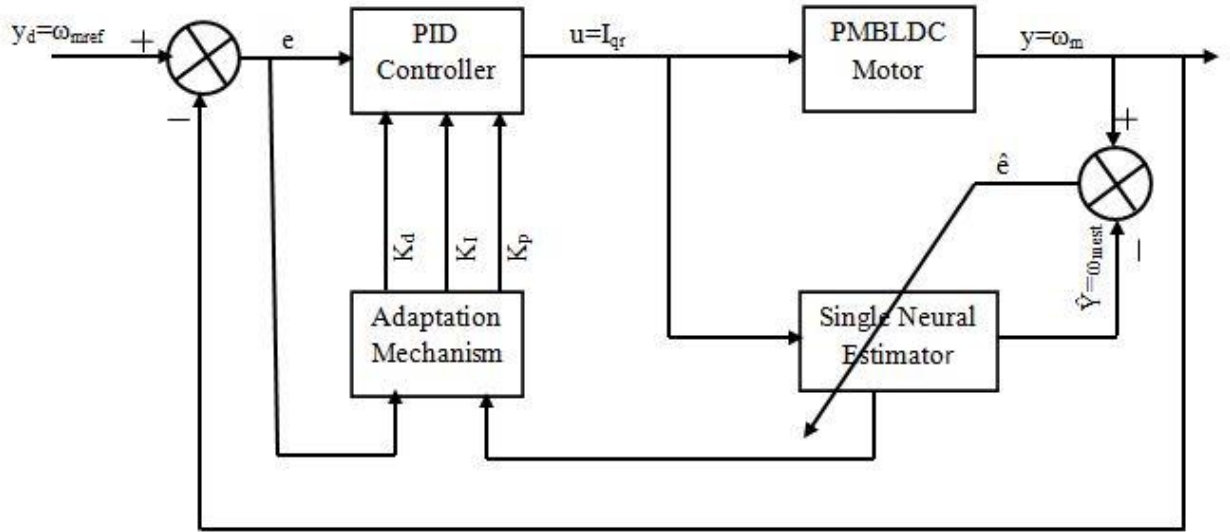


Fig. 5.2: Block Diagram for Tuning Algorithm of PID gains by SNE

5.3 Tuning Algorithm of PID gains by SN estimator

For tuning the PID gains we consider θ first [32]. As shown in Fig. 5.2 the purpose of updating θ is to make the motor speed reach the reference speed. From the error of eq. (5.10), MIT rule of eq. (5.9) and using the chain rule [32] we have, for $i=1, 2, 3$,

$$\theta'_i = -\eta_i e \frac{\partial e}{\partial \theta_i} = -\eta_i e \frac{\partial e}{\partial y} \frac{\partial y}{\partial u} \frac{\partial u}{\partial \theta_i} = \eta_i e \frac{\partial y}{\partial u} \frac{\partial u}{\partial \theta_i} \quad (5.14)$$

The PID control law is given by

$$u(t) = \left[K_p e(t) + K_i \int_0^t e(\tau) d\tau + K_d \frac{d}{dt} e(t) \right] \quad (5.15)$$

Where K_p , K_i and K_d are Proportional, Integral and Derivative gain respectively [32].

Partial derivative of $\frac{\partial u}{\partial \theta_i}$ in (5.14) easily can be estimated from eq. (5.15)

$$\frac{\partial u}{\partial \theta_i} = \begin{bmatrix} \frac{\partial u}{\partial K_p} \\ \frac{\partial u}{\partial K_I} \\ \frac{\partial u}{\partial K_d} \end{bmatrix} = \begin{bmatrix} e(t) \\ \int_0^t e(\tau) d\tau \\ \frac{d}{dt} e(t) \end{bmatrix} \quad (5.16)$$

The PID controller constants are updated as follows [32]

$$k_p(k) = k_p(k-1) + \Delta k_p(k) \quad (5.17)$$

$$k_I(k) = k_I(k-1) + \Delta k_I(k) \quad (5.18)$$

$$k_d(k) = k_d(k-1) + \Delta k_d(k) \quad (5.19)$$

From the error of eq. (5.11), MIT rule of eq. (5.13) and using the chain rule [32] we have, for $i=1, 2, 3$,

$$\hat{\theta}_i = -\hat{\eta}_i \hat{e} \frac{\partial \hat{e}}{\partial \theta_i} = -\hat{\eta}_i \hat{e} \frac{\partial \hat{e}}{\partial \hat{y}} \cdot \frac{\partial \hat{y}}{\partial \theta_i} = \hat{\eta}_i \hat{e} \cdot \frac{\partial \hat{y}}{\partial \theta_i} \quad (5.20)$$

$$\text{Where, } \frac{\partial \hat{y}}{\partial \theta_i} = \begin{bmatrix} \frac{\partial \hat{y}}{\partial \phi} \\ \frac{\partial \hat{y}}{\partial a} \\ \frac{\partial \hat{y}}{\partial b} \end{bmatrix} = \begin{bmatrix} -\frac{ab}{2} \left(1 + \frac{\hat{y}}{a}\right) \left(1 - \frac{\hat{y}}{a}\right) \\ \frac{\hat{y}}{a} \\ \frac{a \cdot \text{net}}{2} \left(1 + \frac{\hat{y}}{a}\right) \left(1 - \frac{\hat{y}}{a}\right) \end{bmatrix} \quad (5.21)$$

Three adjustable variables ϕ , a and b are updated as follows [32]

$$a(k) = a(k-1) + \Delta a(k) \quad (5.22)$$

$$b(k) = b(k-1) + \Delta b(k) \quad (5.23)$$

$$\phi(k) = \phi(k-1) + \Delta \phi(k) \quad (5.24)$$

Derivate of $\frac{\partial y}{\partial u}$ may be approximated by $\frac{\partial \hat{y}}{\partial u}$ and derivate of $\frac{\partial \hat{y}}{\partial u}$ can be obtained from eq. 5.6 and 5.7 [32].

Also we have

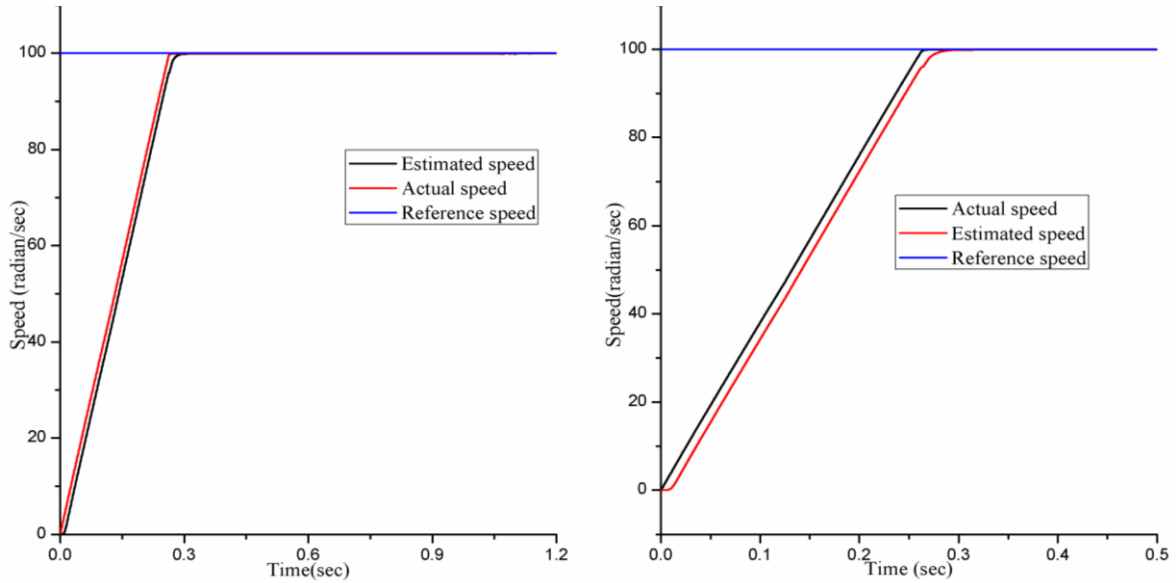
$$\frac{\partial \hat{y}}{\partial u} = \frac{ab}{2} \left(1 + \frac{\hat{y}}{a}\right) \left(1 - \frac{\hat{y}}{a}\right) \quad (5.25)$$

$$\text{Output of the controller is } u = k_p x_1 + k_i x_2 + k_d x_3 \quad (5.26)$$

5.4 Simulation Results

The performance of proposed drive system was tested through simulation. A computer program with C++ code is developed. The system was tested using simulation with RKG routine. For the simulation, parameters of PM Brushless DC Motor are given in Appendix A. The motor was started from rest with a load torque of $T_l = 1.0$ N-m. The set speed was 100 radian per sec. The drive system is found to respond fast to follow the set speed. The motor reaches the set speed in 0.26 sec. No appreciable overshoot and oscillation is noticed in the actual motor speed. Only at the corner point the estimated speed differ reasonably

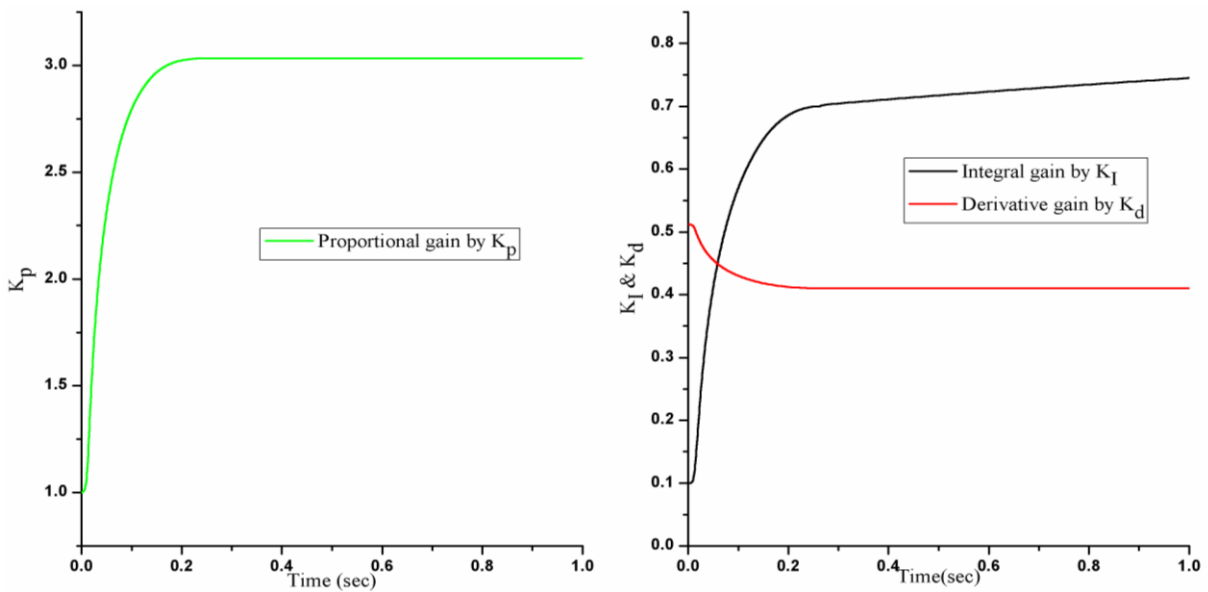
from actual speed. This may be due to improper settings of limiting values or tuning parameters of the controller. Hence, speed of the drive system is working effectively as indicated in Fig5.3 and it is seen that the estimated speed follows the actual speed very closely and the speed control is faster. Response of K_p , K_i and K_d are illustrated in Fig.5.4. It is observed that initial values of K_p and K_i are 1.0 when value of K_d is 0.5. Gradually; these values are updated to adjust motor speed. To stable speed at 100 radian per sec K_p and K_i reach up to 3.1 and 0.7 respectively but K_d is decreased from 0.5 to 0.41



(a) Speed response at starting condition

(b) Zoomed Speed response at starting.

Fig.5.3: Actual speed and estimated speed by SNAPID controller

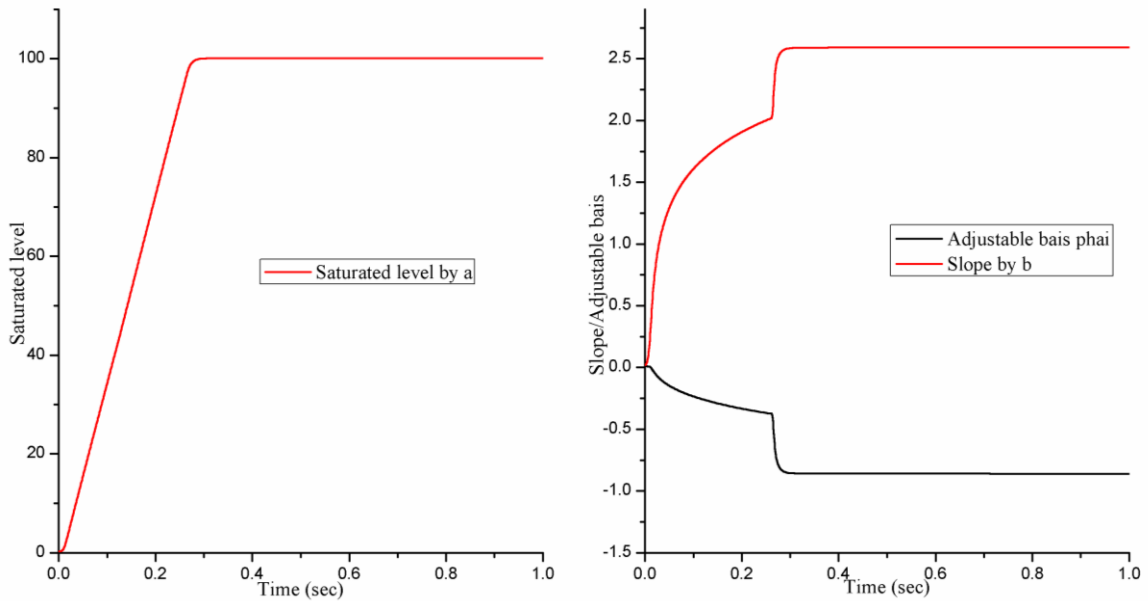


(a) Proportional gain at starting

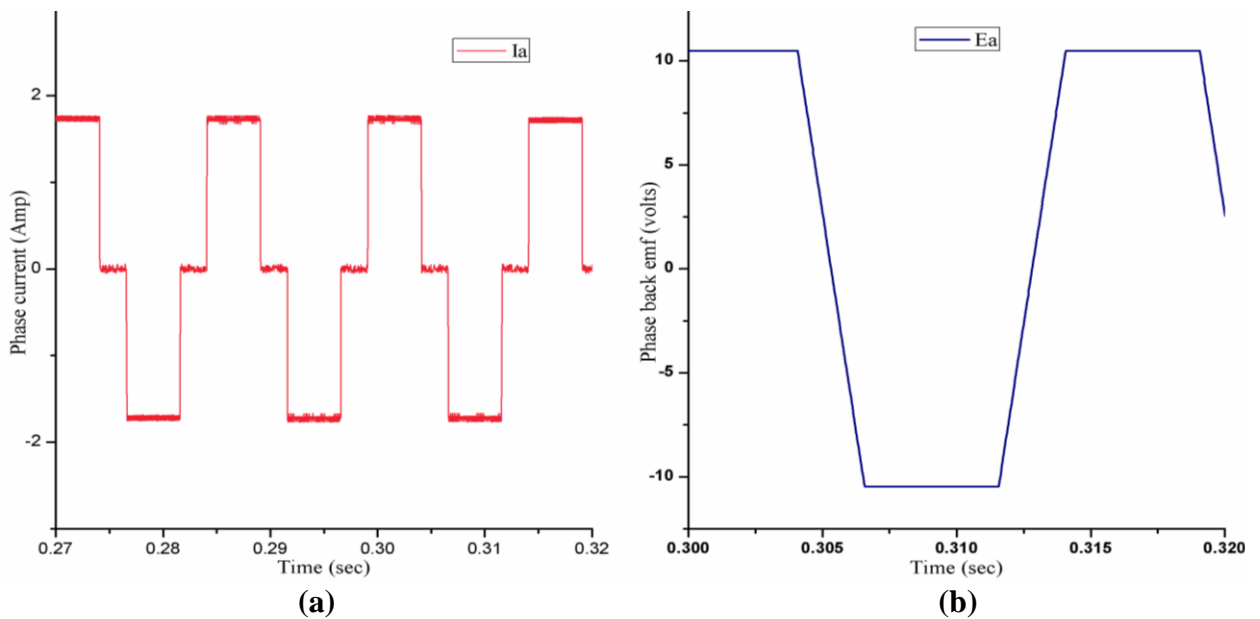
(b) Response of integral and derivative gain

Fig.5.4: Response of K_p , K_i and K_d gain for SNAPID controller

Feature of adjustable bias, saturated level and slope are displayed in Fig.5.5. From this figure it is noticed that saturated level is increased linearly from 0.0 to 100 for controlling motor speed at reference speed. Adjustable bias and slope also are updated up to 2.5 and -0.8 respectively according to reference speed when time is observed 0.26 sec. In this time actual speed is controlled according to update values of slope, adjustable bias and saturated level.



(a). Saturated level in modified tangent function (b) Feature of slope and adjustable bias
 Fig.5.5: Adjustable bias of (a) saturated level and (b) slope with SNAPID controller



(a) (b)
 Fig.5.6: At steady state condition (a) phase current and (b) phase back emf for SNAPID controller

In steady state condition single phase current and single phase back emf are shown in Fig.5.6 (a) and Fig.5.6 (b) respectively. Phase current is like rectangular shape and phase back is trapezoidal shape due to trapezoidal nature of flux.

In field oriented control system, reference quadrature axis current (I_{qr}) is directly proportional to requested load torque. Motor draws phase currents according to response of I_{qr} and developed torque is proportional to motor phase currents. Hence developed torque follows the requested load torque as shown in Fig.5.7. In transient condition of starting, maximum current follows when speed is rising. But it does not exceed 4.0 amp due to current limiter and in this case torque developed is maximum. At 0.26 sec when motor reaches the desired speed, current level of I_{qr} and developed torque decrease according to requested load torque.

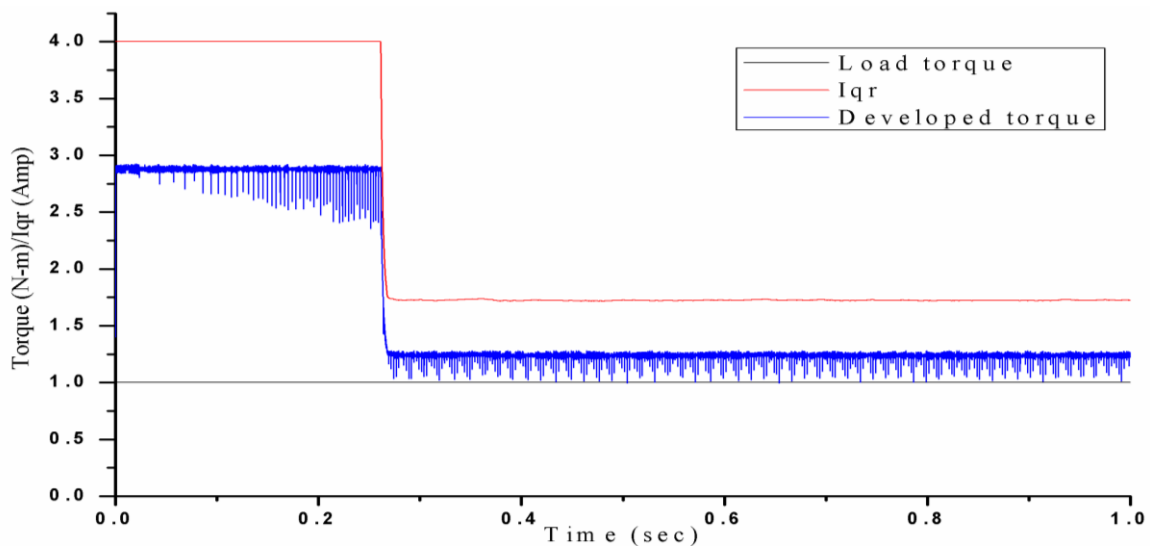


Fig.5.7: Developed torque and quadrature axis current for proposed controller

It is seen that initially induce back emf is zero as shown in Fig.5.8 (a) when motor speed behind the reference speed. When motor reaches its reference speed back emf is set as remain constant. Trapezoidal back emf is illustrated in Fig.5.8 (b). Fig.5.9 (a) displays three phase current and this current is zooming in Fig.5.9 (b). But phase current is controlled as well by proposed controller.

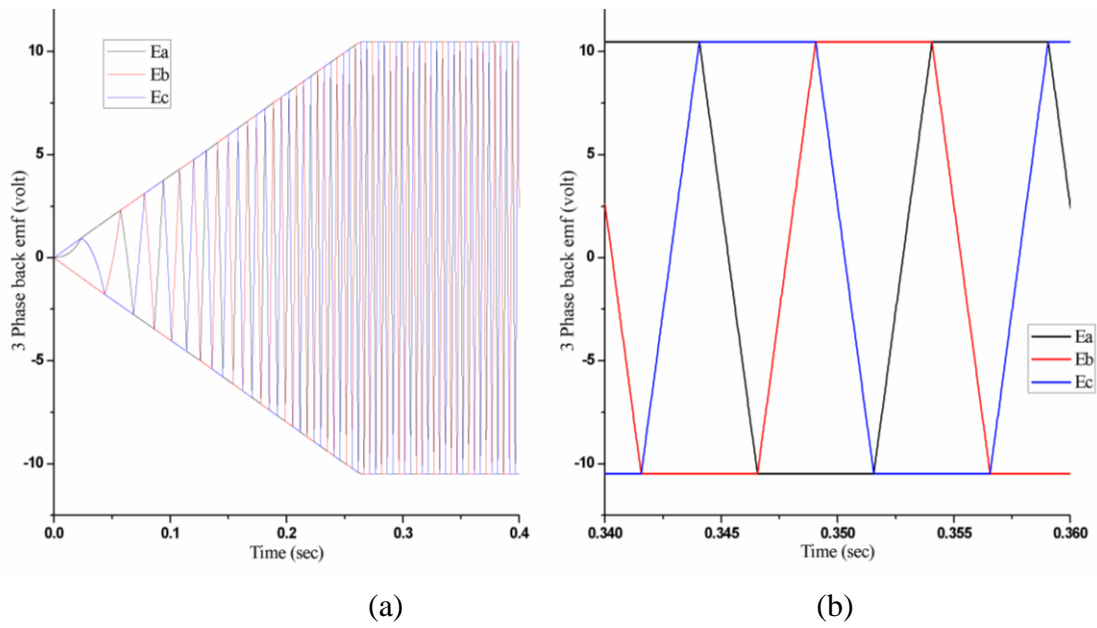


Fig.5.8: Illustration of three phase back emf with nature of trapezoidal back emf by SNAPID controller

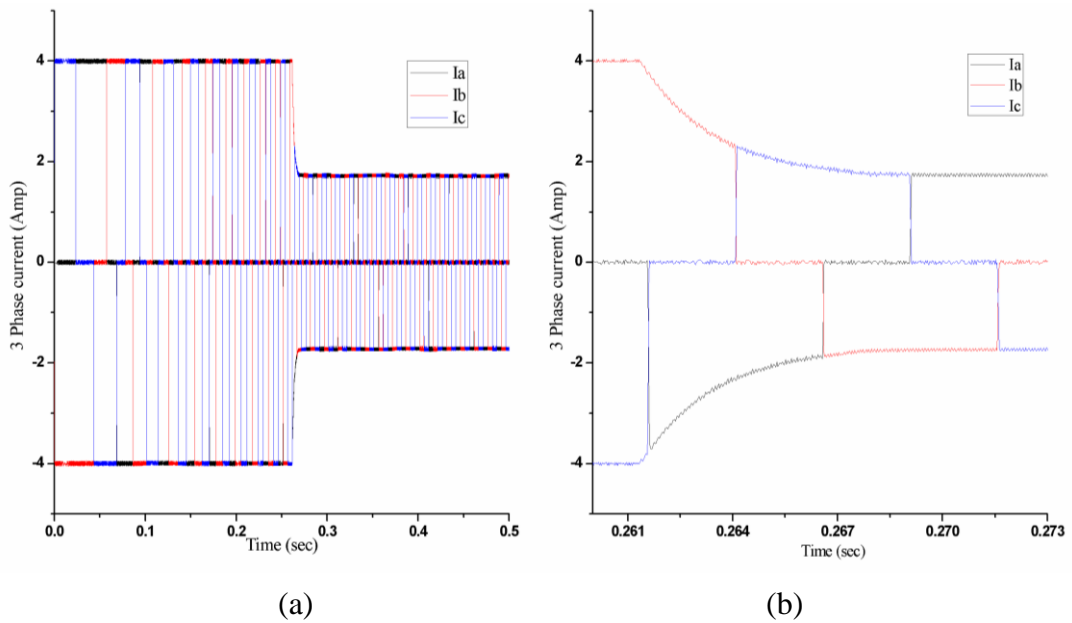


Fig.5.9: Three phase current by SNAPID controller

Fig.5.10 shows trapezoidal phase back emf and it is seen that initially induced phase back emf is low because of rotor takes more time to reach 2π radian. When motor speed error is

minimized rotor reaches 2π radian within very short time and hence induced back emf is maximum of ± 10 volt.

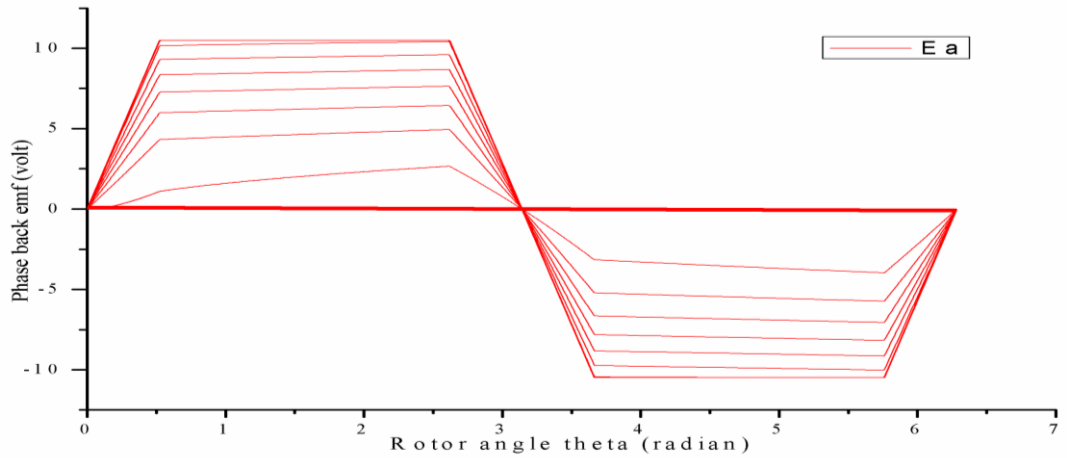


Fig.5.10: Phase back emf with rotor angle theta for proposed technique

At starting condition three phase voltage as shown in Fig.5.11 and it is noticed that phase voltage is changed as well with dc input voltage.

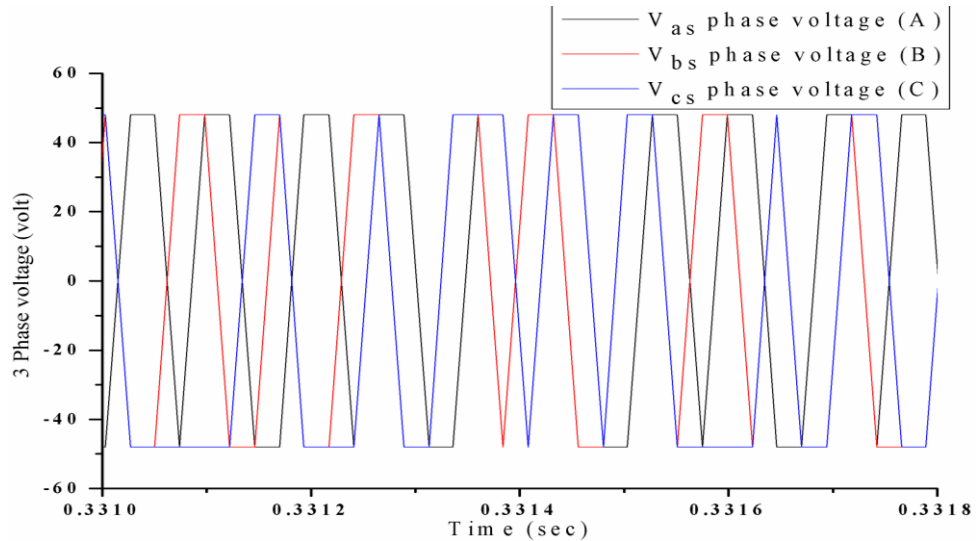


Fig.5.11: Three phase voltage for SNAPID Controller

5.5 Conclusion

In this chapter a single artificial neural network based adaptive PID controller with auto tuning feature for the Permanent Magnet Brushless DC Motor has been presented. The proposed controller also has the estimation capability. The controller constants are updated by online tuning process. It has been observed through simulation that the system works fast and with no appreciable oscillations. The estimator can be utilized for estimating other variables or parameters of the system.

CHAPTER VI

ANFIS BASED CONTROLLER DESIGN FOR PMBLDC MOTOR

The Chapter at a Glance

Introduction	Section 6.1
ANFIS based Controller with Radial Basis Function and Training Feature	Section 6.2
Architecture of ANFIS	Section 6.3
Training rule of ANFIS	Section 6.4
Identification of Radial Basis Function	Section 6.5
Simulation Results for Training Feature	Section 6.6
ANFIS Controller based on Takagi-Sugeno Model	Section 6.7
Simulation Results based on Takagi -Sugeno Model	Section 6.8
Machine model of PM Brushless DC Motor based on Line Voltage	Section 6.9
Simulation Results for Line Voltage Model	Section 6.10
Conclusion	Section 6.11

6.1 Introduction

Recently, adaptive neuro-fuzzy inference system based controllers are gaining popularity as an innovative research in artificial neural network. An ANFIS is a combination of fuzzy logic and artificial neural network. In this chapter an ANFIS controller and its online training is proposed based on radial basis neural network. To reduce training cost, the Gaussian function is proposed in this research. A PMBLDC Motor drive is a complex system for its multi-variable and nonlinear nature [42]. The motor speed and torque are simultaneously controlled for controlling variable speed drives applications. But it is difficult to control by using conventional PI controller. In order to overcome these problems, the ANFIS based controller is proposed and developed in this chapter. Another ANFIS based system with Takashi-Sugeno architecture is also introduced later on. A line voltage based PMBLDC Motor model is also proposed and used for drive control system. This chapter proposes two ANFIS based Controller for PMBLDC Motor control of phase

and line voltage based models. The effectiveness of the control scheme is tested in a C++ simulation environment.

6.2 ANFIS based Controller with Radial Basis Function and Training Feature

The performance of an ANFIS based controller depends on only three factors, viz number of parameters, membership functions and number of membership functions. In this research Gaussian membership function is proposed which has the premise parameters as c_i , b_i , C_j and B_j . Three membership functions receive two inputs that are error $x_2(k)$ and error difference rate $x_1(k)$ where k indicates as discrete sample instant. ANFIS based controllers with radial basis function is depicted in Fig.6.1. Radial basis function takes three inputs which are $u(k)$, $y(k)$ and estimated error difference $e(k)$ between $y(k)$ and $y_{model}(k)$. It provides Jacobin output $\partial y(k)/\partial u(k)$ which is denoted as $\partial y(k)/\partial u(k)$ [42].

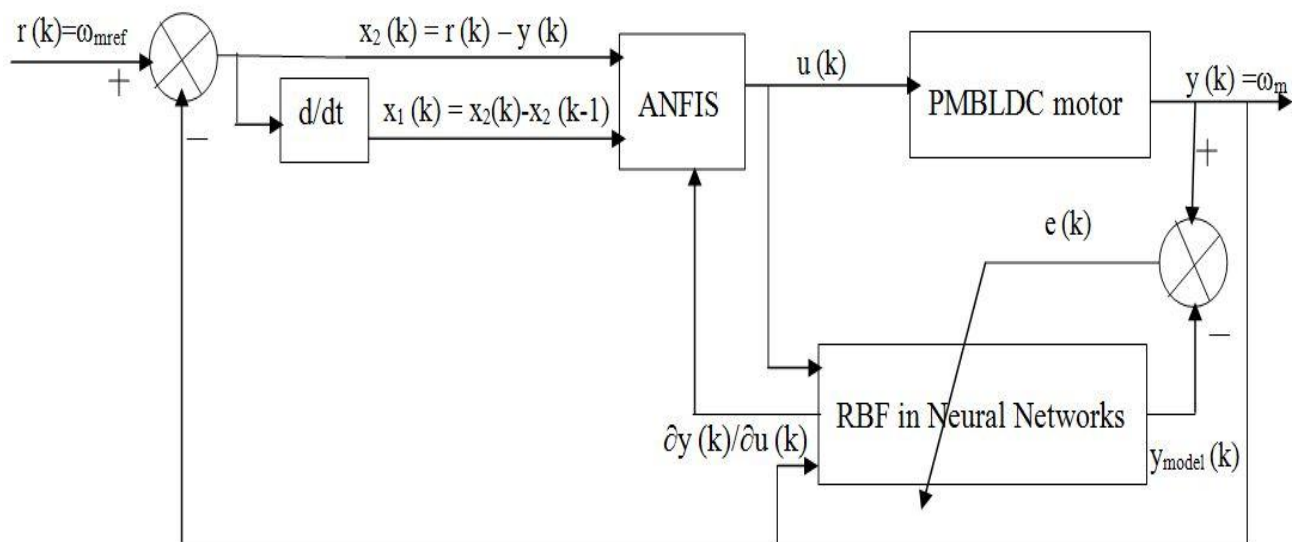


Fig.6.1: Block diagram of ANFIS based controller with radial basis function and PMBLDC Motor

6.3 Architecture of ANFIS

ANFIS based controller is well known as Sugeno fuzzy model having five layer and fuzzy “If-Then” rule is applied to this system. Fourth and first layer are indicated as an adaptive layer and remain layer are fixed layer. ANFIS controller is illustrated as in Fig.6.2 for motor drive system. A_1, A_2, A_3 and B_1, B_2, B_3 are membership functions of set A and B respectively. These functions are Gaussian type with the two inputs written as [42];

$$x_2(k) = r(k) - y(k) = e(k) \quad (6.1)$$

$$x_1(k) = x_2(k) - x_2(k-1) \quad (6.2)$$

Where $r(k)$ and $y(k)$ are defined as motor set speed (ω_{mref}) and actual speed (ω_m) in k discrete time.

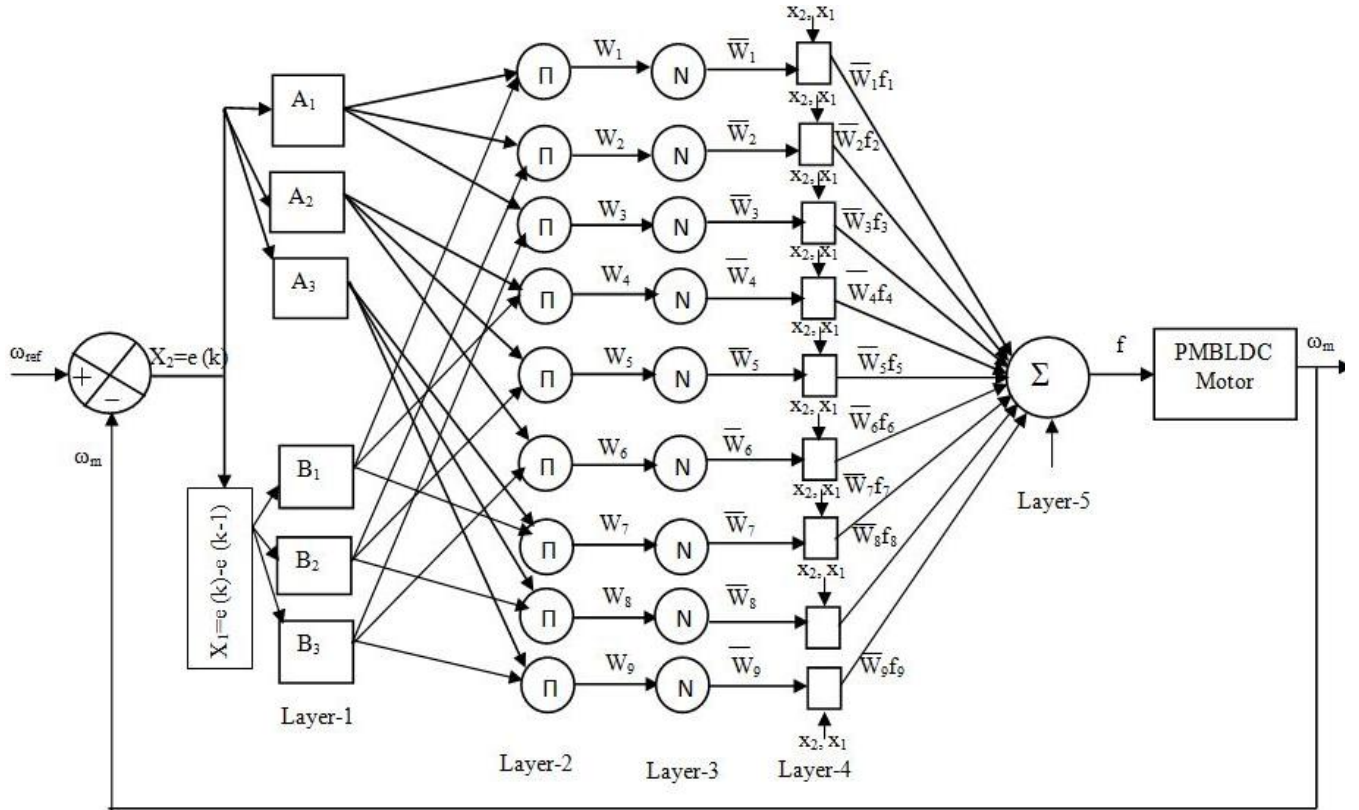


Fig.6.2: ANFIS controller with PMBLDC Motor

1st layer: This layer is fuzzification layer and inputs are passed through membership functions.

Output of Gaussian membership function is indicated as followings [42]

$$O_{1,i} = \mu_{A_i}(k) = \exp\left(-\frac{\|x_2 - c_i\|^2}{2b_i^2}\right), i = 1,2,3 \quad (6.3)$$

$$O_{1,j} = \mu_{B_j}(k) = \exp\left(-\frac{\|x_1 - c_j\|^2}{2B_j^2}\right), j = 1,2,3 \quad (6.4)$$

Where x_2 and x_1 are input variables and c_i , b_i , C_j and B_j are premise parameters which are adjusted by online training.

2nd layer: This layer is marked as Π in the circle and output of this layer is expressed as

$$O_{2,m} = w_m = \mu_{A_i}(k) \cdot \mu_{B_j}(k) \quad (6.5)$$

Where,

$$i = 1,2,3, \quad j = 1,2,3 \quad \text{and} \quad m = 1,2, \dots,9$$

3rd layer: In this layer each node is normalized and it is labeled by N. This normalized equation set is shown as [42]

$$O_{3,m} = \overline{w}_m = \frac{w_m}{\sum_{m=1}^m w_m} = \frac{w_m}{w_{total}}, m = 1,2, \dots,9 \quad (6.6)$$

4th layer: Output of this adaptive layer is calculated by normalized values \overline{w}_m and fuzzy rules f_m .

$$O_{4,m} = \overline{w}_m f_m \quad (6.7)$$

$$\text{Where, } f_m = (p_m x_2 + q_m x_1 + r_m) \quad m = 1,2, \dots,9 \quad (6.8)$$

Here p_m , q_m and r_m are linear consequent parameters those are needed to be adjusted for training purpose [42].

5th layer: This layer is labeled as Σ and output of this layer is fixed that is written as:

$$O_{5,m} = \sum_{m=1}^m \overline{w}_m f_m = \sum_{m=1}^m \frac{w_m}{\sum_{m=1}^m w_m} f_m, m = 1,2, \dots,9 \quad (6.9)$$

This output is considered as input to the PMBLDC Motor drive. In field oriented control system, two current components are considered. These are quadrature axis current component and direct axis current component. The reference direct axis current i_{dref} is considered zero for maximum torque output. The reference quadrature axis current i_{qref} is calculated according to the requested load torque from speed error using Equation from 6.1 to 6.9. Output of controller is considered to generate reference quadrature axis current i_{qref} . The magnitude of reference currents are obtained using Equation 3.5. The square wave shape of reference currents are generated using Equation from 3.6 to 3.12. Reference three phase currents are compared with the actual currents for voltage vector generation using delta modulation. The inverter switches are turned OFF or ON according to a hysteresis controller which was discussed in chapter three.

6.4 Training rule of ANFIS

Radial basis function is employed to train ANFIS network so that consequent parameters $\{p_m, q_m, r_m\}$ and premise parameters $\{c_i, b_i, C_j, B_j\}$ of membership function can be updated. Performance index is calculated in equation (6.10) to minimize error written as [42]

$$E(k) = \frac{1}{2}(e(k))^2 \quad (6.10)$$

For changing c_i , b_i , C_j , B_j

$$c_i(k) = c_i(k-1) - \eta \frac{\partial E(k)}{\partial c_i(k)} \quad (6.11)$$

$$b_i(k) = b_i(k-1) - \eta \frac{\partial E(k)}{\partial b_i(k)} \quad (6.12)$$

For updating p_m , q_m , r_m

$$p_m(k) = p_m(k-1) - \eta \frac{\partial E(k)}{\partial p_m(k)} \quad (6.13)$$

$$q_m(k) = q_m(k-1) - \eta \frac{\partial E(k)}{\partial q_m(k)} \quad (6.14)$$

$$r_m(k) = r_m(k-1) - \eta \frac{\partial E(k)}{\partial r_m(k)} \quad (6.15)$$

Derivatives form of above equations are written as

$$\begin{aligned} \frac{\partial E(k)}{\partial c_i(k)} &= \frac{\partial E(k)}{\partial e(k)} \frac{\partial e(k)}{\partial y(k)} \frac{\partial y(k)}{\partial u(k)} \frac{\partial u(k)}{\partial c_i(k)} \\ \frac{\partial E(k)}{\partial c_i(k)} &= -e(k) \frac{\partial y(k)}{\partial u(k)} \frac{1}{w_{tot}} (Sum_i) \exp\left(-\frac{\|x_2 - c_i\|^2}{2b_i^2}\right) (x_2 - c_i) \frac{1}{b_i^2} \\ \frac{\partial E(k)}{\partial b_i(k)} &= \frac{\partial E(k)}{\partial e(k)} \frac{\partial e(k)}{\partial y(k)} \frac{\partial y(k)}{\partial u(k)} \frac{\partial u(k)}{\partial b_i(k)} \end{aligned} \quad (6.16)$$

$$\begin{aligned} \frac{\partial E(k)}{\partial b_i(k)} &= -e(k) \frac{\partial y(k)}{\partial u(k)} \frac{1}{w_{tot}} (Sum_i) \exp\left(-\frac{\|x_2 - c_i\|^2}{2b_i^2}\right) (x_2 - c_i)^2 \frac{1}{b_i^3} \\ \frac{\partial E(k)}{\partial C_j(k)} &= \frac{\partial E(k)}{\partial e(k)} \frac{\partial e(k)}{\partial y(k)} \frac{\partial y(k)}{\partial u(k)} \frac{\partial u(k)}{\partial C_j(k)} \end{aligned} \quad (6.17)$$

$$\begin{aligned} \frac{\partial E(k)}{\partial C_j(k)} &= -e(k) \cdot \frac{\partial y(k)}{\partial u(k)} \cdot \frac{1}{w_{tot}} \cdot (Sum_j) \exp\left(-\frac{\|x_1 - C_j\|^2}{2B_j^2}\right) \cdot (x_1 - C_j) \frac{1}{B_j^2} \\ \frac{\partial E(k)}{\partial B_j(k)} &= \frac{\partial E(k)}{\partial e(k)} \frac{\partial e(k)}{\partial y(k)} \frac{\partial y(k)}{\partial u(k)} \frac{\partial u(k)}{\partial B_j(k)} \end{aligned} \quad (6.18)$$

$$\begin{aligned} \frac{\partial E(k)}{\partial B_j(k)} &= -e(k) \frac{\partial y(k)}{\partial u(k)} \frac{1}{w_{tot}} (Sum_j) \cdot \exp\left(-\frac{\|x_1 - C_j\|^2}{2B_j^2}\right) (x_1 - C_j)^2 \frac{1}{B_j^3} \\ \frac{\partial E(k)}{\partial p_m(k)} &= \frac{\partial E(k)}{\partial e(k)} \frac{\partial e(k)}{\partial y(k)} \frac{\partial y(k)}{\partial u(k)} \frac{\partial u(k)}{\partial p_m(k)} \end{aligned} \quad (6.19)$$

$$\begin{aligned} \frac{\partial E(k)}{\partial p_m(k)} &= -e(k) \frac{\partial y(k)}{\partial u(k)} \left(\frac{w_m}{w_{tot}}\right) \cdot x_1(k) \\ \frac{\partial E(k)}{\partial q_m(k)} &= \frac{\partial E(k)}{\partial e(k)} \frac{\partial e(k)}{\partial y(k)} \frac{\partial y(k)}{\partial u(k)} \frac{\partial u(k)}{\partial q_m(k)} \end{aligned} \quad (6.20)$$

$$\frac{\partial E(k)}{\partial q_m(k)} = -e(k) \frac{\partial y(k)}{\partial u(k)} \left(\frac{w_m}{w_{tot}} \right) \cdot x_2(k) \quad (6.21)$$

$$\frac{\partial E(k)}{\partial r_m(k)} = \frac{\partial E(k)}{\partial e(k)} \frac{\partial e(k)}{\partial y(k)} \frac{\partial y(k)}{\partial u(k)} \frac{\partial u(k)}{\partial r_m(k)}$$

$$\frac{\partial E(k)}{\partial r_m(k)} = -e(k) \frac{\partial y(k)}{\partial u(k)} \left(\frac{w_m}{w_{tot}} \right) \quad (6.22)$$

For Sum_i (6.23)

$$\text{When, } i=1, \quad Sum_i = \mu_{B1}(k)f_1 + \mu_{B2}(k)f_2 + \mu_{B3}(k)f_3$$

$$\text{When, } i=2, \quad Sum_i = \mu_{B1}(k)f_4 + \mu_{B2}(k)f_5 + \mu_{B3}(k)f_6$$

$$\text{When, } i=3, \quad Sum_i = \mu_{B1}(k)f_7 + \mu_{B2}(k)f_8 + \mu_{B3}(k)f_9$$

For Sum_j (6.24)

$$\text{When, } j=1, \quad Sum_j = \mu_{A1}(k)f_1 + \mu_{A2}(k)f_2 + \mu_{A3}(k)f_3$$

$$\text{When, } j=2, \quad Sum_j = \mu_{A1}(k)f_4 + \mu_{A2}(k)f_5 + \mu_{A3}(k)f_6$$

$$\text{When, } j=3, \quad Sum_j = \mu_{A1}(k)f_7 + \mu_{A2}(k)f_8 + \mu_{A3}(k)f_9$$

6.5 Identification of Radial Basis Function

In this section $\partial y(k)/\partial u(k)$ is information of Jacobian of controller and it can be found out from inputs $y(k)$, $u(k)$ and estimated error $e(k)$ as shown in Fig.6.1 For this case three input Gaussian radial basis function is defined as [42]

$$h_j = \exp\left(-\frac{\|x-g_j\|^2}{2d_j^2}\right) \quad (6.25)$$

Where x variable is indicated as above for three inputs with corresponding g_j and d_j .

Output of RBF can be written as

$$y_{model}(k) = w_0 + w_1h_1 + w_2h_2 + \dots + w_xh_x \quad (6.26)$$

Rewriting above equation

$$y_{model}(k) = w_0 + \sum_{j=1}^x w_jh_j \quad (6.27)$$

RBF tracking the output error J which is defined as [42]

$$J = \frac{1}{2} ((y(k) - y_{model}(k))^2) \quad (6.28)$$

Changing weight with respect to error J that is shown as [42]

$$\frac{\partial J}{\partial w} = \frac{\partial J}{\partial y_{model}} \frac{\partial y_{model}}{\partial w}$$

$$\frac{\partial J}{\partial w} = (y(k) - y_{model}(k))h_j \quad (6.29)$$

Updated weights between Gaussian function and output of RBF is indicated as [42]

$$w_j(k) = w_j(k-1) + \eta \frac{\partial J}{\partial w}$$

$$w_j(k) = w_j(k-1) + \eta(y(k) - y_{model}(k))h_j + \alpha(w_j(k-1) - w_j(k-2)) \quad (6.30)$$

Where α and η are defined as moment coefficient and learning rate. In a similar way for d_j

$$d_j(k) = d_j(k-1) + \eta \Delta d_j + \alpha(d_j(k-1) - d_j(k-2)) \quad (6.31)$$

Where,

$$\Delta d_j = \frac{\partial J}{\partial d_j} = \frac{\partial J}{\partial y_{model}} \frac{\partial y_{model}}{\partial h_j} \frac{\partial h_j}{\partial d_j}$$

$$\Delta d_j = (y(k) - y_{model}(k))w_j h_j \left(-\frac{\|X - g_j\|^2}{d_j^3} \right)$$

For g_j

$$g_j(k) = g_j(k-1) + \eta \Delta g_j + \alpha(g_j(k-1) - g_j(k-2)) \quad (6.32)$$

Where as

$$\Delta g_j = \frac{\partial J}{\partial g_j} = \frac{\partial J}{\partial y_{model}} \frac{\partial y_{model}}{\partial h_j} \frac{\partial h_j}{\partial g_j}$$

$$\Delta g_j = (y(k) - y_{model}(k))w_j h_j \left(-\frac{\|X - g_j\|^2}{d_j^2} \right)$$

In the radial basis function $\partial y(k)/\partial u(k)$ is unknown and $\partial y_{model}(k)/\partial u(k)$ is calculated by RBF. Assuming $\partial y(k)/\partial u(k)$ is approximated to $\partial y_{model}(k)/\partial u(k)$ [42].

$$\frac{\partial y(k)}{\partial u(k)} \approx \frac{\partial y_{model}(k)}{\partial u(k)} = \frac{\partial y_{model}(k)}{\partial h_j(k)} \frac{\partial h_j(k)}{\partial u(k)}$$

$$\frac{\partial y(k)}{\partial u(k)} \approx \frac{\partial y_{model}(k)}{\partial u(k)} = \sum_{j=1}^x w_j h_j \frac{g_j - x_j}{d_j^2} \quad (6.33)$$

6.6 Simulation Results for Training Feature

The motor was started from standstill condition with a reference speed of 100 rad per sec. It is observed that the motor reaches the set speed in 0.26 sec without any overshoot or undershoot which is very fast response indeed as illustrated in Fig.6.3.

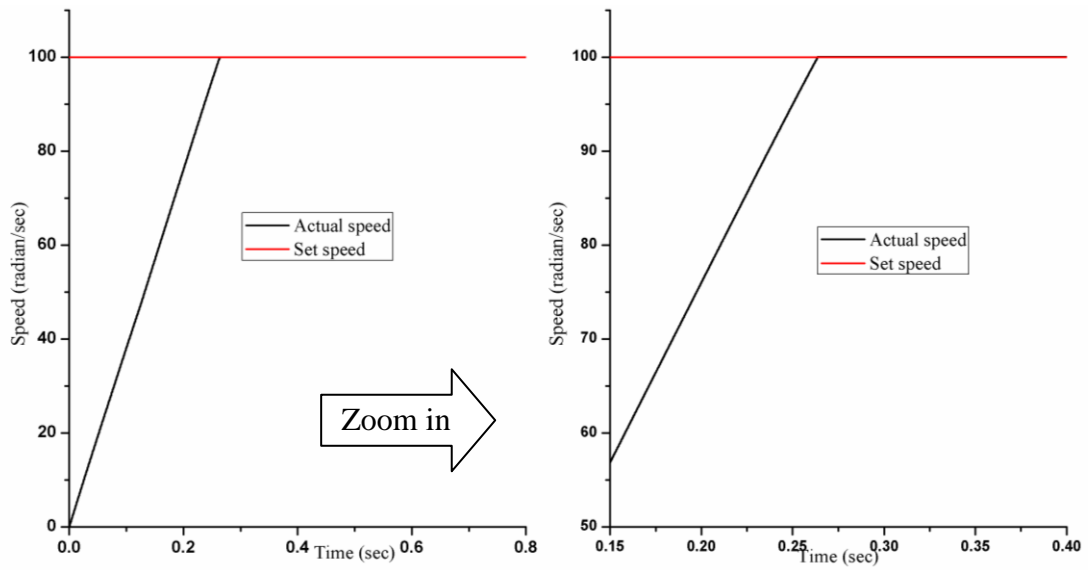


Fig.6.3: Speed response characteristic by ANFIS based controller with RBF

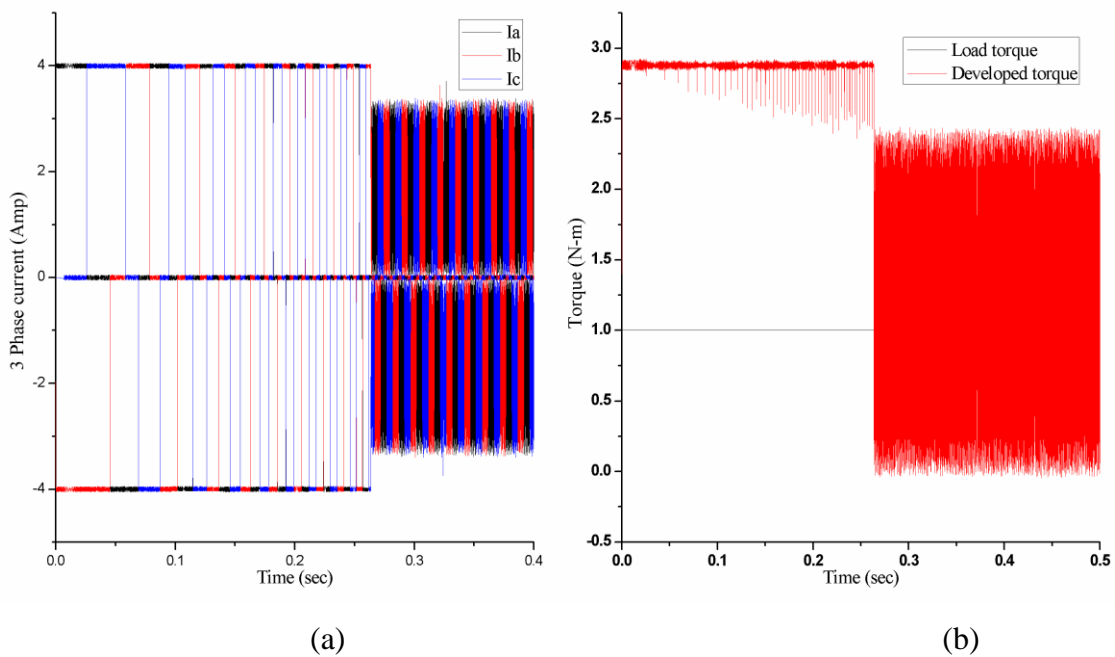


Fig.6.4: (a) Three phase current and (b) developed torque by ANFIS with RBF

It is observed from Fig.6.4 that the developed torque follows the load torque as the motor runs at steady state condition and it is also noticed that phase current is controlled according to load torque. This ANFIS controller has the capability to update the weights and parameters. Weight adjustments are shown in Fig.6.5. Adjustment of consequent parameters p_i , q_i and r_i are shown in Fig.6.6, Fig.6.7 and Fig.6.8 respectively. It is noticed that all weights and parameters are updated according to obtain desire accuracy.

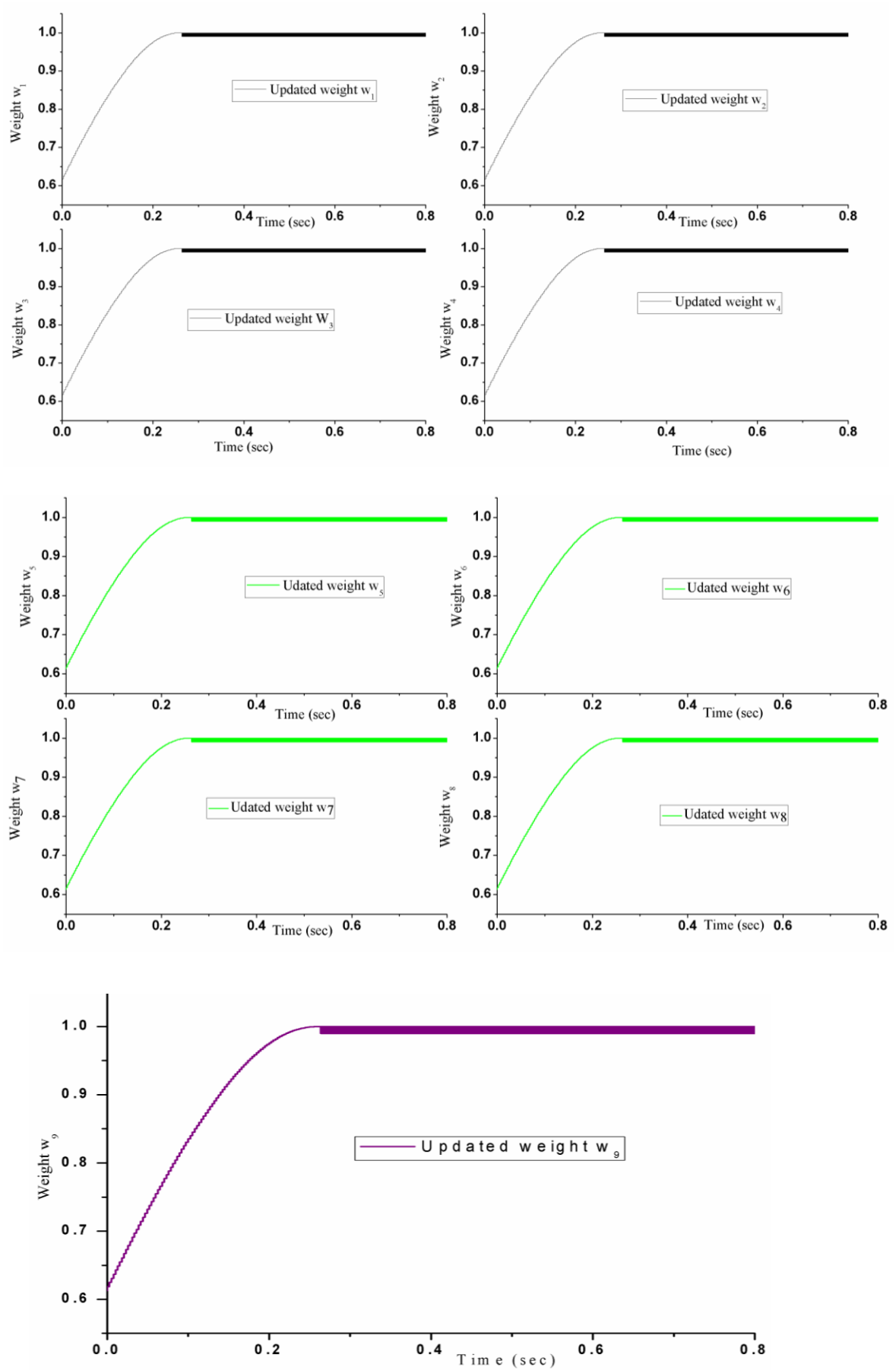


Fig.6.5: Weight update from w_1 to w_9

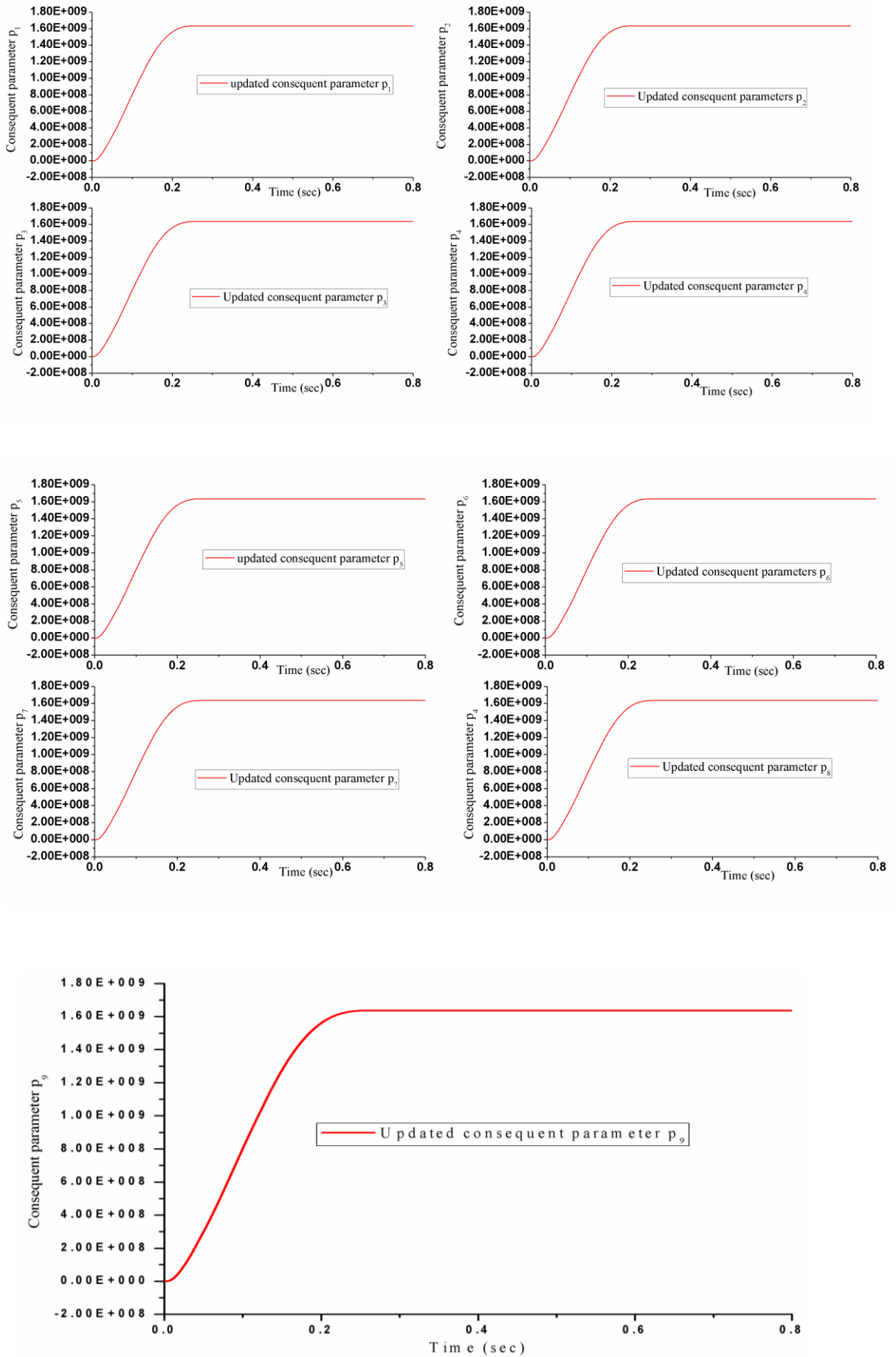


Fig.6.6: Update consequent parameters from p_1 to p_9

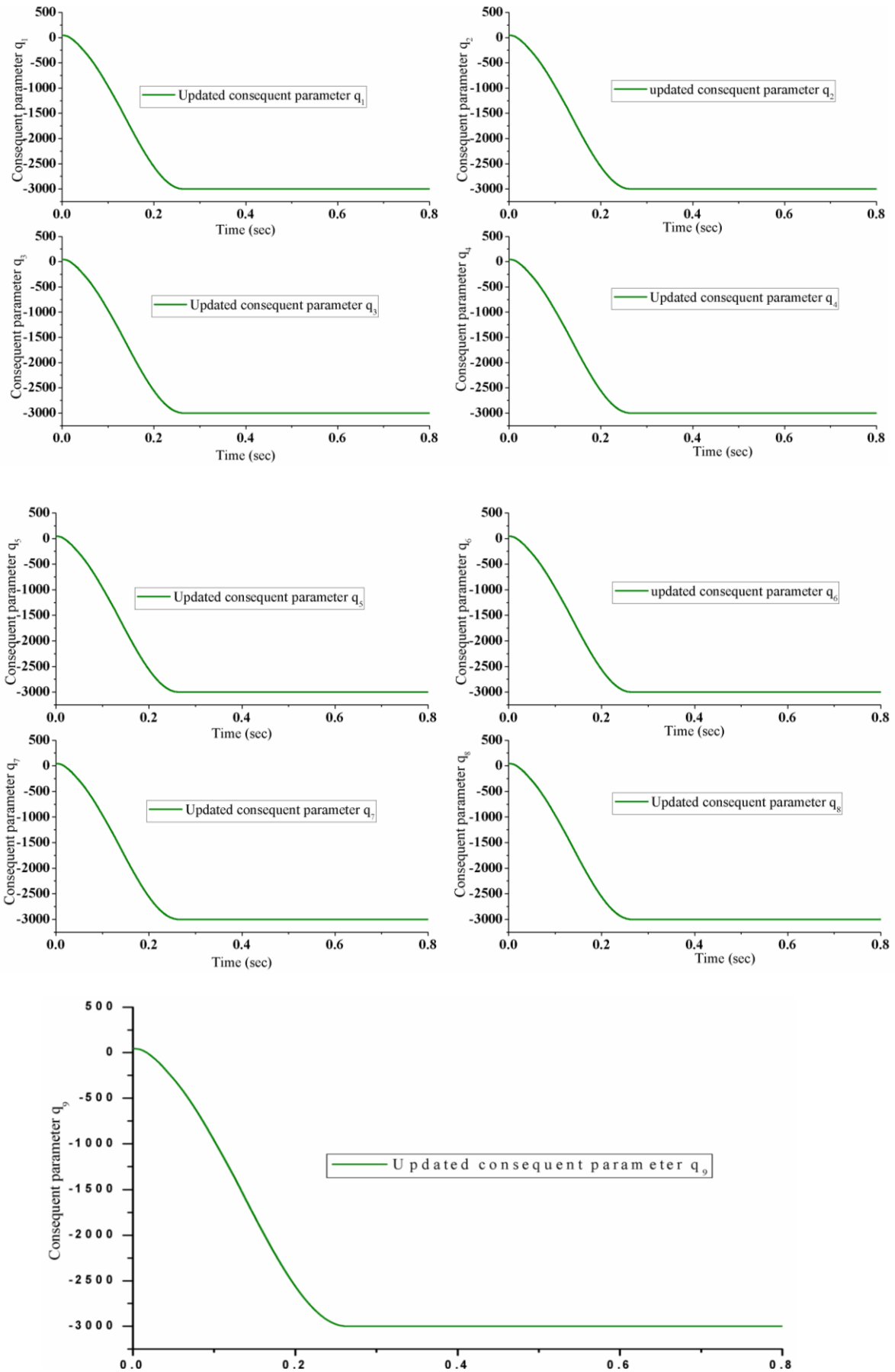


Fig.6.7: Update consequent parameter from q_1 to q_9

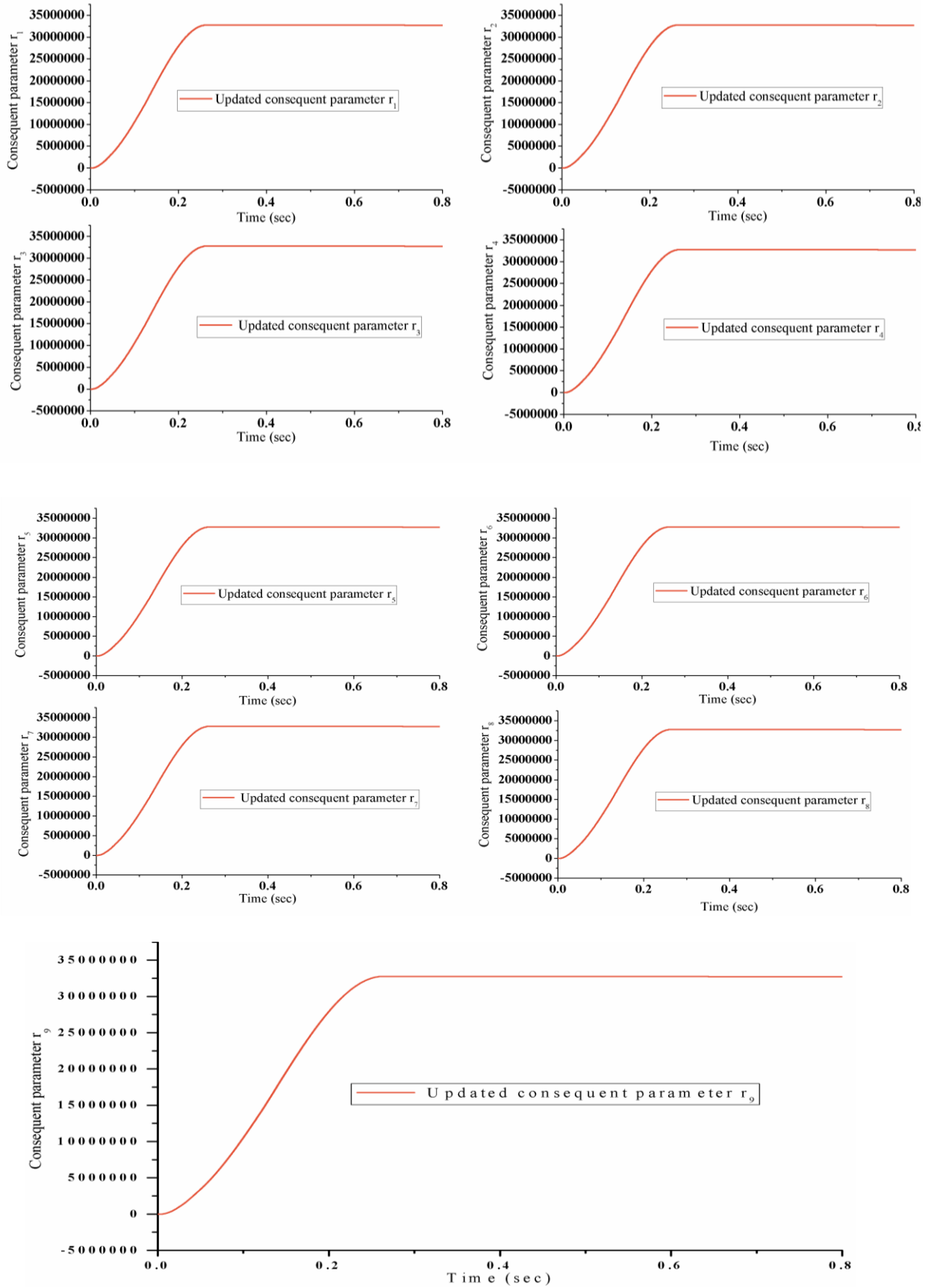


Fig.6.8: Update consequent parameter from r_1 to r_9

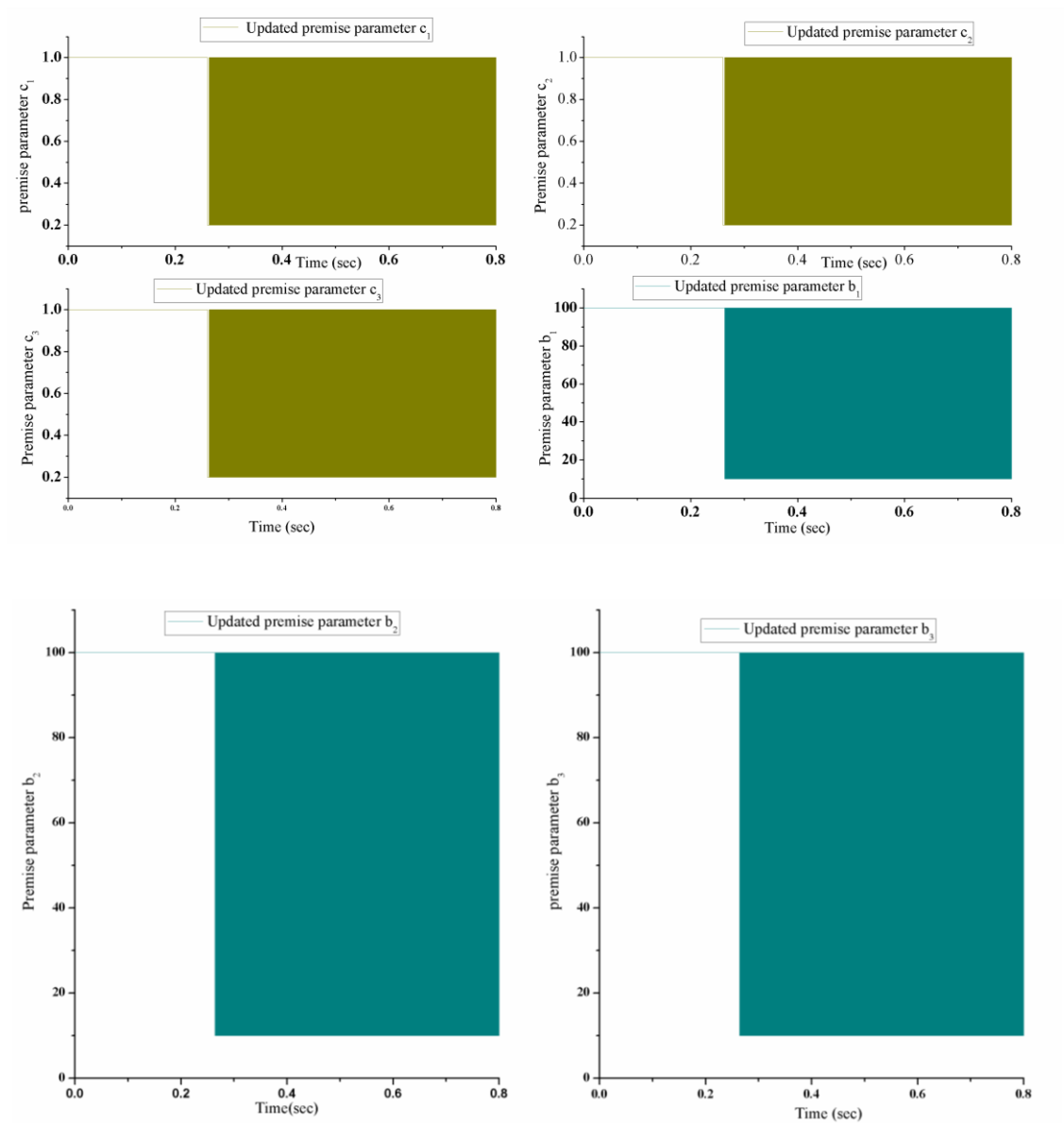


Fig.6.9: Update premise parameters from c_1 to c_3 and b_1 to b_3

It is noticed in Fig.6.9, All premise parameters are changing to adjust desire command.

6.7 ANFIS controller based on Takagi-Sugeno Model

This controller is proposed based on Takagi- Sugeno model and fuzzy logic rule. The structure of ANFIS controller with PMLDC Motor is shown in Fig.6.10. Here two inputs are taking, one is error (x_2) and other is error difference (x_1) as described in previous subsection. Two rules were used in the method of “If-Then” for Takagi- Sugeno model as follows [43, 44]. For this ANFIS structure, the two rules are:

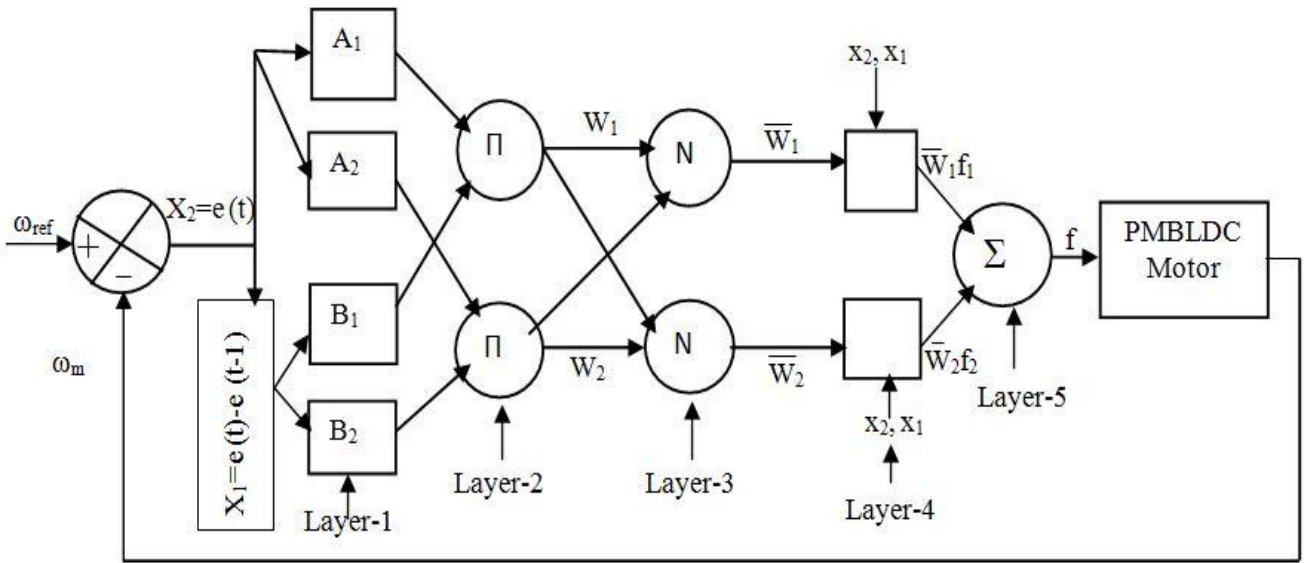


Fig.6.10: ANFIS Controller based on Takagi- Sugeno Model

Rule-1, If x_2 is A_1 and x_1 is B_1 , Then $f_1 = p_1x_2 + q_1x_1 + r_1$

Rule-2, If x_2 is A_2 and x_1 is B_2 , Then $f_2 = p_2x_2 + q_2x_1 + r_2$

Where A_1, A_2 and B_1, B_2 are membership functions having input x_2 and x_1 , while p_i, q_i, r_i are linear consequent parameters.

Layer 1: The membership function can be a Gaussian function, bell function or another type function. In this model, we have used bell function [43] in the following equation (6.32) as membership function for fuzzy set A_i and input x_2 .

$$O_{1i} = \mu_{A_i}(x_2) = \frac{1}{1 + \left| \frac{x_2 - c_i}{a_i} \right|^{2b_i}} \quad i=1, 2 \quad (6.34)$$

Similarly [43] for fuzzy set B_i and input x_1

$$O_{1i} = \mu_{B_i}(x_1) = \frac{1}{1 + \left| \frac{x_1 - c_i}{a_i} \right|^{2b_i}} \quad i=1, 2 \quad (6.35)$$

Where, μ_{A_i} and μ_{B_i} are the degree of membership functions. The parameters $\{a_i, b_i, c_i\}$ are considered fixed.

Layer 2: Every node in this layer is fixed and the circle node is labeled by Π . Outcome of this layer is showed following equations

$$O_{2i} = w_i = \mu_{A_i}(X_2)\mu_{B_i}(X_1), i=1, 2 \quad (6.36)$$

Where, w_i presents the firing strength.

Layer 3: This layer is normalization and fixed layer. Each node is labeled by N and outputs

[43] are written as

$$O_{3i} = \bar{w}_i = \frac{w_i}{\sum_{i=1}^2 w_i} \quad (6.37)$$

Layer 4: In this layer, every node is adaptive node and defuzzification layer. Output of this layer is

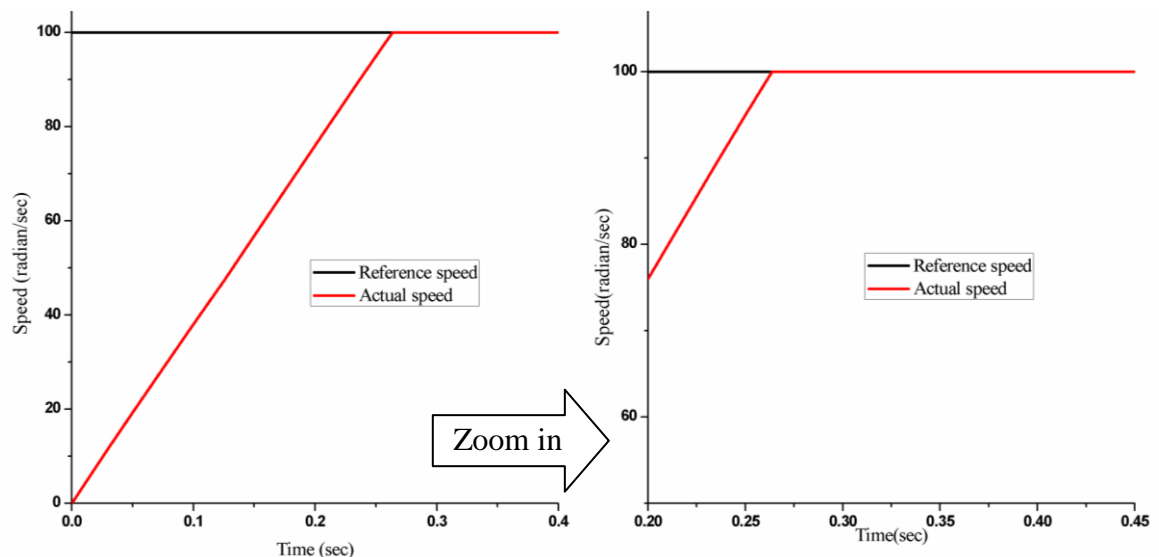
$$O_{4i} = \bar{w}_i f_i = \bar{w}_i (p_i x_2 + q_i x_1 + r_i) \quad (6.38)$$

Layer 5: Node of this layer is fixed and output is the summation of all incoming signals from previous node. Circle node is labeled as Σ . The output equation of the controller is used to find input current of the machine [43].

$$O_{5i} = \sum_{i=1}^2 \bar{w}_i f_i = \frac{\sum_{i=1}^2 w_i f_i}{\sum_{i=1}^2 w_i} \quad (6.39)$$

6.8 Simulation Results based on Takagi-Sugeno Model

A C++ program code is written for field oriented based ANFIS Control system of PM Brushless DC Motor. The effectiveness of the drive system is studied through simulation. The parameters of the motor are tabulated in Appendix A. Parameters of ANFIS system are selected on trial and error method for obtaining fast response. The motor was started from rest condition. The results are shown in Fig. 6.11. It is observed that the motor reaches to reference speed 100 rad per sec very fast about 0.26 sec. No appreciable overshoot or undershoot is noticed in speed.



(a). Speed characteristic

(b) Zoomed speed characteristic

Fig.6.11: Speed characteristic by ANFIS controller based on Takagi-Sugeno Model

In field oriented control system, three phases stator current is directly proportional to requested load torque. Hence developed torque follows the requested load torque as shown in Fig.6.12. In

starting condition, a high current follows when the motor accelerates. But current is limited at 4 Amp. At 0.26 second motor reaches the reference speed, these phases current and developed torque are decreased according to load torque.

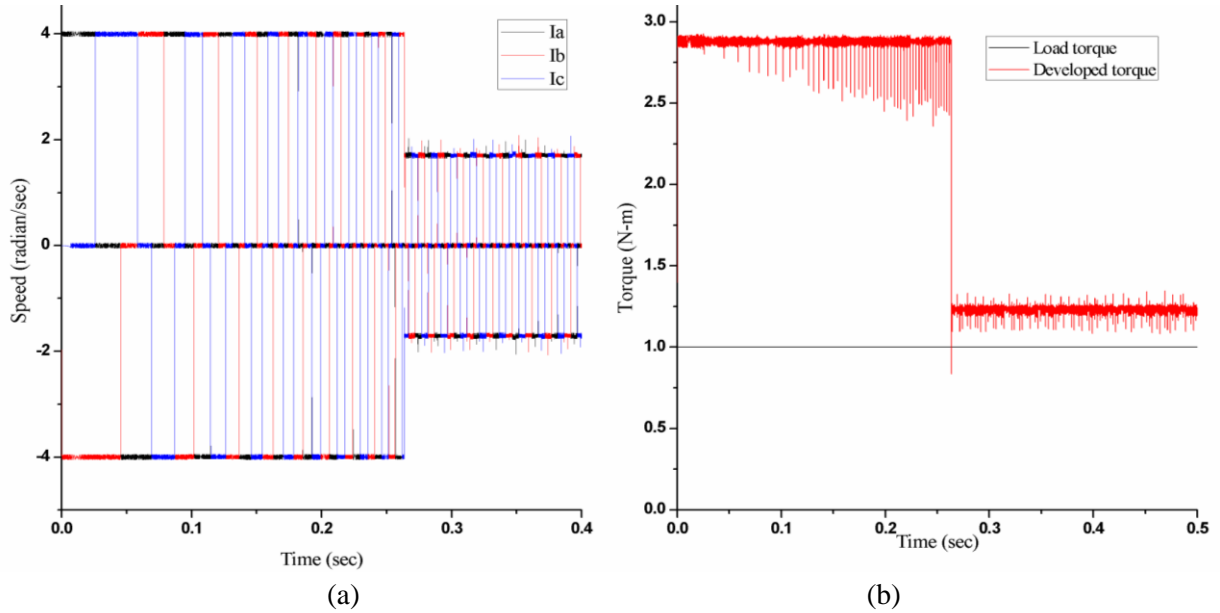


Fig.6.12: Illustration of (a) three phase current and (b) developed torque

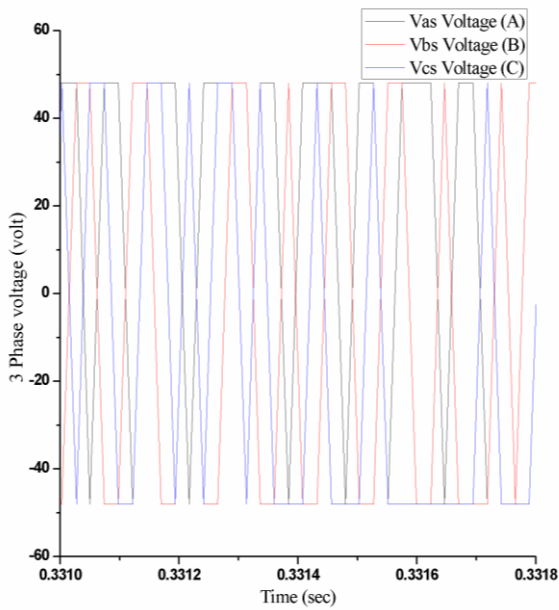


Fig.6.13: Three phases voltage

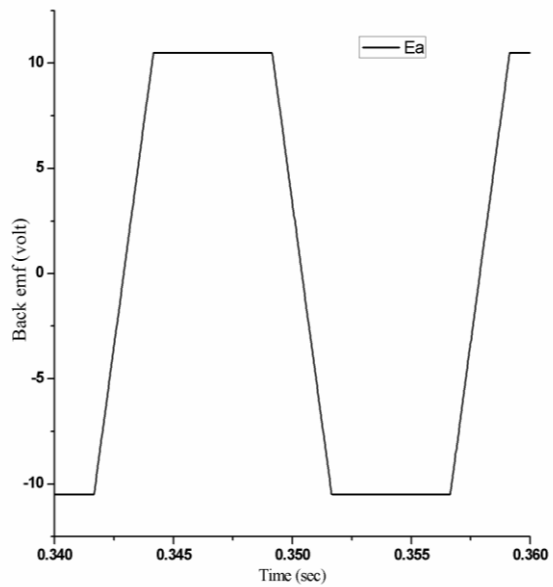


Fig.6.14: Single phase back emf

Inverter output is 3-phase voltages which put into 3 phase windings of PMSM Motor. As we can see phase voltages in Fig. 6.13. Steady state back emf is also shown in Fig.6.14

6.9 Machine Model of PM Brushless DC motor based on Line Voltages

For a small duration if phases become unbalanced there is a current flow in neutral wire for star connected motor drive. For this reason we have to replace the phase voltages by line voltages. Following conversion of the motor equations are done in an ANFIS based field oriented control technique for simplification of the program. From Equation (2.14) by substituting the voltages, we get [28]

$$\begin{bmatrix} V_{as} - V_{bs} \\ V_{bs} - V_{cs} \\ V_{cs} - V_{as} \end{bmatrix} = \begin{bmatrix} R_s & 0 & 0 \\ 0 & R_s & 0 \\ 0 & 0 & R_s \end{bmatrix} \begin{bmatrix} i_a - i_b \\ i_b - i_c \\ i_c - i_a \end{bmatrix} + \frac{d}{dt} \begin{bmatrix} L - M & 0 & 0 \\ 0 & L - M & 0 \\ 0 & 0 & L - M \end{bmatrix} \begin{bmatrix} i_a - i_b \\ i_b - i_c \\ i_c - i_a \end{bmatrix} + \begin{bmatrix} e_a - e_b \\ e_b - e_c \\ e_c - e_a \end{bmatrix} \quad (6.40)$$

$$V_{ab} = V_{as} - V_{bs} \quad (6.41)$$

$$V_{bc} = V_{bs} - V_{cs} \quad (6.42)$$

$$V_{ca} = V_{cs} - V_{as} \quad (6.43)$$

$$\begin{bmatrix} V_{ab} \\ V_{bc} \\ V_{ca} \end{bmatrix} = \begin{bmatrix} R_s & 0 & 0 \\ 0 & R_s & 0 \\ 0 & 0 & R_s \end{bmatrix} \begin{bmatrix} i_a - i_b \\ i_b - i_c \\ i_c - i_a \end{bmatrix} + \frac{d}{dt} \begin{bmatrix} L - M & 0 & 0 \\ 0 & L - M & 0 \\ 0 & 0 & L - M \end{bmatrix} \begin{bmatrix} i_a - i_b \\ i_b - i_c \\ i_c - i_a \end{bmatrix} + \begin{bmatrix} e_a - e_b \\ e_b - e_c \\ e_c - e_a \end{bmatrix} \quad (6.44)$$

From Equation (6.44) by substituting V_{ab} by V_{bc} , substituting V_{bc} by V_{ca} , substituting V_{ca} by V_{ab} we get [28]

$$\begin{bmatrix} V_{ab} - V_{bc} \\ V_{bc} - V_{ca} \\ V_{ca} - V_{ab} \end{bmatrix} = \begin{bmatrix} R_s & 0 & 0 \\ 0 & R_s & 0 \\ 0 & 0 & R_s \end{bmatrix} \begin{bmatrix} i_a - i_b - i_b + i_c \\ i_b - i_c - i_c + i_a \\ i_c - i_a - i_a + i_b \end{bmatrix} + \frac{d}{dt} \begin{bmatrix} L - M & 0 & 0 \\ 0 & L - M & 0 \\ 0 & 0 & L - M \end{bmatrix} \begin{bmatrix} i_a - i_b - i_b + i_c \\ i_b - i_c - i_c + i_a \\ i_c - i_a - i_a + i_b \end{bmatrix} + \begin{bmatrix} e_a - e_b - e_b + e_c \\ e_b - e_c - e_c + e_a \\ e_c - e_a - e_a + e_b \end{bmatrix} \quad (6.45)$$

From equation (2.12)

$$i_a - i_b - i_b + i_c = -3i_b \quad (6.46)$$

$$i_b - i_c - i_c + i_a = -3i_c \quad (6.47)$$

$$i_c - i_a - i_a + i_b = -3i_a \quad (6.48)$$

From Equation (6.45)

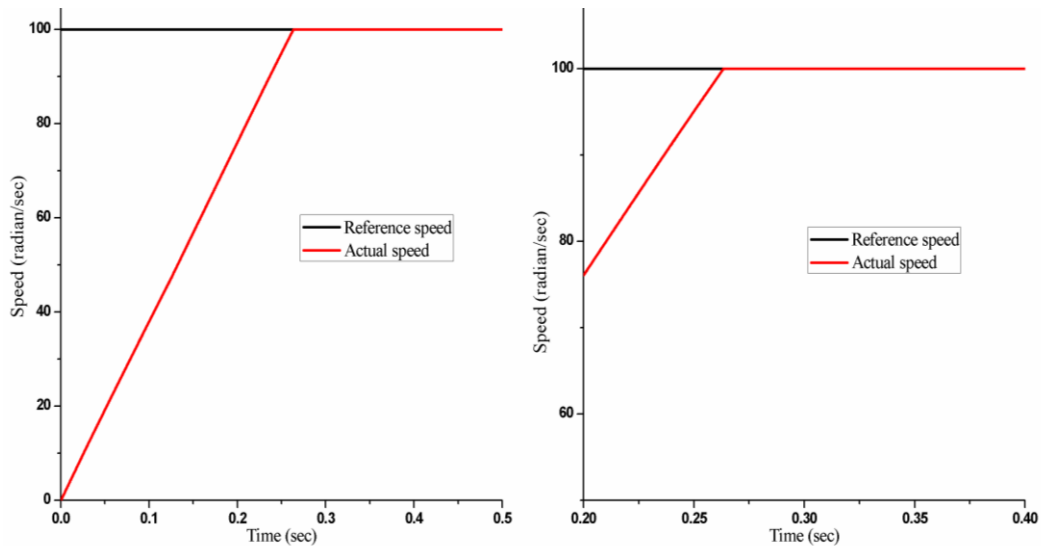
$$\begin{bmatrix} V_{ab} - V_{bc} \\ V_{bc} - V_{ca} \\ V_{ca} - V_{ab} \end{bmatrix} = \begin{bmatrix} R_s & 0 & 0 \\ 0 & R_s & 0 \\ 0 & 0 & R_s \end{bmatrix} \begin{bmatrix} -3i_b \\ -3i_c \\ -3i_a \end{bmatrix} + \frac{d}{dt} \begin{bmatrix} L - M & 0 & 0 \\ 0 & L - M & 0 \\ 0 & 0 & L - M \end{bmatrix} \begin{bmatrix} -3i_b \\ -3i_c \\ -3i_a \end{bmatrix}$$

$$+ \begin{bmatrix} e_a - e_b - e_b + e_c \\ e_b - e_c - e_c + e_a \\ e_c - e_a - e_a + e_b \end{bmatrix} \quad (6.49)$$

So, the equation 6.49 is known as new machine model for line voltage input. A new program is developed for new machine model because of replacing equation 2.14 by equation 6.49 in mathematical section of chapter 2. This new machine model is controlled by field oriented based ANFIS control system which is explained in previous section in this chapter.

6.10 Simulation Results for Line Voltage Model

A software using C++ program code is written for field oriented based ANFIS controller system of new machine model. The effectiveness of the drive system was studied through simulation in a PC environment. The parameters of the motor for simulation are given in Appendix A. For new machine model, the drive system was started from rest condition with reference speed of 100 radian per sec and load torque of 1.0 N-m. Speed characteristic is illustrated in Fig.6.15. From this figure, it is seen that PM Brushless DC motor based on ANFIS field oriented control drive takes 0.26 seconds to gain desire speed having no under or over shoot.



(a). Speed characteristic at starting condition (b) Speed response in zooming
 Fig.6.15: Speed characteristic for PMBLDC Motor based on Line Voltage Model

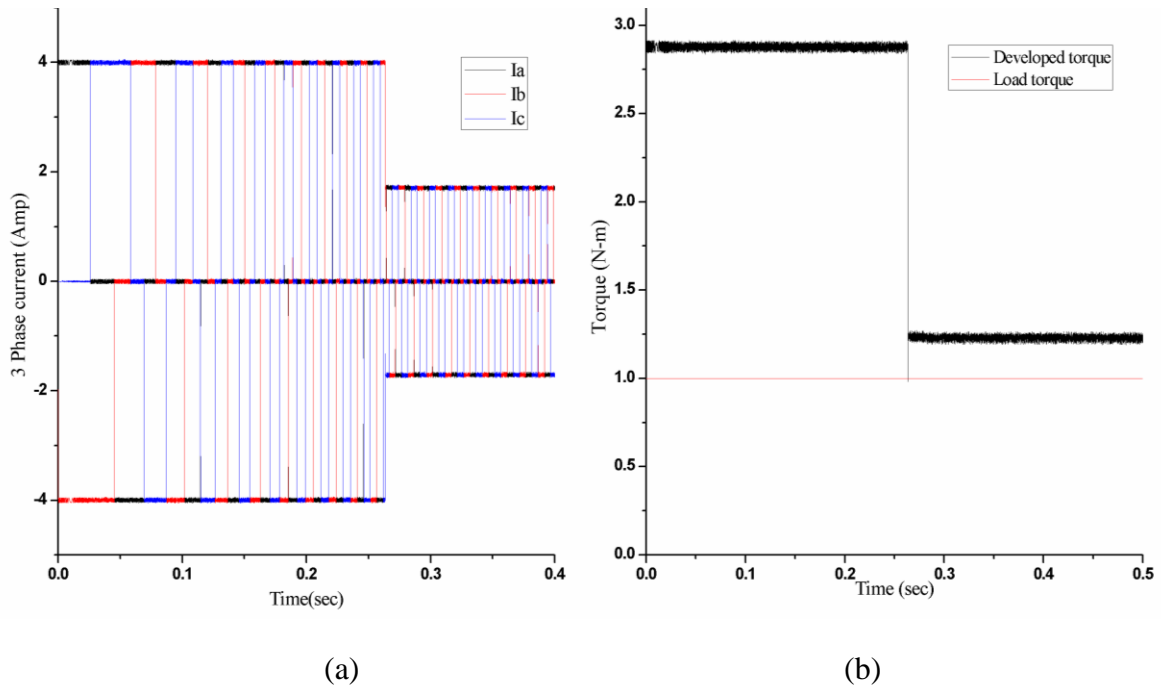


Fig.6.16: Illustration of (a) three phase current and (b) developed torque

Three phases current is controlled as well by requested load torque as shown in Fig.6.16 (a) and developed torque follows the requested load torque as shown in Fig.6.16 (b).

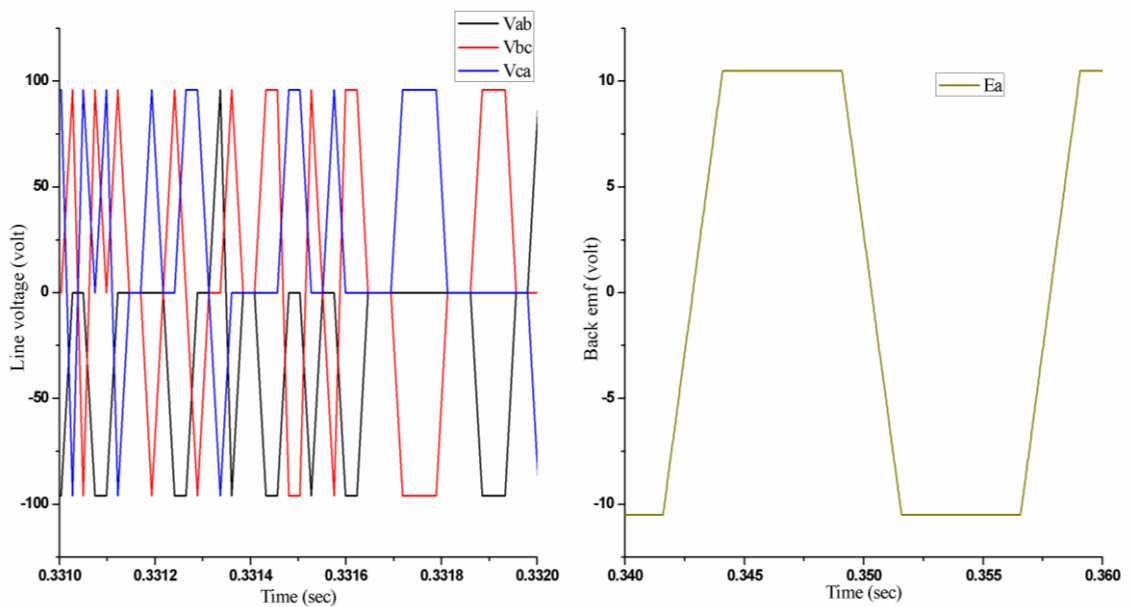


Fig.6.17: Illustration of (a) Line voltage and (b) Back emf based on Line Voltage Model

At starting condition, Fig.6.17 shows line voltage and single phase back emf based on line voltage model. Inverter output voltages are controlled according to requested dc input voltage and these line to line voltages are received by three phase stator winding in

Fig.6.17 (a). In steady state time single phase back emf which is trapezoidal nature as shown in Fig.6.17 (b).

6.11 Conclusion

In this chapter a new approach is studied to control PM Brushless DC Motor drive based on ANFIS types controllers which is designed on RBF, Takagi –Sugeno Model and Line voltage Model. From the simulation results we have seen that these controllers work effectively in closed loop control without any disturbance and ANFIS based controller with RBF updates all consequent and premise parameters to adjust motor speed. However it has large oscillation in motor phase current and developed torque. ANFIS controller based on Takagi- Sugeno Model has very negligible spikes in developed torque and phase current. Finally it is also seen that ANFIS Controller based on Line voltage model works as well.

CHAPTER VII

A CONTROLLER DESIGNED BASED ON WAVELET NEURAL NETWORK

The Chapter at a Glance

Introduction	Section 7.1
Structure of biological and artificial neuron	Section 7.2
Design of a Controller based on Wavelet Neural Network	Section 7.3
Gradient Descent Learning Rule	Section 7.4
Simulation Results	Section 7.5
Conclusion	Section 7.6

7.1 Introduction

Generally, artificial neural network is designed based on an easy mathematical model which has three functions such as summation, multiplication and activation function. It is called artificial neural network when more than one artificial neuron are interconnected with each other. In a general sense artificial neuron is an information processor. It receives input signals (multiplication of weight and information signal) on its body and sums these incoming signals. When sufficient incoming input signals are received, the neuron creates a pulse. An activation function is used to create this pulse which is also called transfer function. Hence artificial neural network has a capability to solve complex problem by adjusting weights between neuron connections. In this chapter wavelet is proposed in the hidden layer neuron as activation function that can locate input function by name of translation and dilation parameters. Combination of artificial neural network and wavelet is defined as wavelet neural networks (WNN). WNN has better performance to process information signal than conventional neural network [45]. Hence in this chapter a controller is designed based on wavelet neural networks for PM Brushless DC Motor drive. Gradient descent is used as a learning rule to train data so that weight, translation and dilation parameter can be update in automatically. The Performance is tested through Simulation by development in C++ software environment.

7.2 Structure of biological and artificial neuron

Artificial neuron works in similar way of biological neuron. Basic structure of biological neuron is depicted in Fig.7.1. Elementary nerve cell defined as biological neuron. It has three main parts those are dendrite, cell body (soma) and axon. Dendrite receives signal or information (input) from previous cells and carries it to cell body. Soma processes signal as well as passes it (output) on via axon. Axon carries this message away from cell body to next cell body. End of axon has terminal which gives the information to dendrite of next neuron and it is called axon terminal. End part of axon terminal and in face at dendrite of next neuron located synapse which carries the information from terminal and gives input to dendrite of next neuron. Artificial neuron is illustrated in Fig.7.2. Three inputs $x_1(k)$, $x_2(k)$ and $x_3(k)$ with corresponding weight $w_1(k)$, $w_2(k)$ and $w_3(k)$ come on artificial neuron body, where k indicates in discrete time. Then each input is multiplied with an individual weight and neuron body sums weighted inputs, bias. Finally processes it and passes process signal through an activation function to get output $y(k)$ [45].

$$y(k) = F \left(\sum_{i=0}^3 w_i(k)x_i(k) + b \right) \quad (7.1)$$

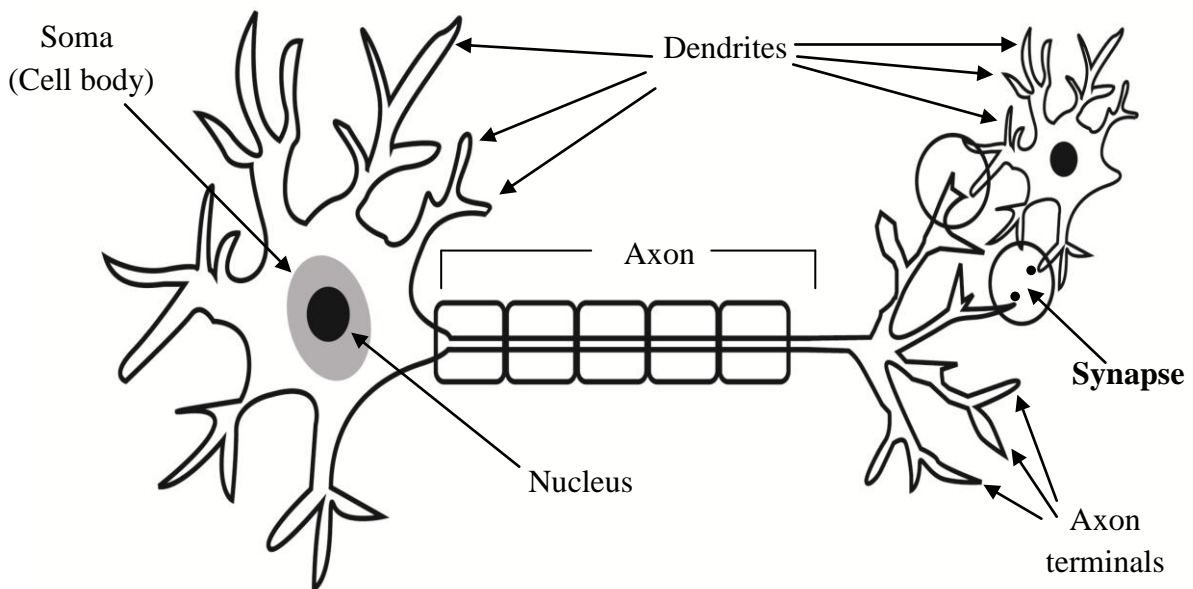


Fig.7.1: Structure of biological neuron

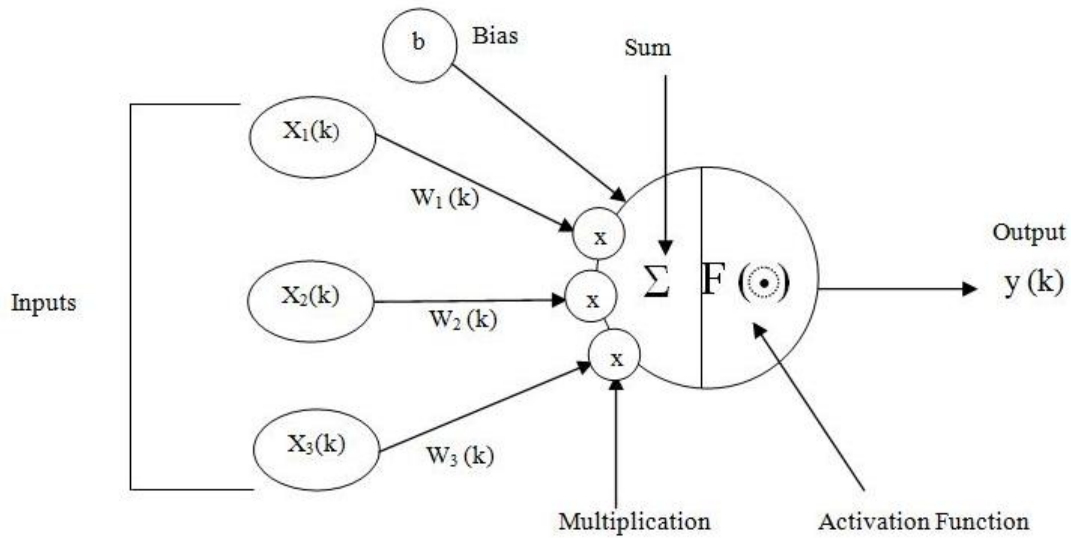


Fig.7.2: Structure of artificial neuron

7.3 Design of a Controller base on Wavelet Neural Network

A controller is designed based on WN network which consists of wavelet theory and feed-forward based neural network as shown in Fig.7.3. There are three layer in this controller such as k th, j th and i th layer which are present as input, hidden and output layer respectively. Input layer takes three inputs which is speed error, error difference between recent error and previous error in speed, error difference between error difference and error difference in previous time. Wavelet theory is proposed in hidden layer neuron so this neuron is called wavlon. Single neuron is placed in output layer that receives signal from hidden layer and gives an output which is input to PMBLDC motor [36].

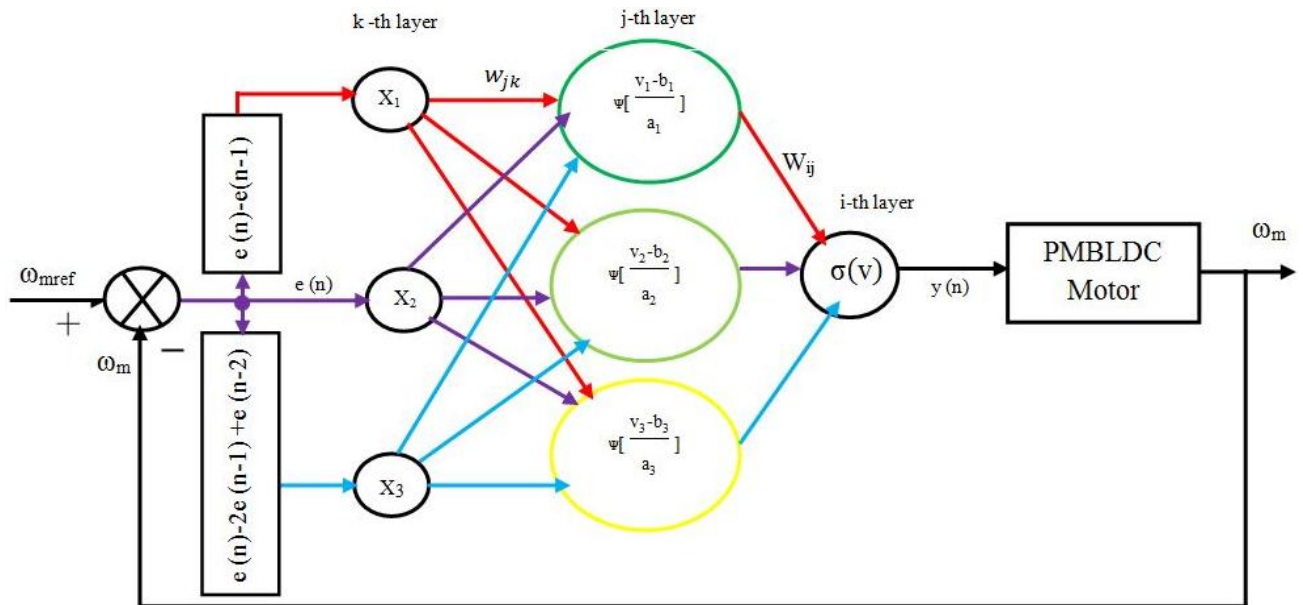


Fig.7.3: Controller based on WNN with PM Brushless DC motor

In this Figure $w_{jk}(n)$, $w_{ij}(n)$, $b_j(n)$ and $a_j(n)$ present as weight between hidden and input layer, weight between output and hidden layer, translating and dilation coefficients at n discrete time. Summation of multiplied weight and input variable at j -th hidden layer is written as [36]

$$V_j(n) = \sum_{k=0}^M w_{jk}(n) \cdot x_k(n) \quad (7.2)$$

Then $V_j(n)$ is passed into wavelet function that is indicated as

$$\psi_{a,b}[V_j(n)] = \psi\left[\frac{V_j(n)-b_j(n)}{a_j(n)}\right] \quad (7.3)$$

Gaussian derivative is a function which is indicated as wavelet function and written as

$$\psi(n) = -x \cdot e^{-0.5x^2} \quad (7.4)$$

Summation of multiplied weight (w_{ij}) and output $\psi_{a,b}[V_j(n)]$ of hidden layer is denoted as

$$V(n) = \sum_{j=0}^N w_{ij}(n) \cdot \psi_{a,b}[V_j(n)] \quad (7.5)$$

When $v(n)$ is passed through nonlinear activation function, output of this controller is found as [36]

$$y(n) = \sigma[V(n)] \quad (7.6)$$

In this research sigmoid activation is proposed.

$$\sigma(n) = K_k \frac{1}{1+e^{-x}} \quad (7.7)$$

Where, K_k is a factor of sensitivity.

7.4 Gradient Descent Learning Rule

Gradient descent learning rule works effectively in neural network to change dilation and translation coefficient, weight w_{jk} and w_{ij} which is identified in previous section. To get better performance cost function is defined as in n discrete time [36]

$$E(n) = 0.5e^2(n) = 0.5[y(n) - d(n)]^2 \quad (7.8)$$

The changing weight between hidden and input layer can be update as

$$\Delta w_{jk}(n+1) = -\eta \cdot \frac{\partial E(n)}{\partial w_{jk}(n)} + \mu \cdot \Delta w_{jk}(n) = \eta e(n) \sigma'[V(n)] \cdot w_{ij}(n) \psi_{a,b}'[V_j(n)] \cdot \frac{x_k(n)}{a_j(n)} + \mu \cdot \Delta w_{jk}(n) \quad (7.9)$$

Where, learning rate is indicated as η . The changing weight between j -th and i -th layer can be adjusted as [36].

$$\Delta w_{ij}(n+1) = -\eta \cdot \frac{\partial E(n)}{\partial w_{ij}(n)} + \mu \cdot \Delta w_{ij}(n) = \eta e(n) \sigma' [V(n)] \cdot w_{ij}(n) \psi_{a,b} [V_j(n)] + \mu \Delta w_{ij}(n) \quad (7.10)$$

In the j-th layer changing of translation can be updated as following equation [36]

$$\Delta b_j(n+1) = -\eta \cdot \frac{\partial E(n)}{\partial b_j(n)} + \mu \cdot \Delta b_j(n) = -\eta e(n) \sigma' [V(n)] \cdot w_{ij}(n) \psi_{a,b} [V_j(n)] \cdot \frac{1}{a_j(n)} + \mu \Delta b_j(n) \quad (7.11)$$

Changing of dilation coefficient is written as

$$\Delta a_j(n+1) = -\eta \cdot \frac{\partial E(n)}{\partial a_j(n)} + \mu \cdot \Delta a_j(n) = -\eta e(n) \sigma' [V(n)] \cdot w_{ij}(n) \psi_{a,b} [V_j(n)] \cdot \frac{V_j(n) - b_j(n)}{a_j(n)^2} + \mu \Delta a_j(n) \quad (7.12)$$

7.5 Simulation results

The performance of proposed drive system was tested through the simulation. A C++ program code is developed to generate data and this data is imported in data analysis origin software to obtain result. For the simulation, parameter of PM Brushless DC Motor is given in Appendix A.

Here reference speed is 100 rad/sec and load torque is 1 N-m for proposed controller based on wavelet neural network. Speed response as revealed in Fig.7.4 where the controller tracking the reference speeds within 0.26 sec and it has slight speed overshoot.

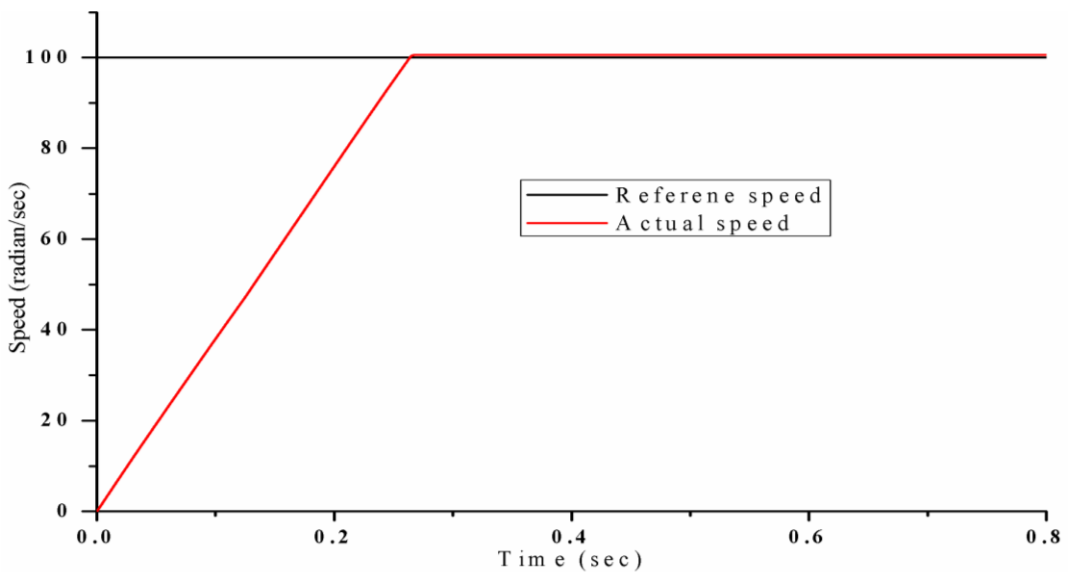


Fig.7.4: Motor speed response is exhibited for WNN based controller

Fig.7.5 illustrates as response of developed torque and quadrature axis current for this proposed controller. It is observed that during starting developed torque and I_{qr} is high and both are fallen when speed tracking the reference speed. It is also seen that developed torque follows load torque at 0.26 sec

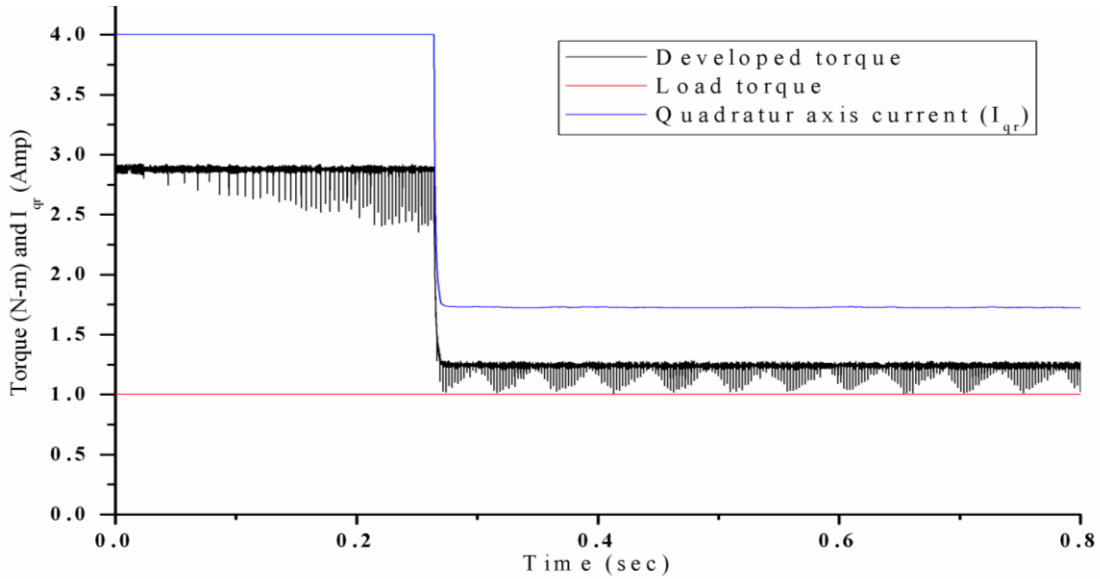


Fig.7.5: Response of developed torque and I_{qr} during starting condition

Fig.7.6 shows stator phase current which is obtained as square wave. Actual speed before reaching reference speed motor draws maximum current of 4.Amp.

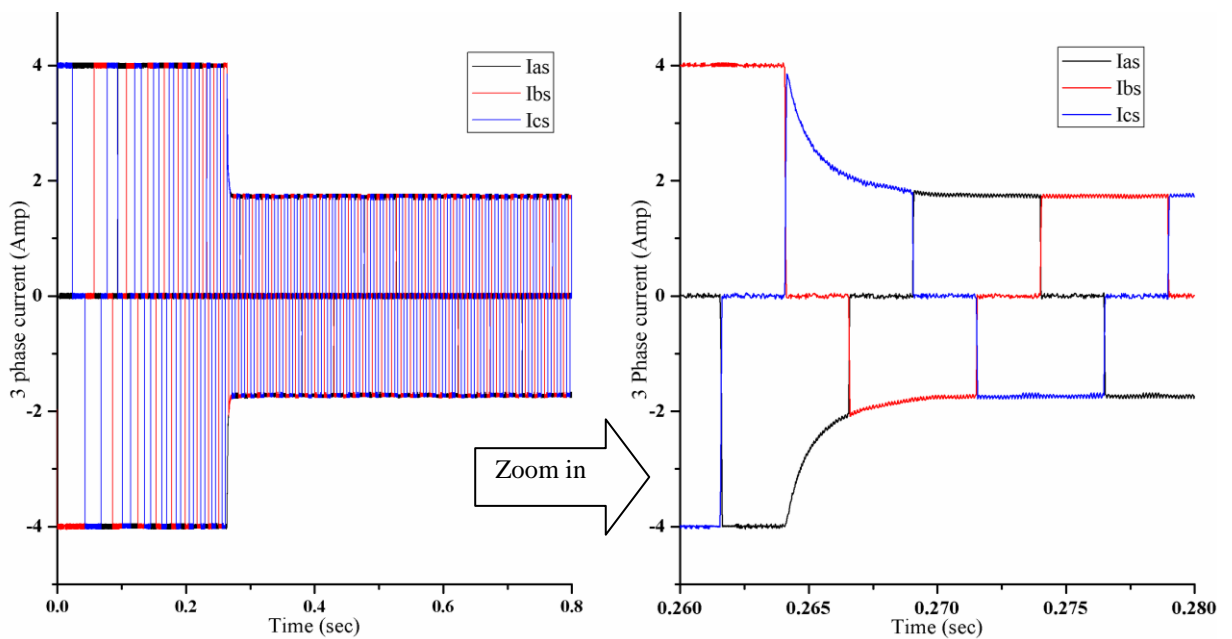


Fig.7.6: Stator phase current is displayed at starting condition for proposed controller

When motor reaches reference speed, phase current is decreased smoothly based on load torque. In this time motor draws near about 1.8 Amp.

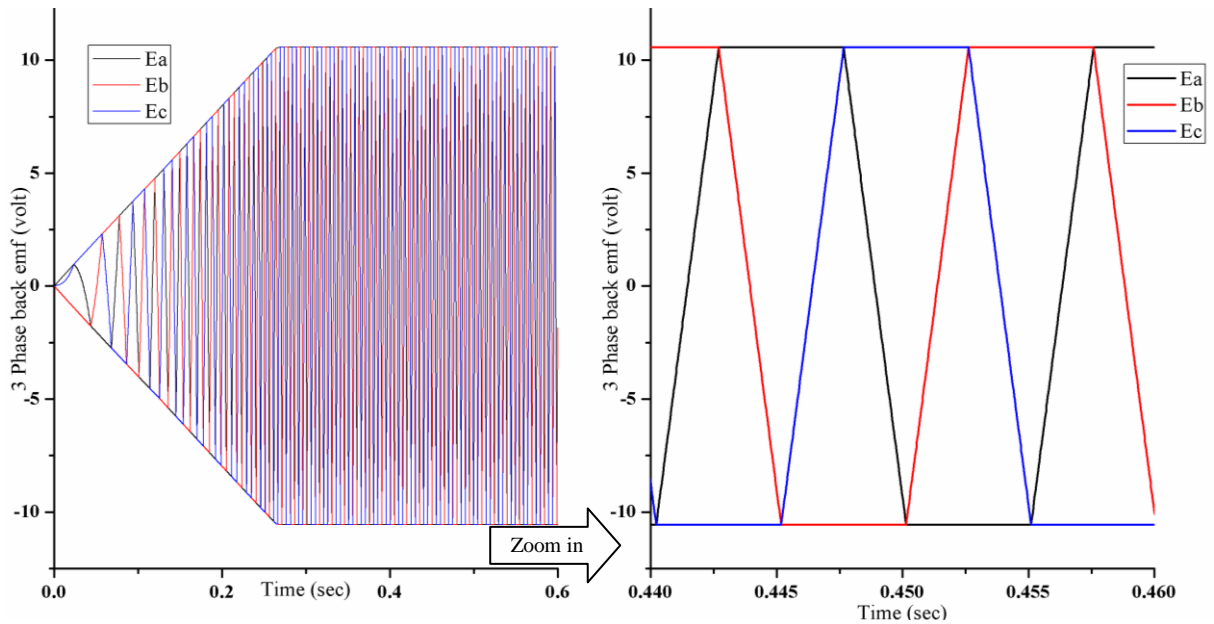


Fig.7.7: Three phase back emf for WNN based controller

At starting condition 3 phase back emf is displayed in Fig.7.7. It is noticed that initial back emf is zero but when motor obtains desire speed then back emf become trapezoidal shape as shown zoom in figure.

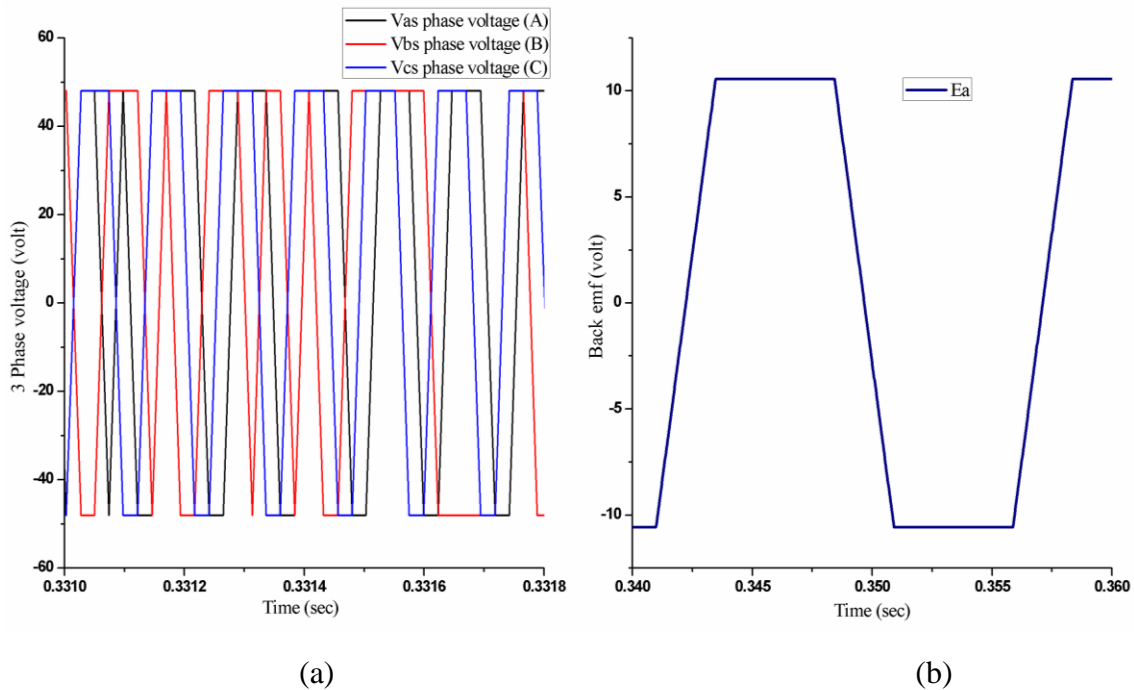


Fig.7.8: Illustration of (a) 3 phase voltage and (b) single phase back emf

At starting condition three phase voltage and single phase back emf are plotted in Fig.7.8. From the Fig.7.8 (a), it is seen that controller output voltages are controlled according to dc input voltage of 48 volt. Single phase back emf in steady state time is looking as smooth trapezoidal nature as shown in Fig.7.8 (b).

7.6 Conclusion

In this chapter it is seen that proposed controller works effectively because of it has better speed and torque control capability. It is also observed that current is controlled smoothly according to load torque. Parameters of weight, dilation and translation are updated based on gradient descent learning rule. This control system becomes introduced newly for PM Brushless DC motor.

CHAPTER VIII

SIMULATION RESULTS AND PERFORMANCE ANALYSIS OF PROPOSED CONTROLLERS

The Chapter at a glance

Introduction	Section 8.1
Performance Analysis for Constant Torque Starting Condition	Section 8.2
Performance Analysis for Speed Variation Condition	Section 8.3
Effect on Performance due to Changing Load Torque	Section 8.4
Effect on Performance due to Changing Parameter	Section 8.5
Conclusion	Section 8.6

8.1 Introduction

In this chapter simulation results and performance are discussed for the controllers we have designed in the earlier chapters, viz. fixed PI, Single Neuron based Adaptive Controller, Single Neuron based Adaptive PID Controller, Wavelet Neural Network (WNN) based Controller and ANFIS type Controller. Drive performance is compared applying these controllers under different operating conditions. In this research closed loop speed and current control are employed which are defined as outer and inner control loop respectively. Square wave reference current and sinusoidal wave reference current are generated from this current control loop. These reference currents are proposed as input current of PMBLDC Motor. In chapter III, we observed that motor speed response is faster when motor input current is proposed as square wave reference current. Hence in this research square wave reference is proposed to get better performance. The performance of drive system is tested under different dynamic conditions such as constant torque starting condition, sudden load torque change, speed variation and changing parameters. Finally, results are compared among proposed controllers through C++ simulation tools.

8.2 Performance Analysis for Constant Torque Starting Condition

At constant load torque starting condition, drive performance was tested with a reference speed of 100 radian per sec as step function and constant load torque of 1.0 N-m for the controllers (1) Fixed PI Controller, (2) Single Neuron based Adaptive (SNA) Controller, (3) Single Neuron based Adaptive PID (SNAPID) Controller, (4) ANFIS based Controller with Radial Basis Function, (5) ANFIS Controller based on Takagi-Sugeno Model, (6) ANFIS Controller based on Line voltage model and (7) Wavelet Neural Network (WNN) based Controller. Actual motor speeds using all these controllers reach the desired or set speed around 0.26 sec as shown within Fig.3.3, Fig.4.3, Fig.5.3, Fig.6.3, Fig.6.11, Fig.6.15 and Fig.7.4. But some overshoot is observed in Fig.3.3 and Fig.7.4 with fixed PI and WNN based controller respectively. With other controllers no oscillations is observed and the response is ramp variation. Developed torques for all cases with the controllers settle closer to load torque as the speed reaches to reference value at near about 0.26 sec as shown in Fig.3.7 (b), Fig.4.8, Fig.5.7, Fig.6.4 (b), Fig.6.12 (b), Fig.6.16 (b) and Fig.7.5. Developed torques of all controllers based drives follow load torque as well with insignificant oscillation at steady state conditions.

Three phase currents are adjusted when actual motor speed accelerating to reach the reference speed as indicated in Fig.3.8, Fig.4.10, Fig.5.9, Fig.6.4 (a), Fig.6.12 (a), Fig.6.16 (a) and Fig.7.6. It is seen that phase currents are controlled for the all proposed controllers. Three phase voltage for all controllers are changed as well as shown in Fig.3.5, Fig.4.11, Fig.5.11, Fig.6.13, Fig.7.8 and line voltage is also controlled as well in Fig.6.17 (a).

8.3 Performance Analysis for Speed Variation Condition

For speed variation condition, the motor was run with set speed of 100 rad/ sec and load torque of 1.0 N-m. After 0.45 sec set speed was decreased from 100 radian per sec to 50 rad/sec., after then 0.80 sec set speed was increased from 50 rad/sec to 150 rad/sec. The speed response and other performance were tested for the same controllers mentioned in Art 8.2 with the PMSBLDC Motor drive system. Actual speed follows set speed promptly by fixed PI controller as shown in Fig.8.1 (a) but it has small speed overshoot and undershoot. The back emf is shown in Fig.8.1 (b) but it is seen that back emf increases or decreases smoothly with increasing or decreasing speed. When set speed is changed at 0.45 sec from 100 rad/sec to 50 rad/sec no high value of transient current exists as indicated in

Fig.8.1 (c). It is observed that phase current is increased to overcome inertia for increasing speed from (50 to 100) rad/sec at 0.8 sec.

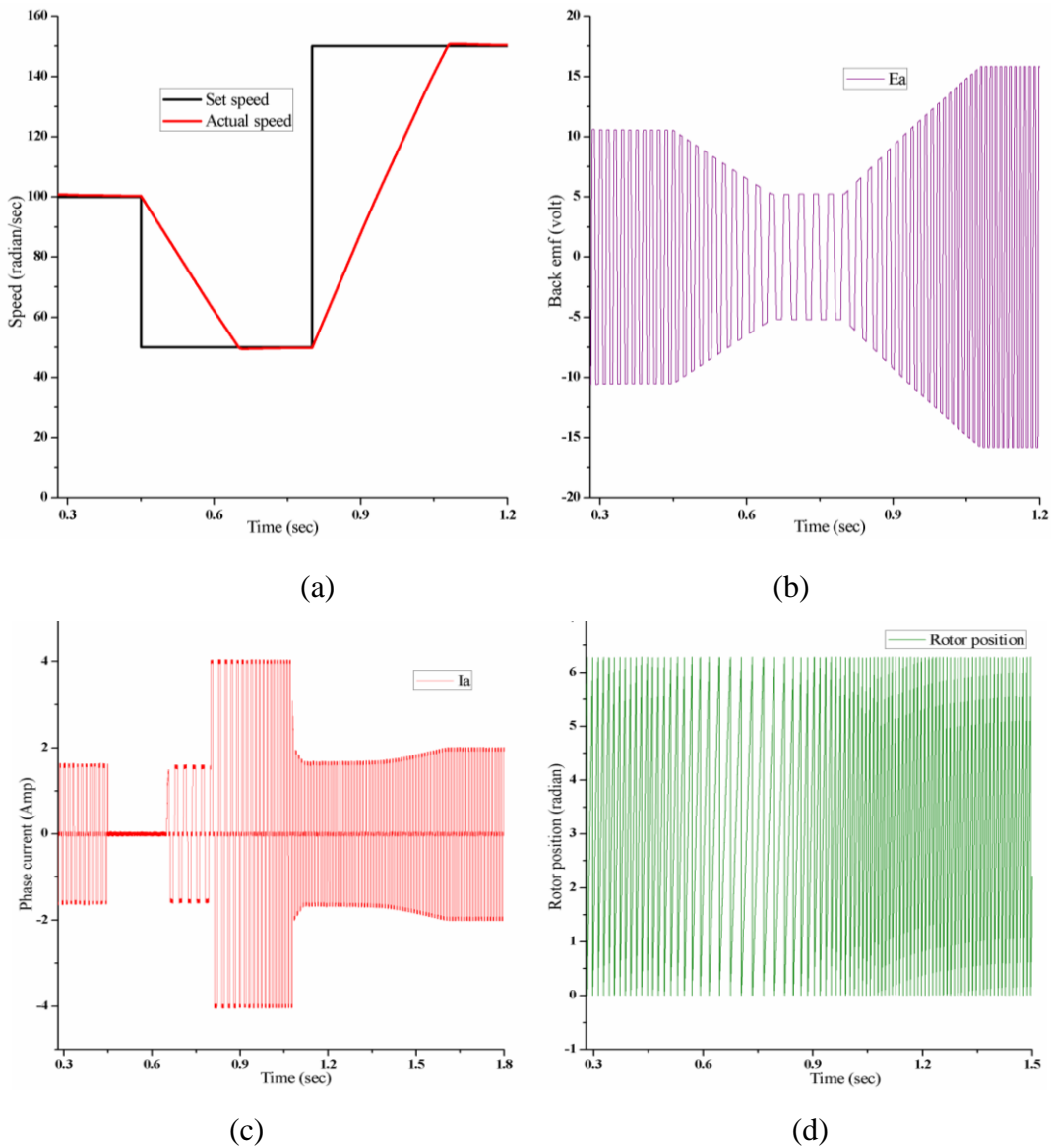


Fig.8.1: (a) Speed response, (b) Single phase back emf, (c) Phase current and (d) Rotor position by fixed PI controller

Unidirectional rotor position is changed from 0 to 6.2832 radian as shown in Fig.8.1 (d). Its position is changed according to command of set speed but it has some spikes. Now performance was tested by Single Neuron based Adaptive controller and it is noticed that actual speed follows the set speed sharply having no overshoot or undershoot in speed as illustrated in Fig.8.2 (a). Back emf variation is changed smoothly by speed variation in Fig.8.2 (b). Motor phase current is controlled as well as shown in Fig.8.2 (c) when set speed is decreased at 0.45 sec and increased at 0.80 sec. Rotor position variation as

depicted in Fig.8.2 (d) and it is observed that rotor position is changed slowly and firstly for the decrement and increment of set speed at time 0.45 sec and 0.80 sec.

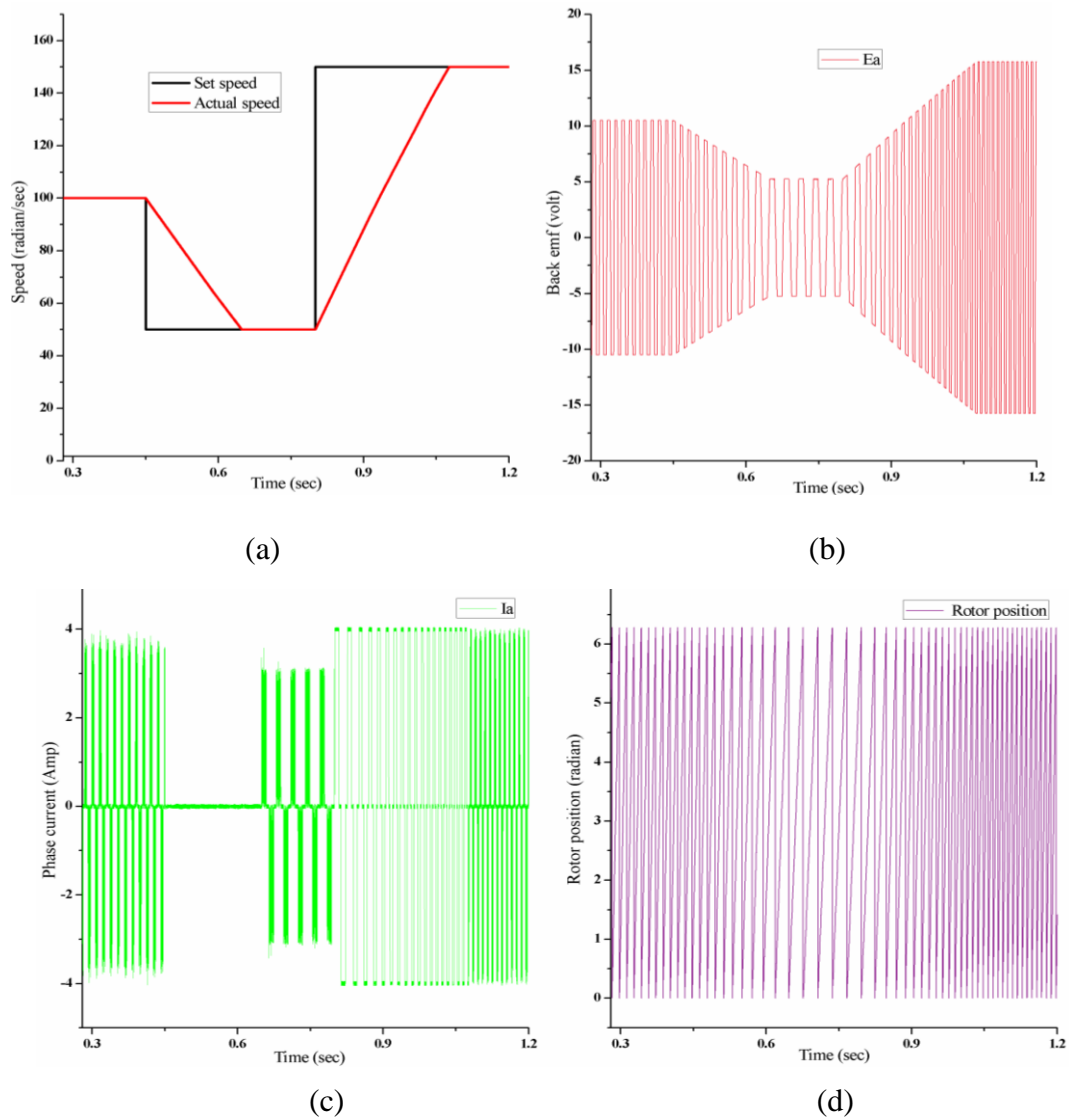


Fig.8.2: (a) Speed response, (b) Single phase back emf, (c) Phase current and (d) Rotor position by SNA controller

Fig.8.3 shows that all weights are updated through online to adjust motor speed by Single Neuron based Adaptive Controller. Initially weight w_{11} is updated from -0.055 to 0.00 and weight w_{22} is updated from 425000 to 0.0 obtaining set speed 100 rad/sec but weight w_{33} varies between 0.020 and -0.020. Gradually variation of w_{33} becomes 0.0 that is indicated in Fig.8.3(c). All weights remain unchanged when speed is decreased at 0.45 sec. Finally, if set speed is increased from (50 to 150) rad/sec at time 0.80 sec then all weights are updated in the similar way as that of initial step change in speed.

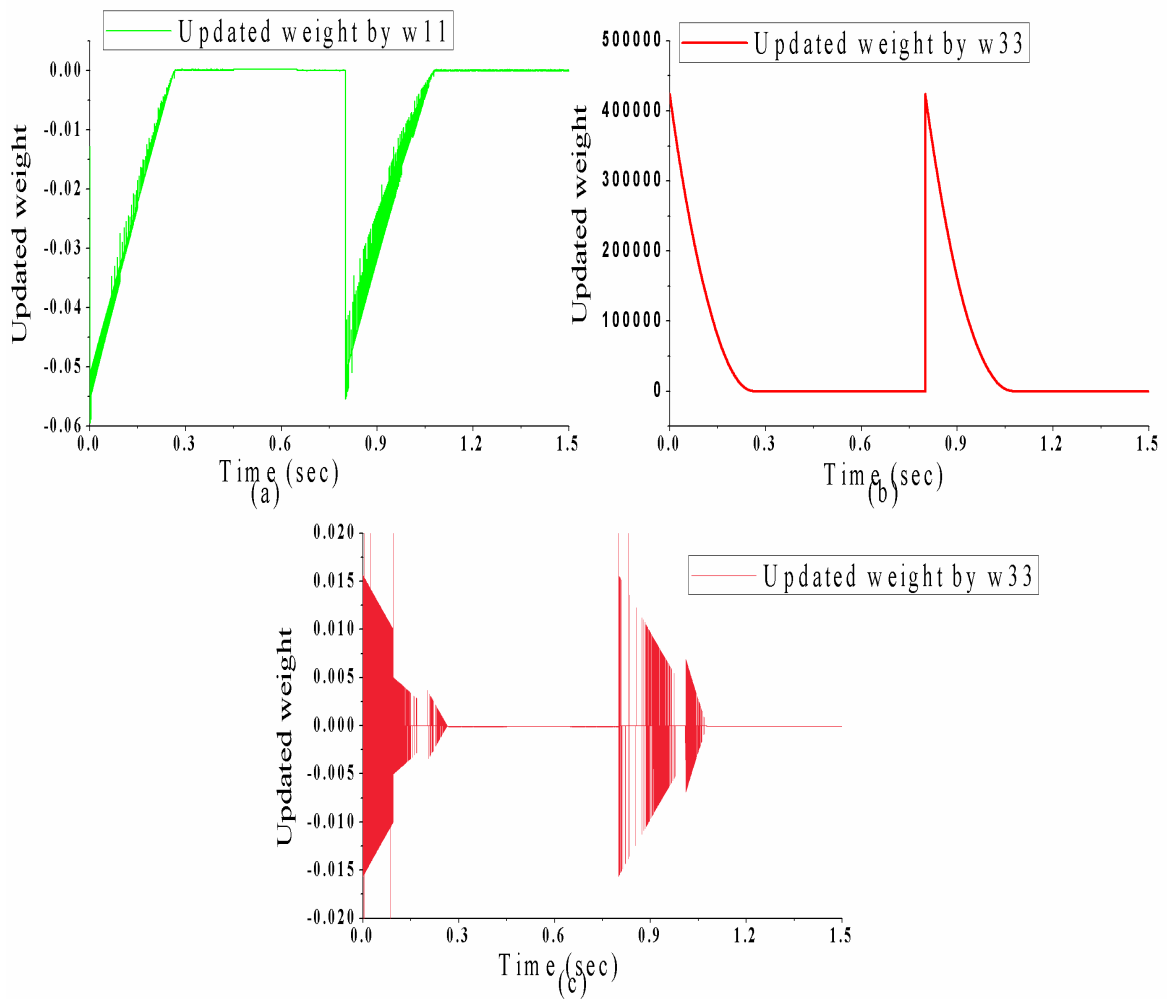


Fig.8.3: Updated weights with SNA controller

Speed variation performance is tested using ANFIS based controller with RBF. At 0.45 sec set speed is reduced to 50 rad/sec in that time motor speed tracks the set speed at 0.65 sec as shown in Fig.8.4 (a). Finally, it reaches set speed almost 1.5 sec later for the speed increasing to 150 rad/sec following the reference. Back emf and rotor position is controlled smoothly according to command speed as shown in Fig.8.4 (b) and Fig.8.4 (d) respectively. It is noticed that motor phase currents are controlled as shown in Fig.8.4 (c).

To follow the reference speed weight is updated from 0.63 to 1.0 as indicated in Fig.8.5 (a). Then it is decreased rapidly and its value is increased from 0.88 to 1.0 when set speed is decreased to 50 rad/sec at 0.45 sec. Finally, again, it is decreased in the previous way and its value is increased from 0.61 to 1.0 when command speed is increased to 150 rad/sec at 0.80 sec. Consequent parameter p_i increases linearly for the increment of set

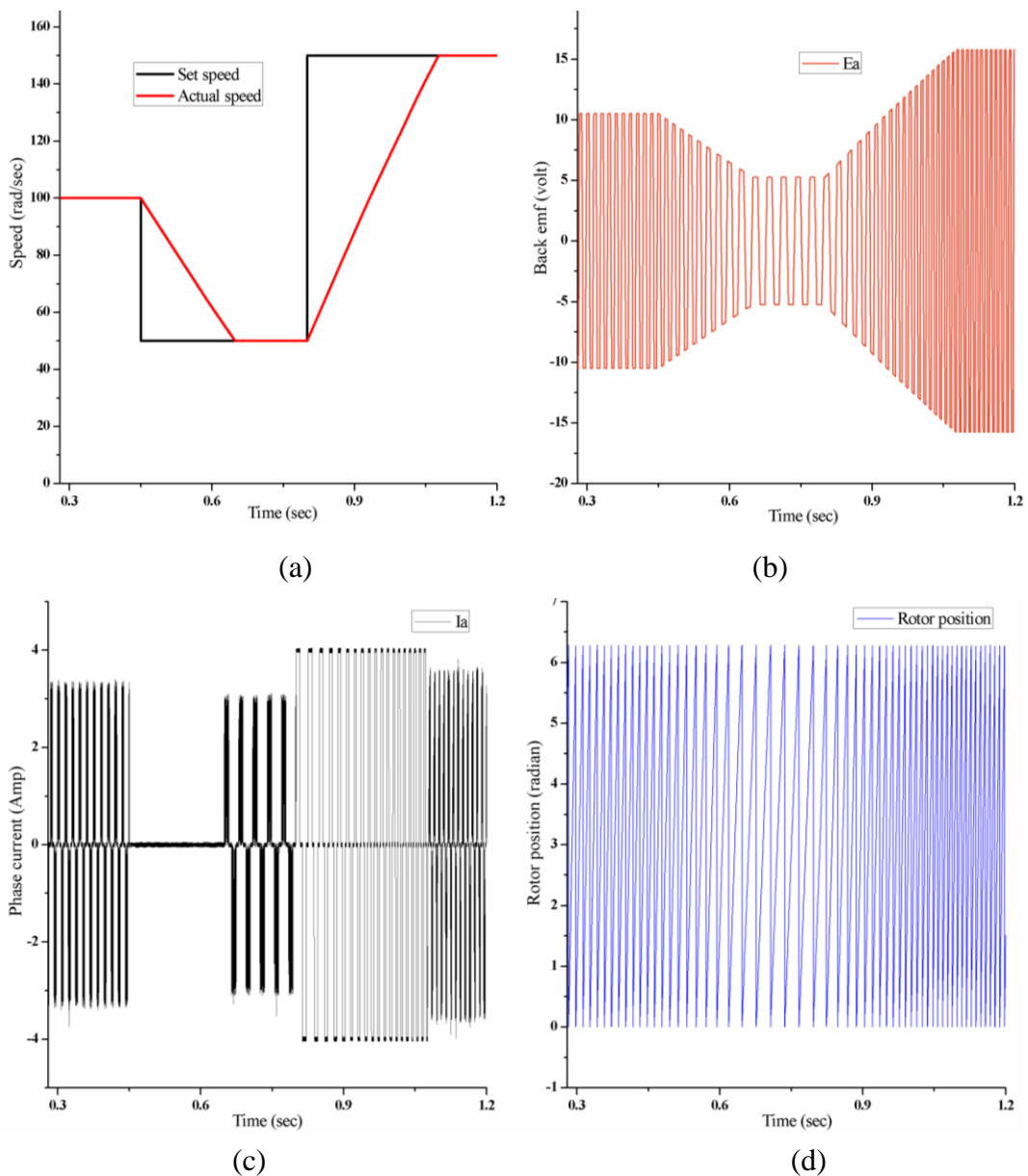
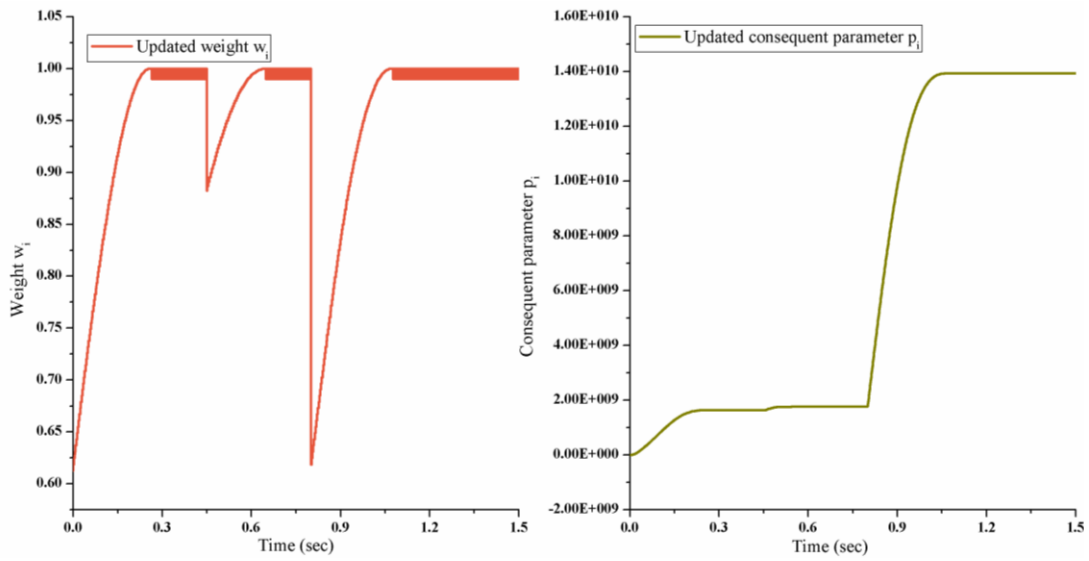


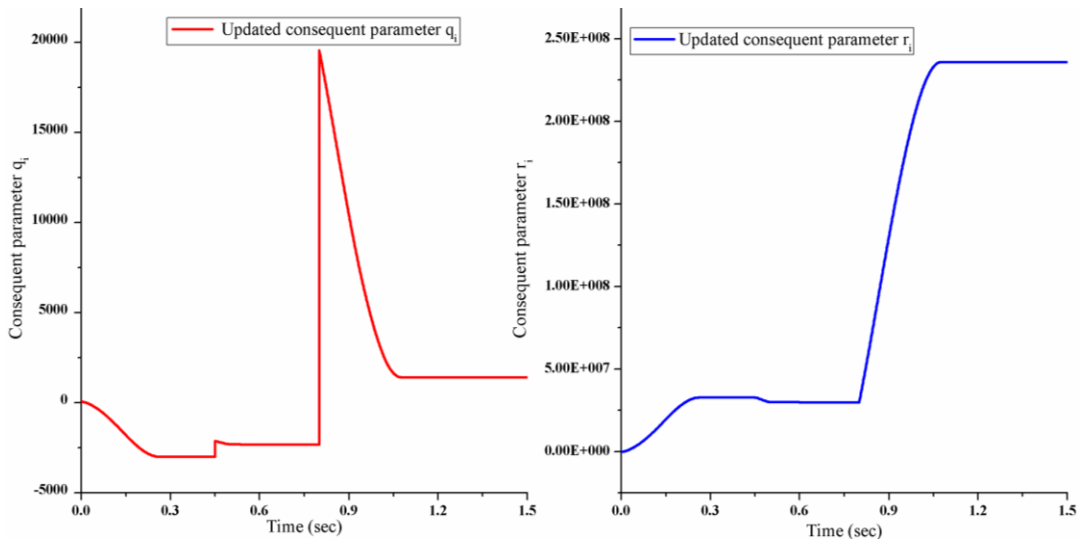
Fig.8.4: (a) Speed response, (b) Back emf, (c) Phase current and (d) Rotor position for the ANFIS based controller with RBF

speed as shown in Fig.8.5 (b) but p_i also increases slightly when command speed is decreased at 0.45 sec. Parameter r_i is updated in the same way of p_i but it has a different value, Also r_i is decreased slightly when speed is decreased at 0.45 sec as shown in Fig.8.5 (d). Initially q_i decreases gradually and its value becomes constant when motor speed reaches set speed. After that it increases slightly for decreasing speed at 0.45 sec and becomes constant gradually. Finally, its value increases very rapidly when set speed is changed from 50 to 150 rad/sec and the drive reaches that at time 0.80 sec and becomes stable as shown in Fig.8.5 (c).



(a)

(b)



(c)

(d)

Fig.8.5: (a) Weight w_i , (b) Consequent parameter p_i , (c) Consequent parameter q_i and Consequent parameter r_i by ANFIS based controller with RBF

The drive performance was tested with ANFIS controller based on Takagi- Sugeno Model. Motor speed follows set speed having no oscillation as shown in Fig.8.6 (a). Back emf depends on motor speed and it is found to change smoothly as shown in Fig.8.6 (b). The rotor position is changed slowly or firstly with respect to lower or higher speed as shown in Fig.8.6 (d). Motor phase current is rapidly decreased or increased for the decrement or increment of set speed as illustrated in Fig.8.6 (c).

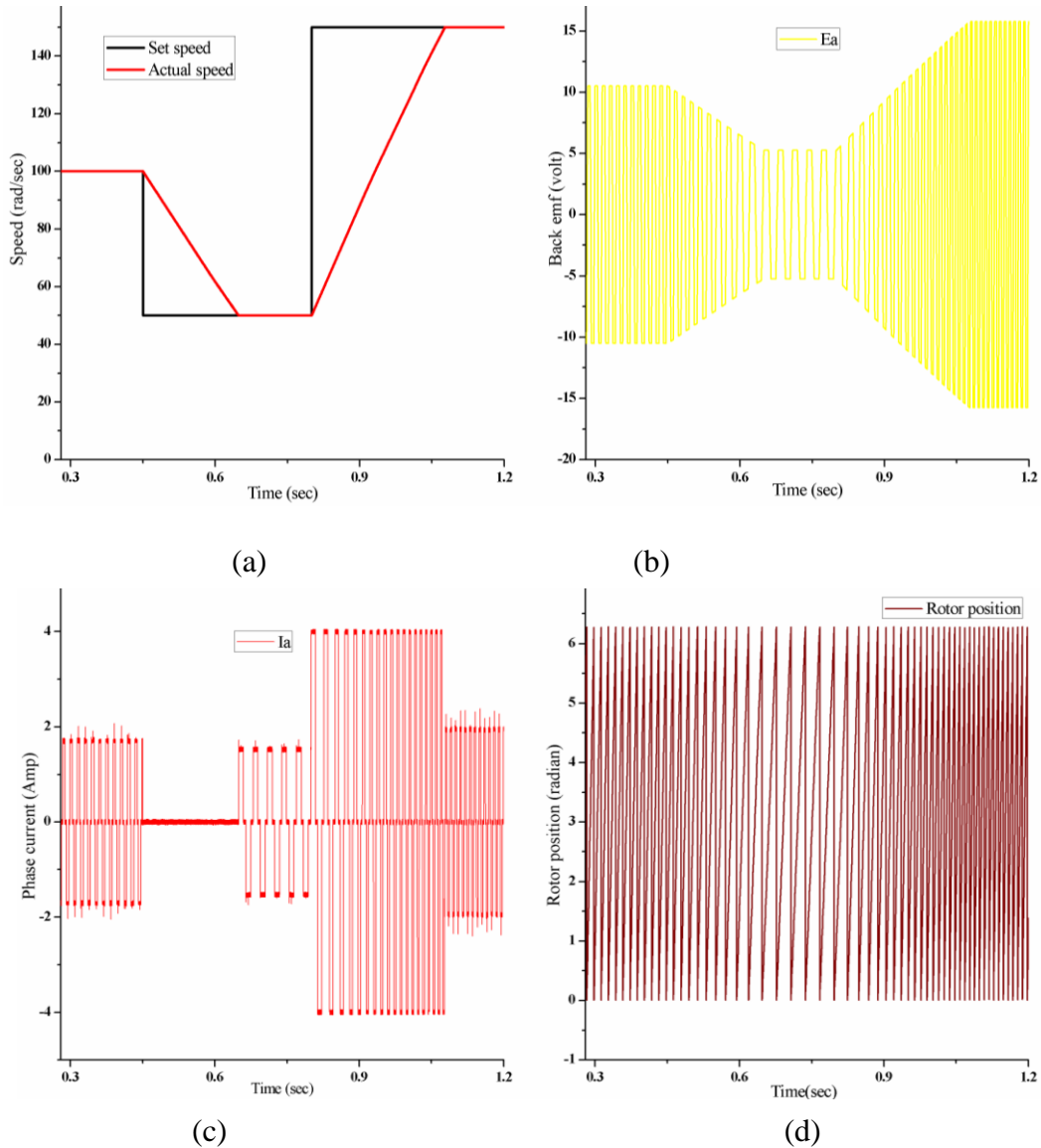


Fig.8.6: (a) Speed characteristic, (b) Back emf, (c) Phase current and (d) Rotor position by ANFIS Controller based on Takagi-Sugeno Model

The drive performance was tested by ANFIS controller based on Line Voltage Model. Fig.8.7 (a) shows that actual speed having no appreciable change and it tracks set speed smoothly at all speed changing conditions. Back emf is changed as well when set speed mode is changed as depicted in Fig.8.7 (b). Motor phase current is controlled as well and it has no spikes in all speed changing cases as displayed in Fig.8.7 (c). Fig.8.7 (d) shows rotor position is changed in three cases; those are fastly, slowly and more rapidly with respect to speeds of 100 rad/sec, 50 rad/sec and 150 rad/sec.

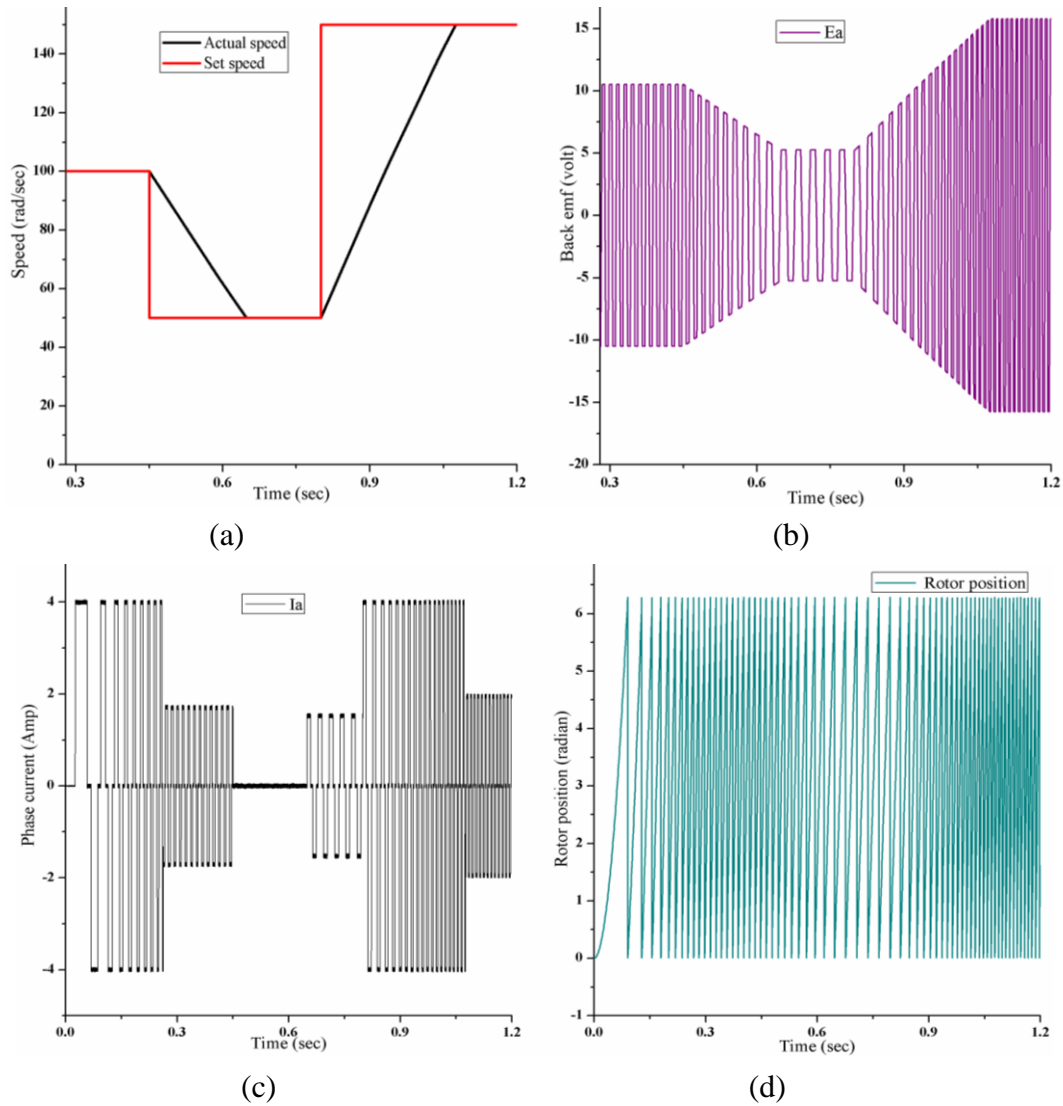
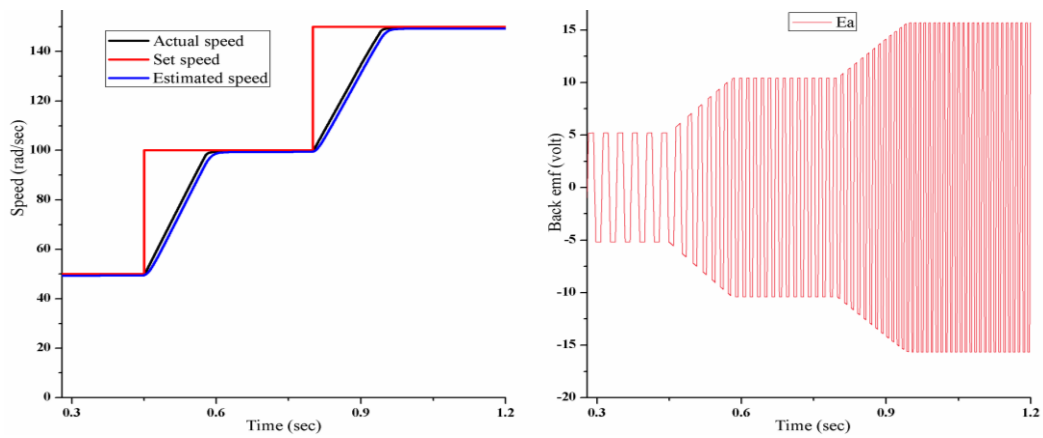


Fig.8.7: (a) Speed characteristic, (b) Single phase back emf, (c) Phase current and (d) Rotor position by ANFIS Controller based on Line Voltage Model

Now performance of the drive system is tested by Single Neuron based Adaptive PID controller with a single neuron based speed estimator. At the beginning motor was run with a set speed of 50 rad/sec and load torque of 1.0 N-m. Fig.8.8 (a) shows that actual speed and estimated speed track set speed very closely. Estimated speed differs only slightly from the actual speed as shown speed. Set speed was changed to 100 rad/sec and 150 rad/sec at time of 0.45 sec and 0.80 sec respectively. For this reason the drive reaches the set speed within 0.60 sec and 0.975 sec respectively. Fig.8.8 (b) indicates back emf which is directly proportional to motor speed i.e. back emf is increased when speed is increased. Back emf remains stable when motor speed becomes constant. Motor phase current is increased slightly to overcome additional mechanical inertia with increment of motor

speed as shown in Fig.8.8(c). Rotor position is changed as well as shown in Fig.8.8 (d) at different speed changed modes.



(a)

(b)

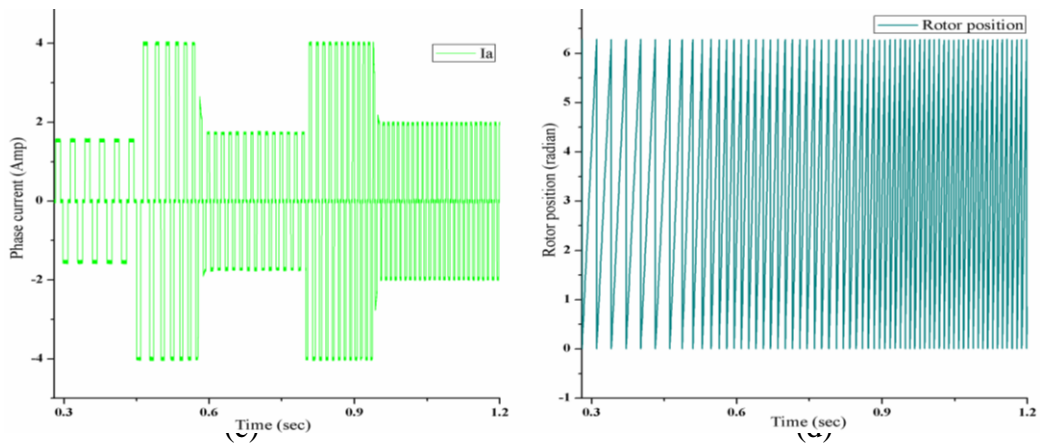
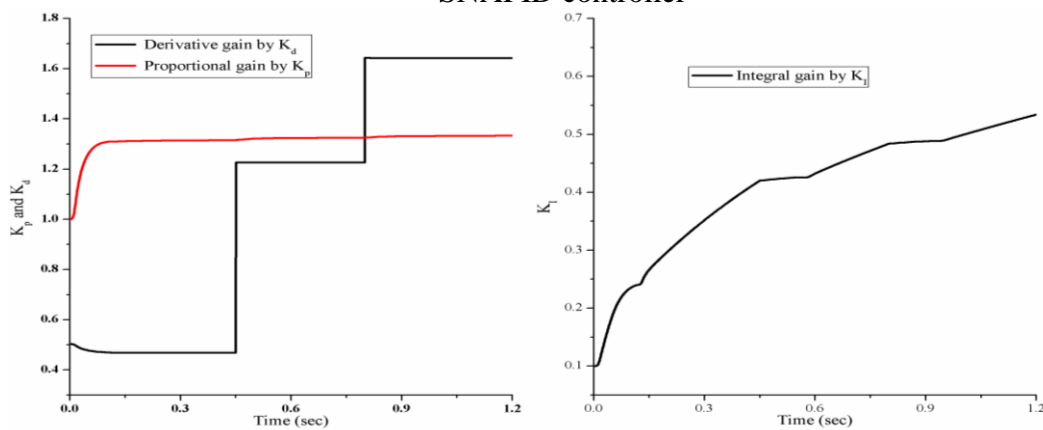


Fig.8.8: (a) Speed characteristic, (b) Back emf, (c) Phase current and (d) Rotor position by SNAPID controller



(a) Proportional and Derivative gain

(b) Integral gain

Fig.8.9: Response of K_p , K_i and K_d gain by SNAPID controller

Fig.8.9 (a) shows values of K_p and k_d which are increased with increment of set speed. K_d is increased very rapidly but k_p is increased very slowly when set speed is increased. Value of K_i is increased linearly when motor command speed is increased in Fig.8.9 (b).

The drive performance was checked by WNN based controller. Actual speed follows set speed but it has slight speed overshoot as shown in Fig.8.10 (a). Back emf variation is changed as well in Fig.8.10 (b). Phase current is controlled smoothly in all speed changed modes as indicated in Fig.8.10(c). Rotor position is also changes as well in different speed changing modes as illustrated in Fig.8.10 (d).

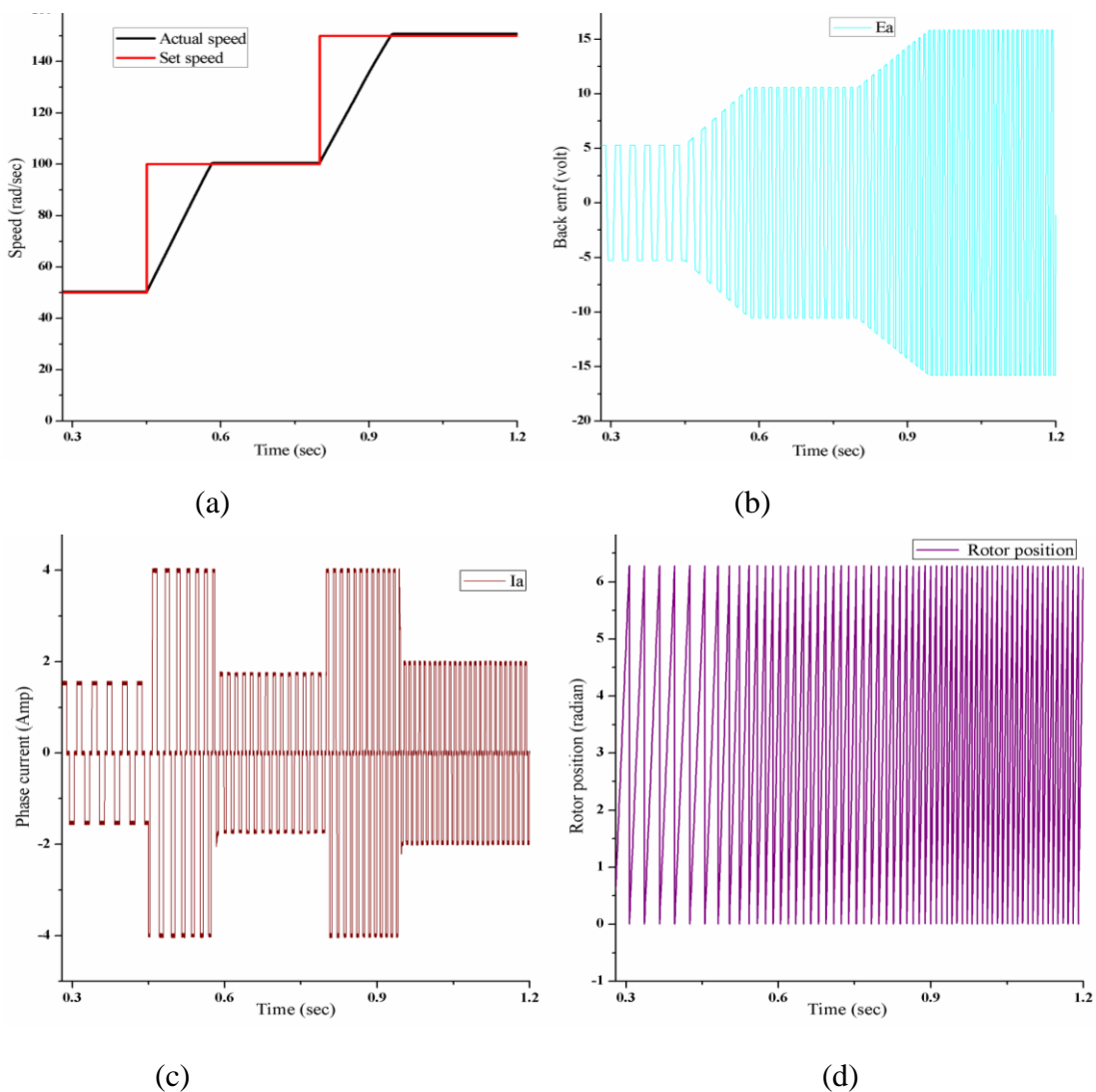


Fig.8.10: (a) Speed characteristic, (b) Back emf, (c) Phase current and (d) Rotor position by WNN based controller

8.4 Effect on Performance due to Changing Load Torque

Firstly motor was run with load torque of 1.0 N-m and reference speed of 100 rad/s. At 0.45 sec load torque was increased by 50 % of initial torque. The drive system performance was tested for the Fixed PI Controller. It is observed that motor speed is fall due to increment of load torque as given in Fig.8.11 (a) and small back is also changed as shown in Fig.8.11 (b) due to increment of load torque. Fig.8.11 (c) presents motor phase current and it is clear that motor draws more phase current at 0.45 sec causing load torque increment. It is also seen that developed torque is increased as shown in Fig.8.11 (d) for the increment of demand torque.

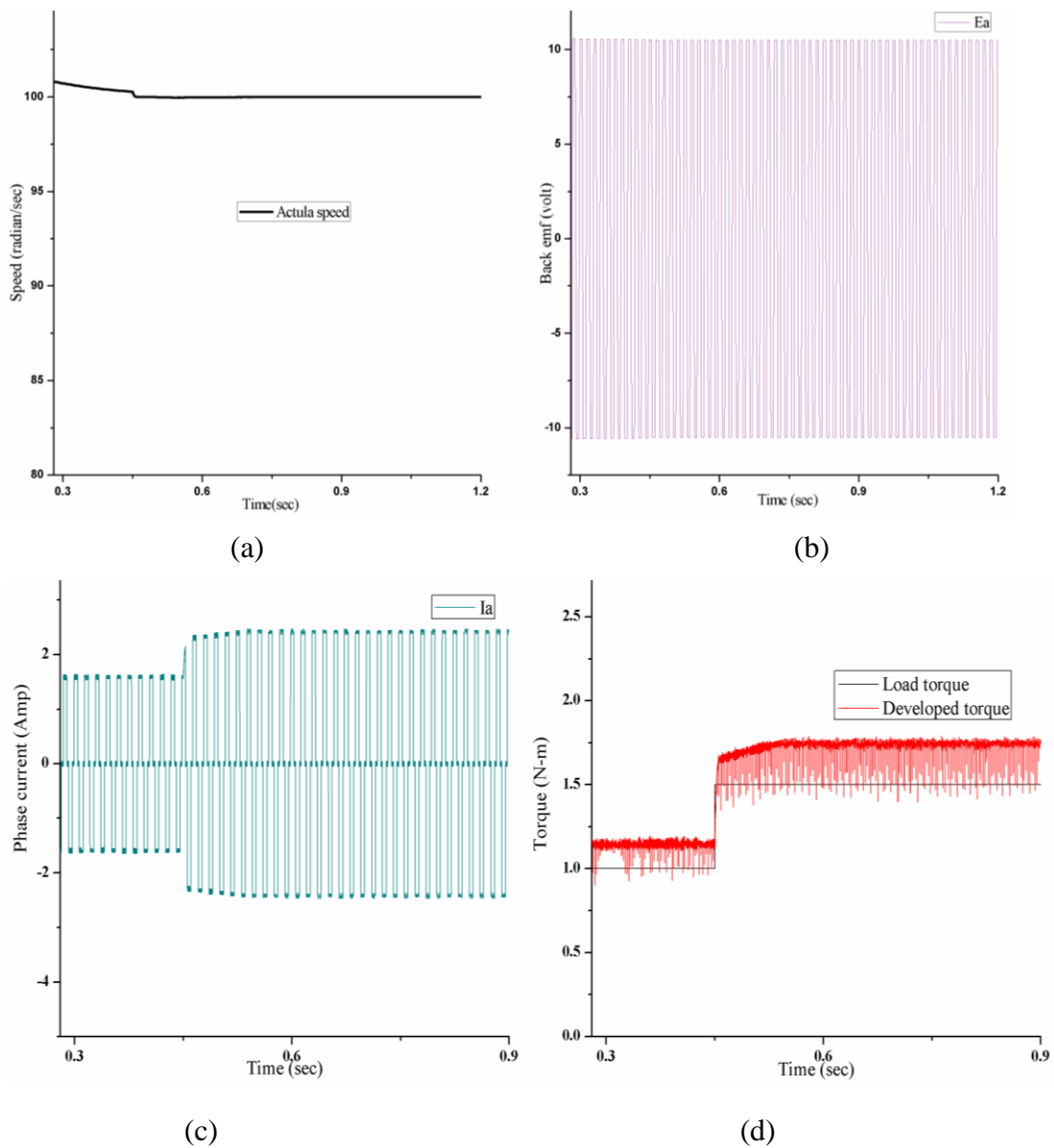


Fig.8.11: (a) Speed response, (b) Back emf, (c) Phase current and (d) Torque response by fixed PI controller

Drive effectiveness was tested for Single Neuron based Adaptive controller. Fig.8.12 (a) and Fig.8.12 (b) show speed characteristic and phase back emf respectively. It is seen that no appreciable change in motor speed and phase back emf for the increment of 50% load torque. Fig.8.12 (c) indicates motor phase current which draws more current for load torque changing mode. Developed torque is controlled according to demand torque that is predicted in Fig.8.12 (d) indicates very fast controller.

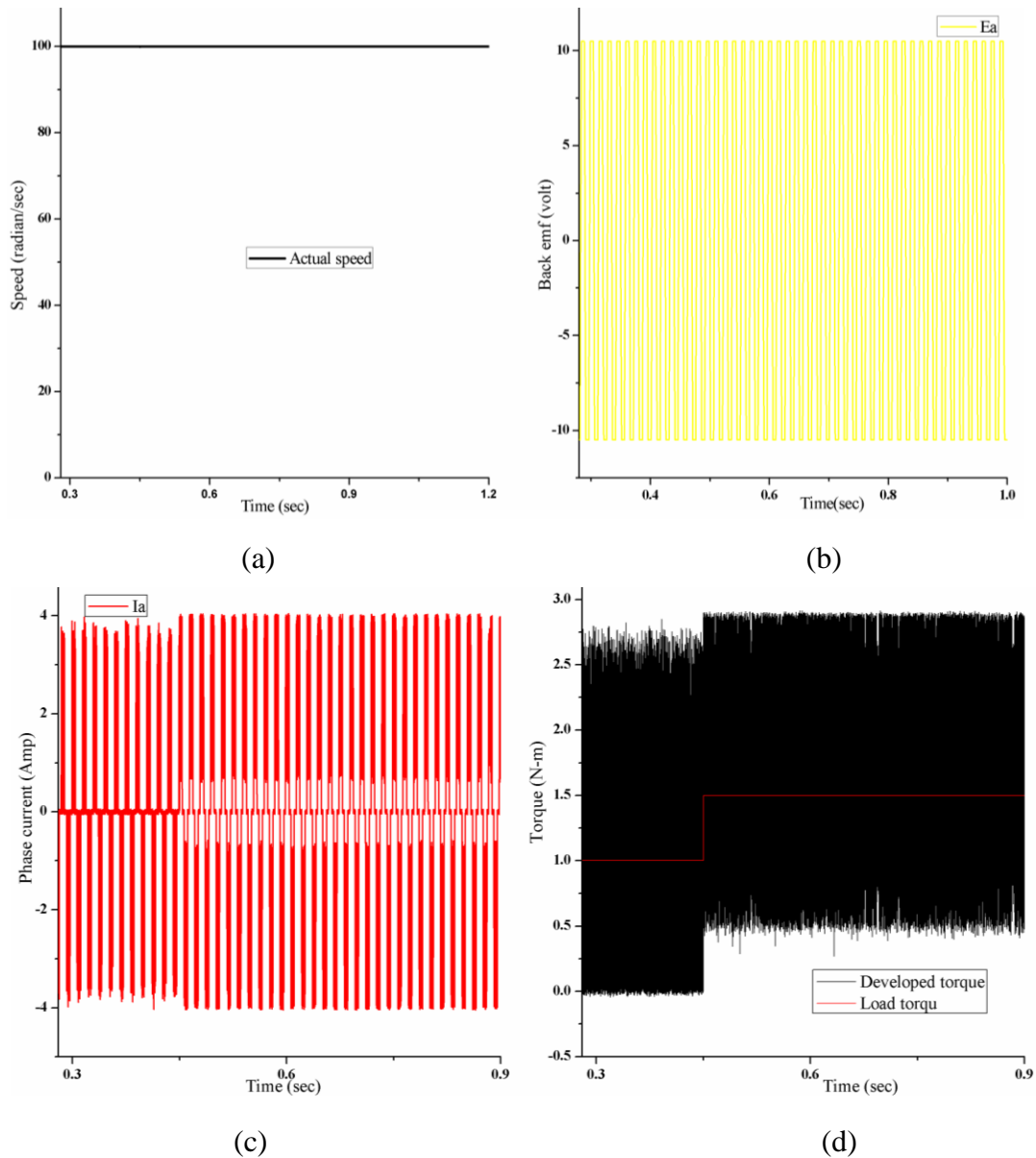


Fig.8.12: (a) Speed characteristic, (b) Phase back emf, (c) Phase current and (d) Torque response by SNA Controller

Here drive effectiveness was tested through Single Neuron based Adaptive PID controller with a speed estimator. Fig.8.13 (a) indicates speed responses which have a speed fall as dip when load torque is increased to 50% of 1 N-m. Also having slight change in back emf

because of speed dip as described in Fig.8.13 (b). Referring to the phase current of Fig.8.13 (c), it is clear that phase current is increased with increment of 50% load torque at time 0.45 sec. Also developed torque was increased according to load torque as shown in Fig.8.13 (d).

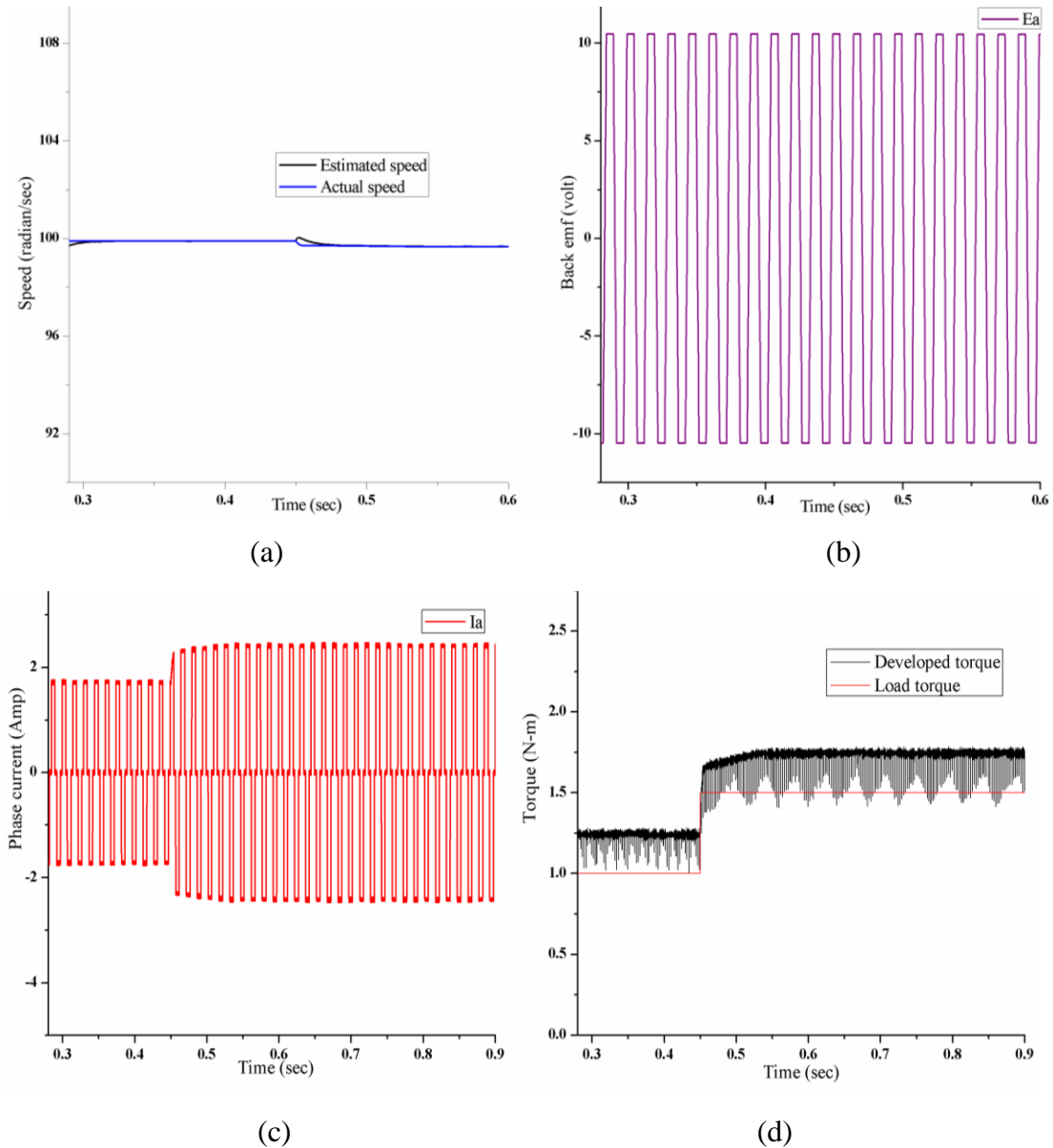


Fig.8.13: Response of (a) Speed, (b) Back emf, (c) Phase current and (d) Torque by SNAPID Controller

Drive performance was tested through ANFIS based on RBF and there is no appreciable change in motor speed and phase back emf are observed when torque was changed from 1.0 N-m to 1.5 N-m. Speed response and back emf are shown in Fig.8.14 (a) and Fig.8.14 (b) respectively. Fig.8.14 (c) specifies motor phase current which increased with increment

of load torque. Fig.8.14 (d) exits as torque response curve which is controlled according to demand torque.

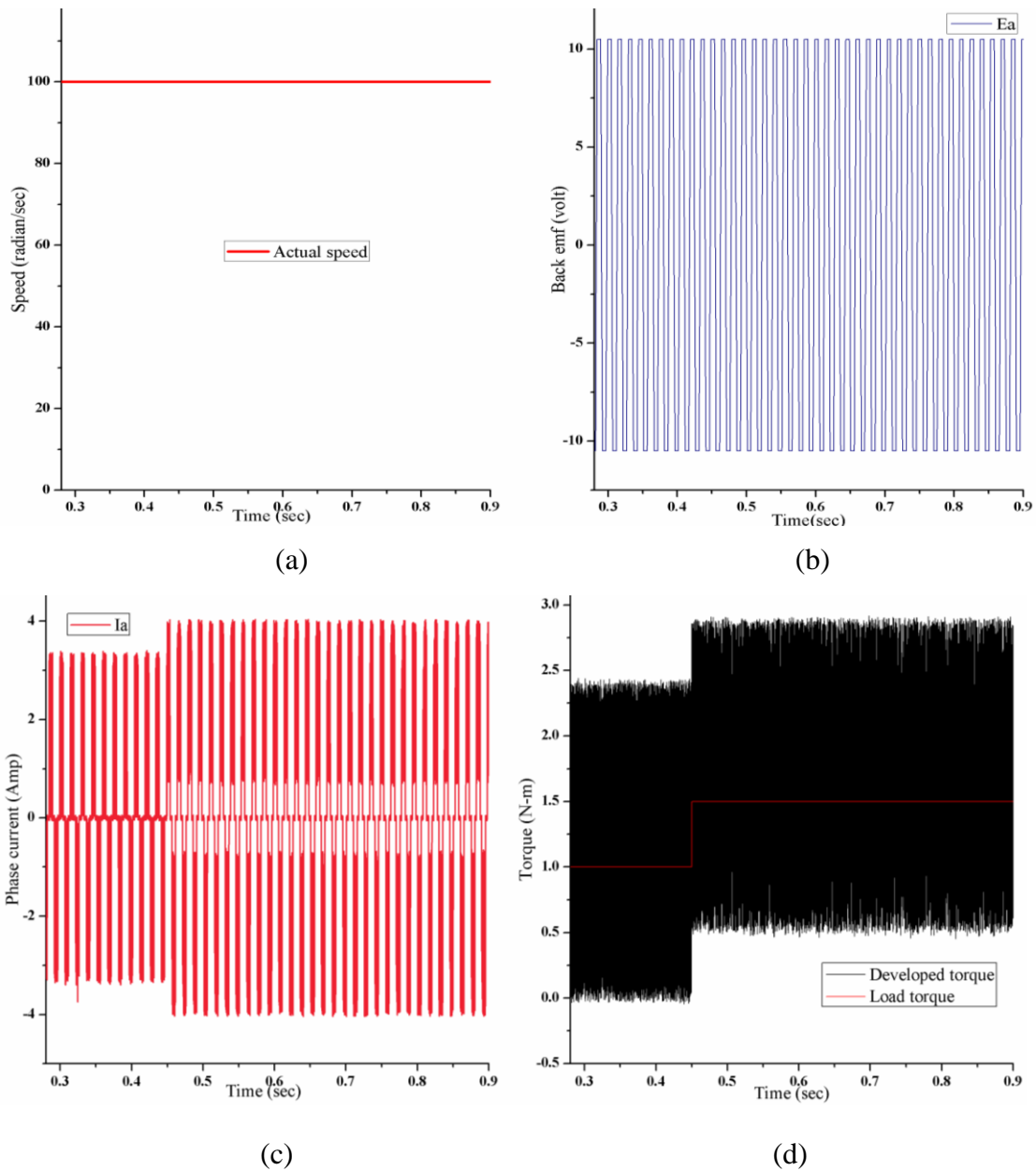


Fig.8.14: (a) Speed response, (b) Back emf, (c) Phase current and (b) Torque response by ANFIS based controller with RBF

The motor performance was checked out by ANFIS controller based on Takagi-Sugeno Model. Fig.8.15 (a) and Fig.8.15 (b) describe speed and phase back emf characteristics under this case. It is seen that no undershoot or overshoot occurred in speed curve and also seen that phase back emf is changed as well in torque changing mode at time 0.45 see. Fig.8.15(c) shows motor phase current which was increased as well when load torque was

increased to 50% of 1 N-m at 0.45 sec. In this case developed torque is also increased when load torque is increased as shown in Fig.8.15 (d).

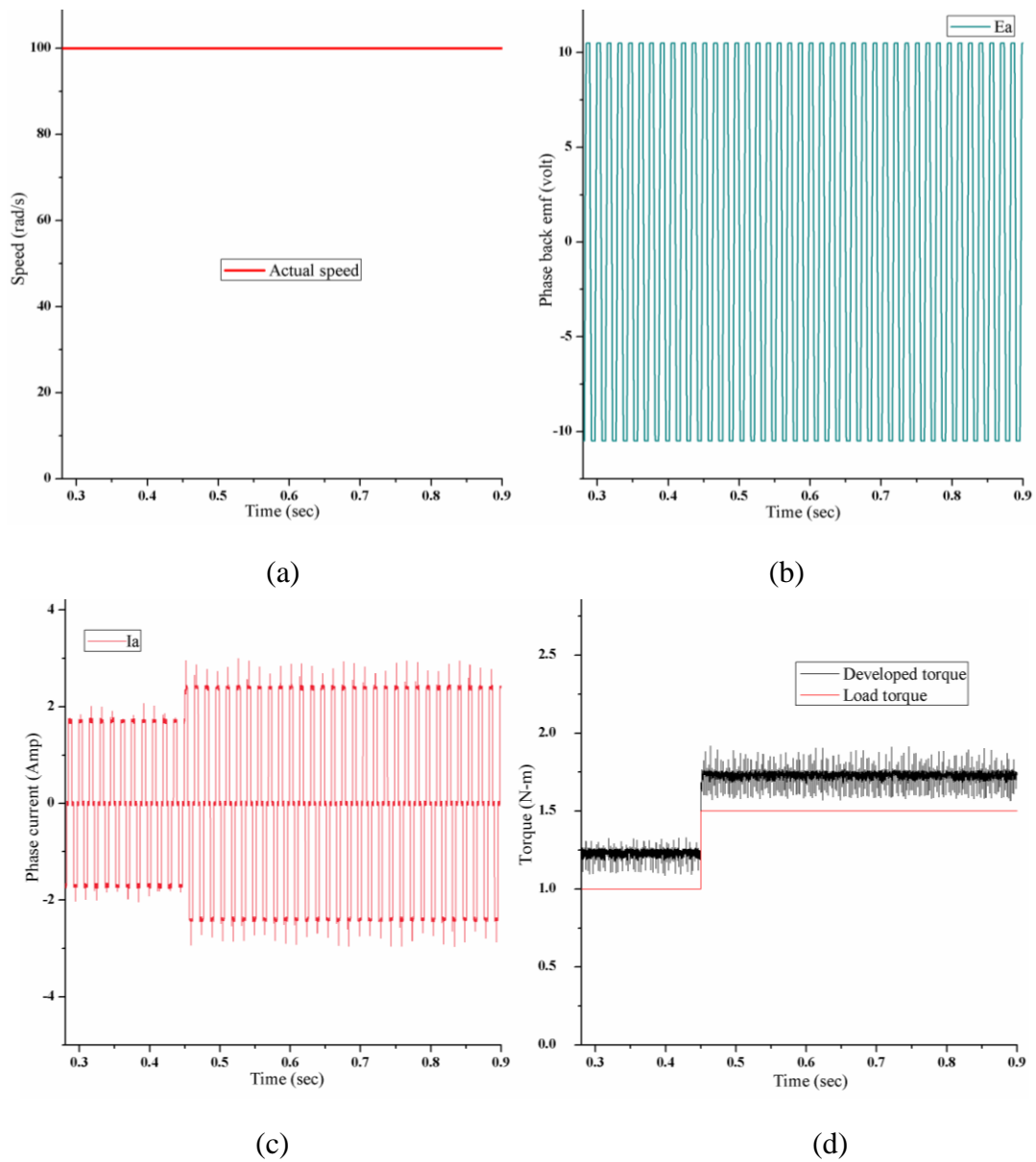


Fig.8.15: (a) Speed response, (b) Phase back emf, (c) Phase current and (b) Torque response by ANFIS controller based on Takagi-Sugeno Model

PMBLDC Motor drive performance was checked with ANFIS controller based on Line voltage Model. Here is no impact on motor speed because of increasing load torque as shown in Fig.8.16 (a). Back emf is controlled smoothly but no effect on load torque changing mode as shown in Fig.8.16 (b). Motor phase current was increased slightly when load torque was increased to 50% of its initial value at 0.45 sec that was displayed in Fig.8.16 (c). In this case developed torque was also increased in well as shown in Fig.8.16 (d).

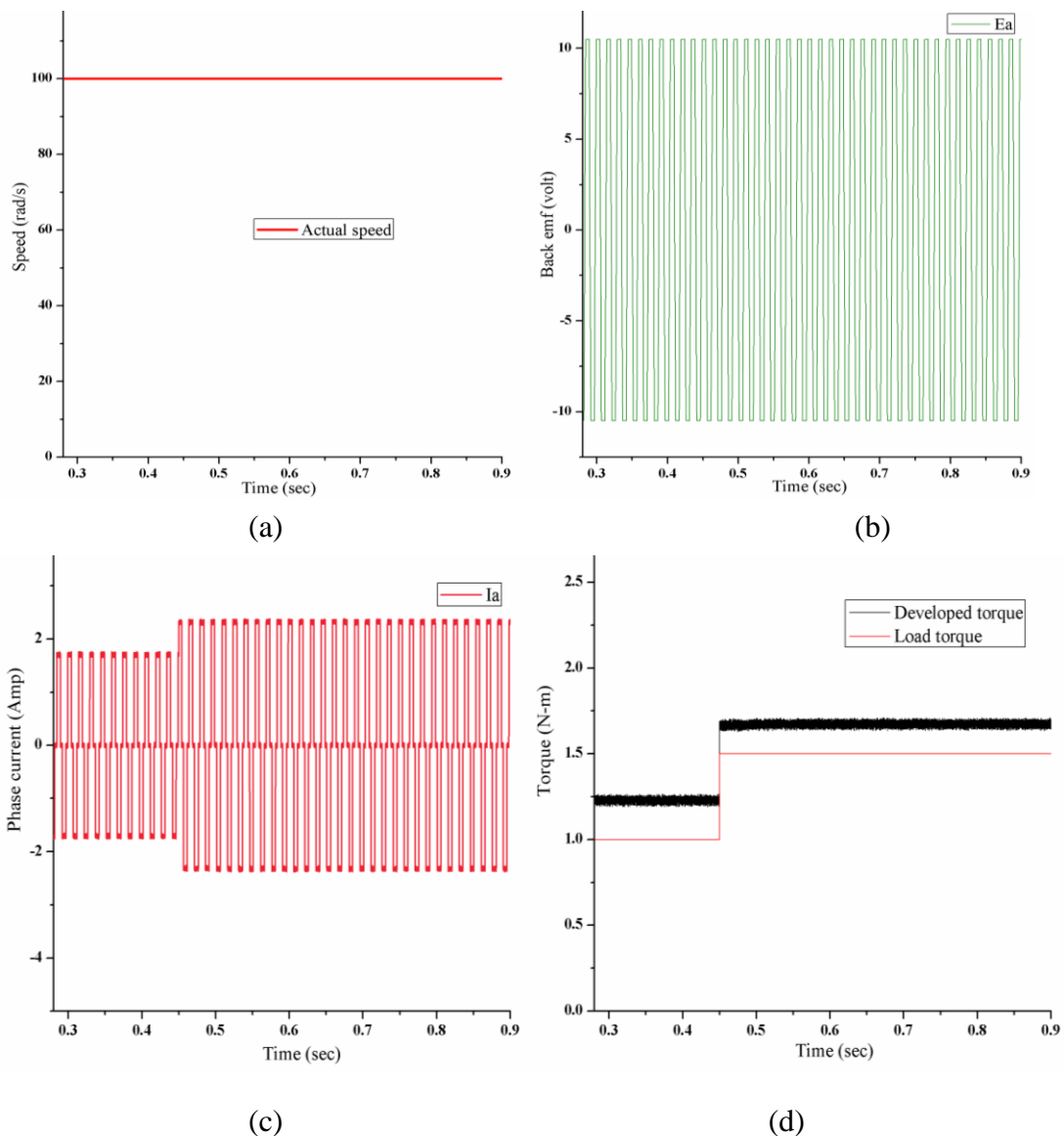


Fig.8.16: (a) Speed response, (b) Back emf, (c) Phase current and (b) Load torque with ANFIS Controller based on Line voltage Model

Motor speed and back emf were controlled with WNN based controller at load torque changing mode as shown in Fig.8.17 (a) and Fig.8.17 (b). It is clear that when load torque is increased then motor speed is reduced slightly and back emf is also changed by a negligible amount with decrement of speed.

Phase current and back emf are shown in Fig.8.17 (c) and Fig.8.17 (d) respectively. It is noticed that motor phase current and torque were increased smoothly at time 0.45 sec for an increment of 50% load torque.

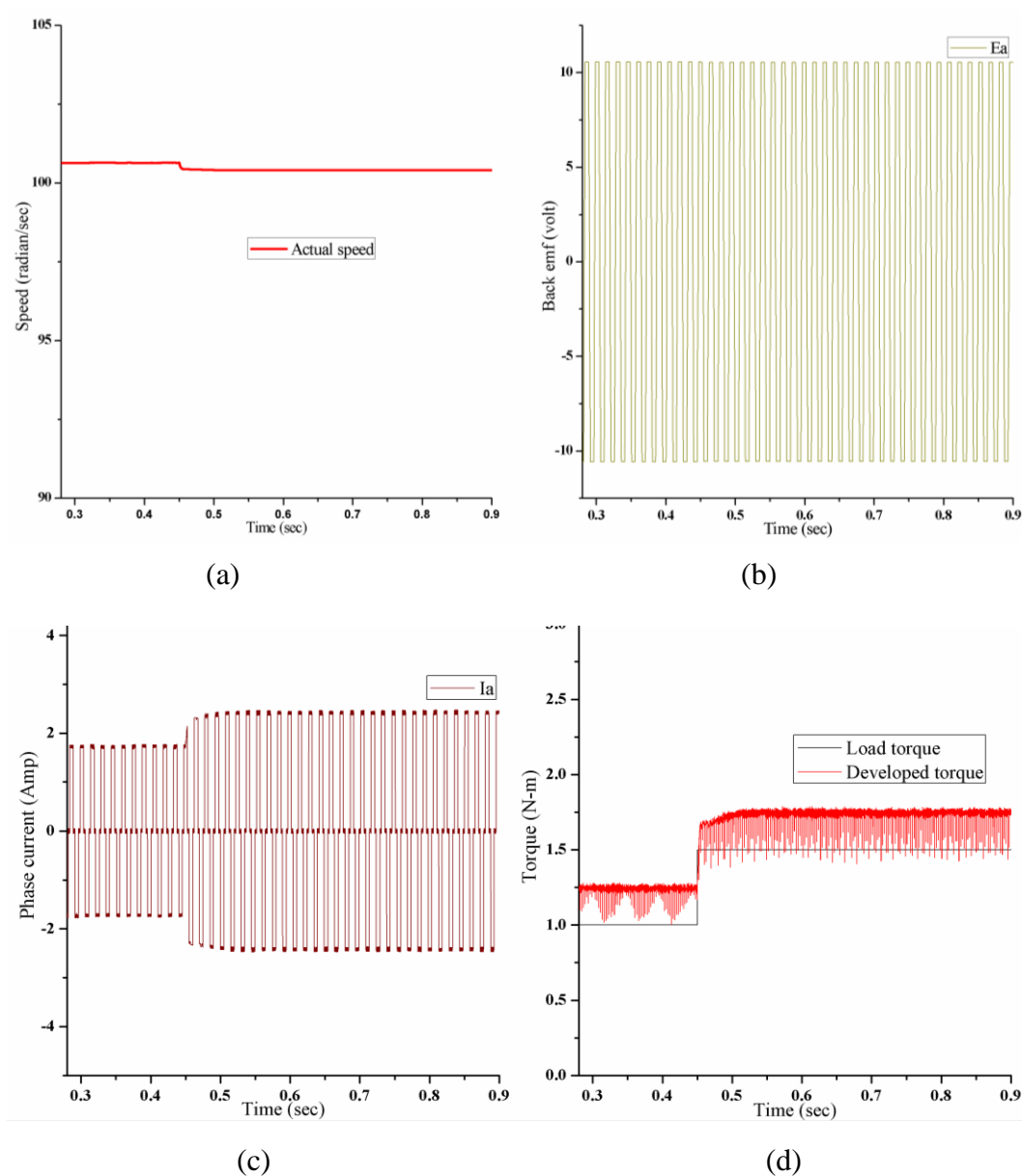


Fig.8.17: Illustration of (a) Speed response, (b) Back emf, (c) Phase current and (b) Torque response with WNN based controller

8.5 Effect on Performance due to Changing Parameter

Stator resistance was increased by 50% of rated value when the motor speed is 100 rad/sec and load torque is 1.0 N-m at 0.45 sec. The drive performance was tested by fixed PI controller. Having very slight speed undershoot and in addition torque control is shown in Fig.8.18 (a) and Fig.8.18 (b) respectively. It is observed that a distortion was seen at peak of phase current for the increment of stator resistance as describe in Fig.8.19.

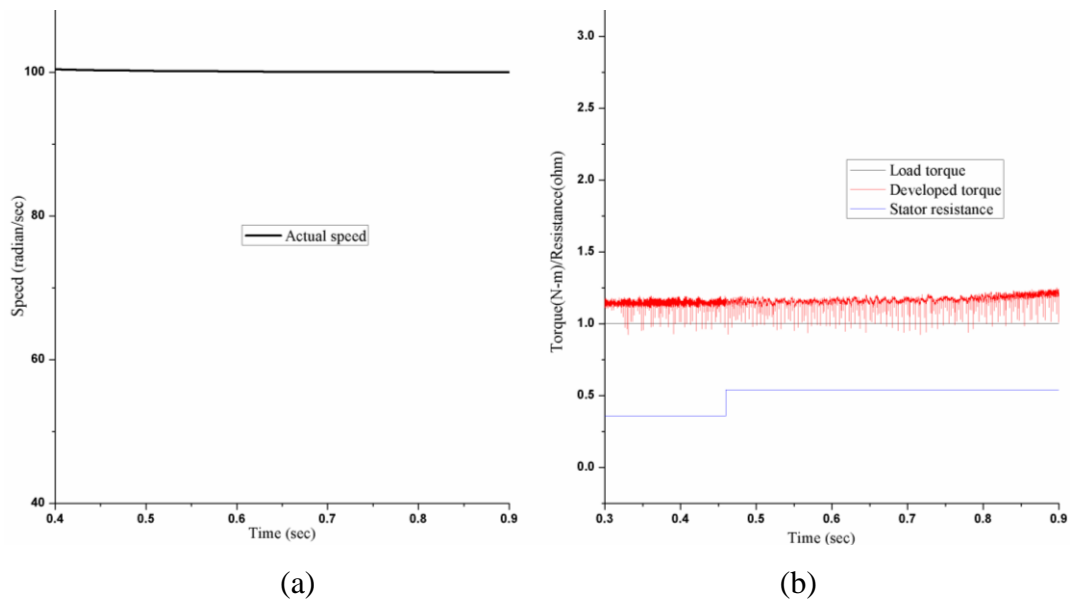


Fig.8.18: (a) Speed response and (b) Torque response by fixed PI controller

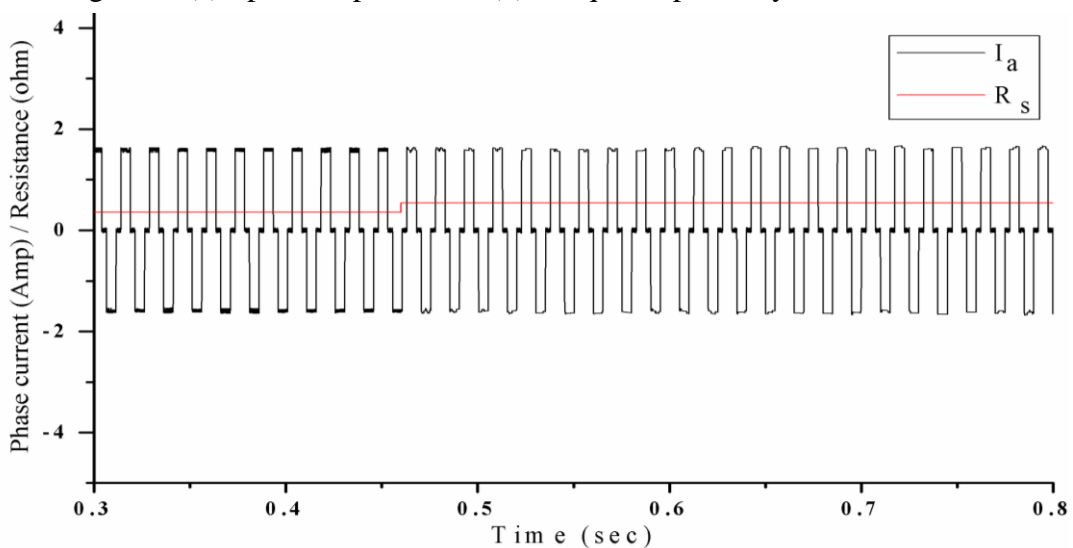


Fig.8.19: Response of phase current with fixed PI controller

In this case drive effectiveness was tested with Single Neuron based Adaptive controller. Here is no impact on motor speed due to increasing parameter as shown in Fig.8.20 (a). Increment of stator resistance produces no effect on developed torque that is shown in Fig.8.20 (b).

It is also seen that motor phase current has no effect on changing parameter as shown in Fig.8.21.

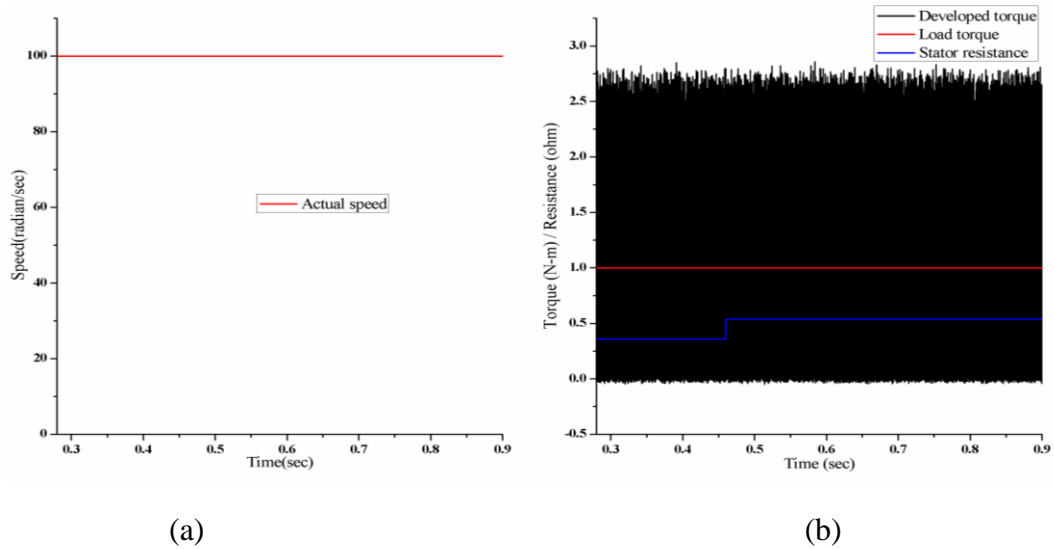


Fig.8.20: (a) Speed characteristic and (b) Torque characteristic with Single Neuron based Adaptive (SNA) controller

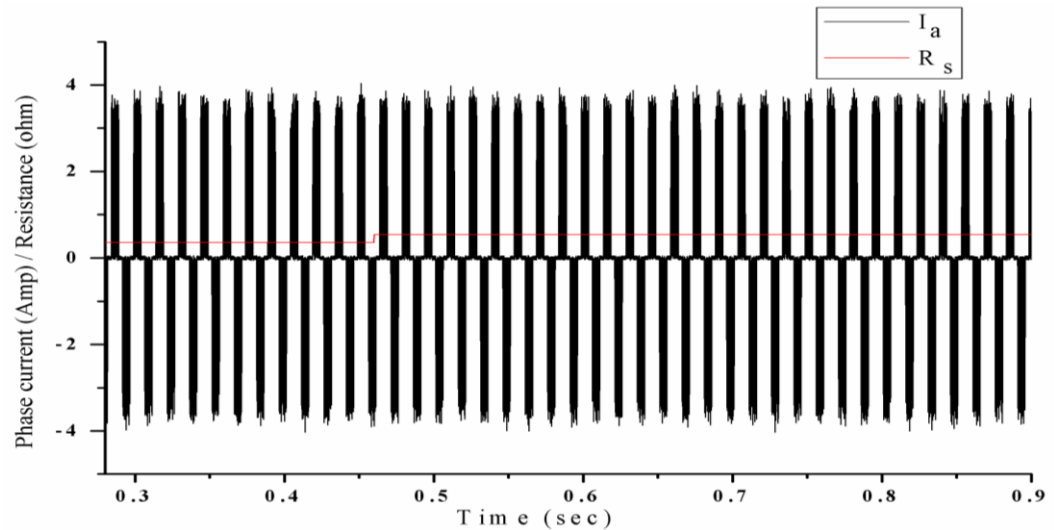


Fig.8.21: Motor phase current with SNA controller

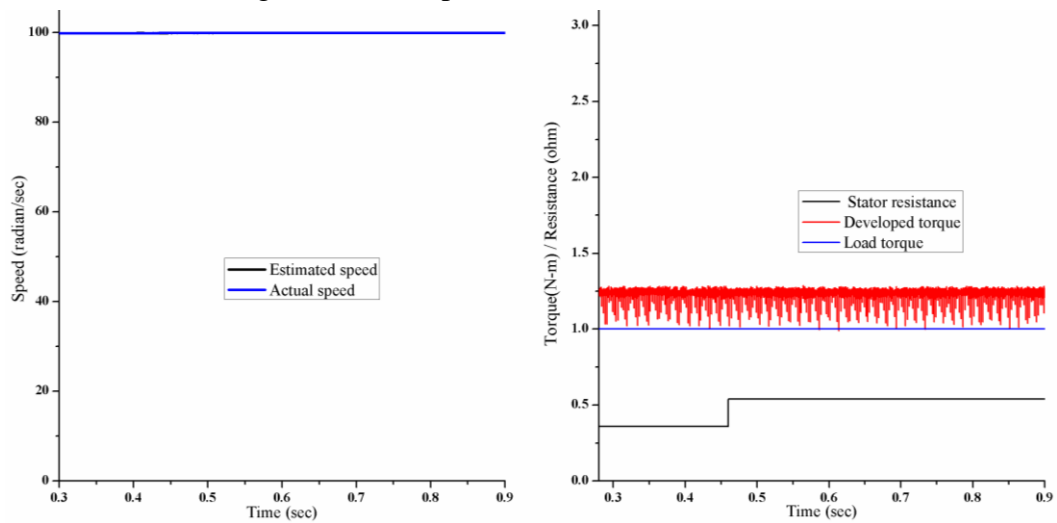


Fig.8.22: Response of (a) Speed and (b) Torque with Single Neuron based Adaptive PID controller

Single Neuron based Adaptive PID controller was applied to test drive performance based on 50 % increment of stator resistance. There is no appreciable change in motor speed, torque or phase current which are described in Fig.8.22 (a), Fig.8.22 (b) and Fig.8.23 respectively.

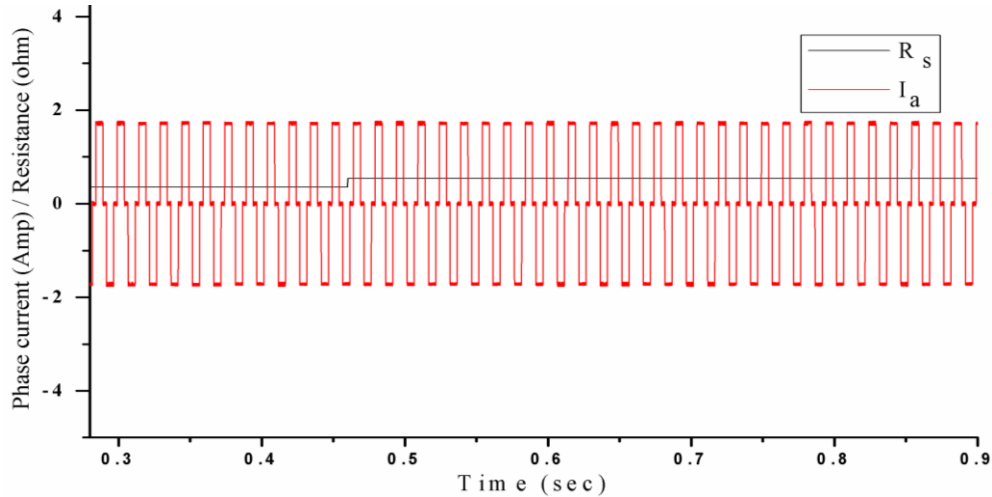


Fig.8.23: Motor phase current with SNAPID controller

ANFIS based controller with Radial Basis Function was employed to test drive effectiveness with stator resistance increment of 50 % (of 0.36Ω). Fig.8.24 (a) shows speed response and it is seen that motor speed remains stable. It also observed that no impact on developed torque and phase current which are shown in Fig.8.24 (b) and Fig.8.25 shows phase current with the increment of stator resistance.

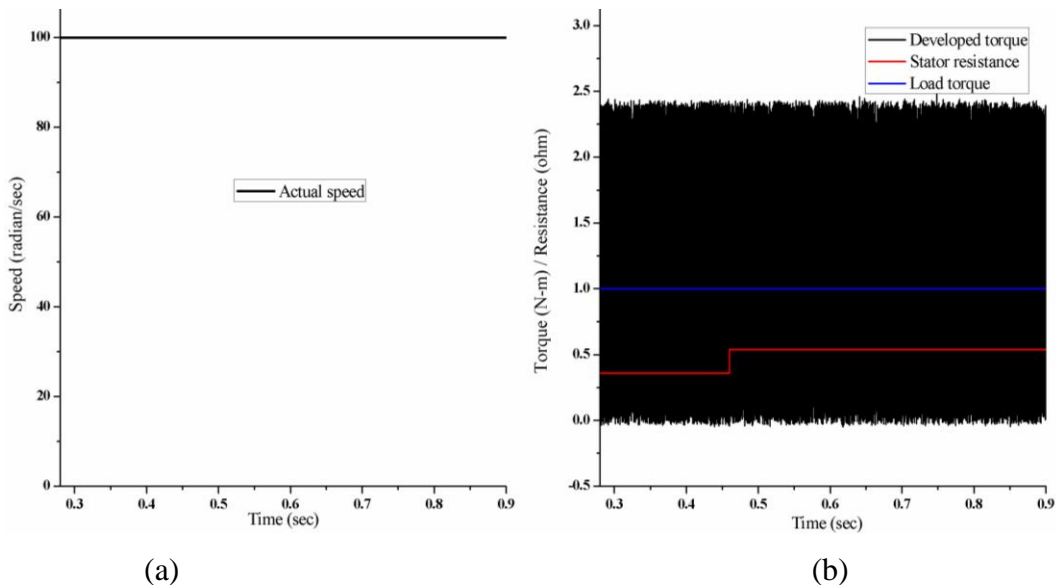


Fig.8.24: (a) Speed response and (b) Torque response by ANFIS based Controller with RBF

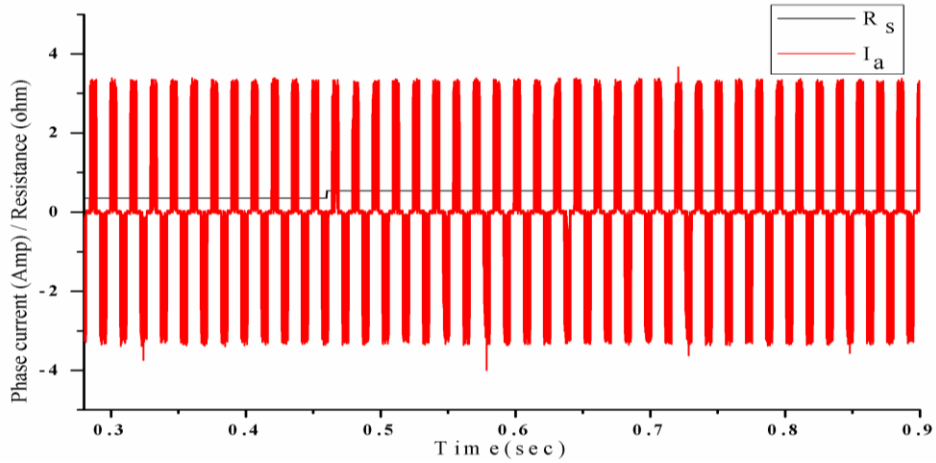


Fig.8.25: Motor phase current by ANFIS based Controller with RBF

Effectiveness of PMBLDC motor drive was tested by ANFIS controller based on Takagi-Sugeno Model. Responses of speed, torque and phase current are given in Fig.8.26 (a), Fig.8.26 (b) and Fig.8.26 (c) respectively. It is noticed that no appreciable change in speed, torque and phase current is caused due to changing resistance at 0.45 sec.

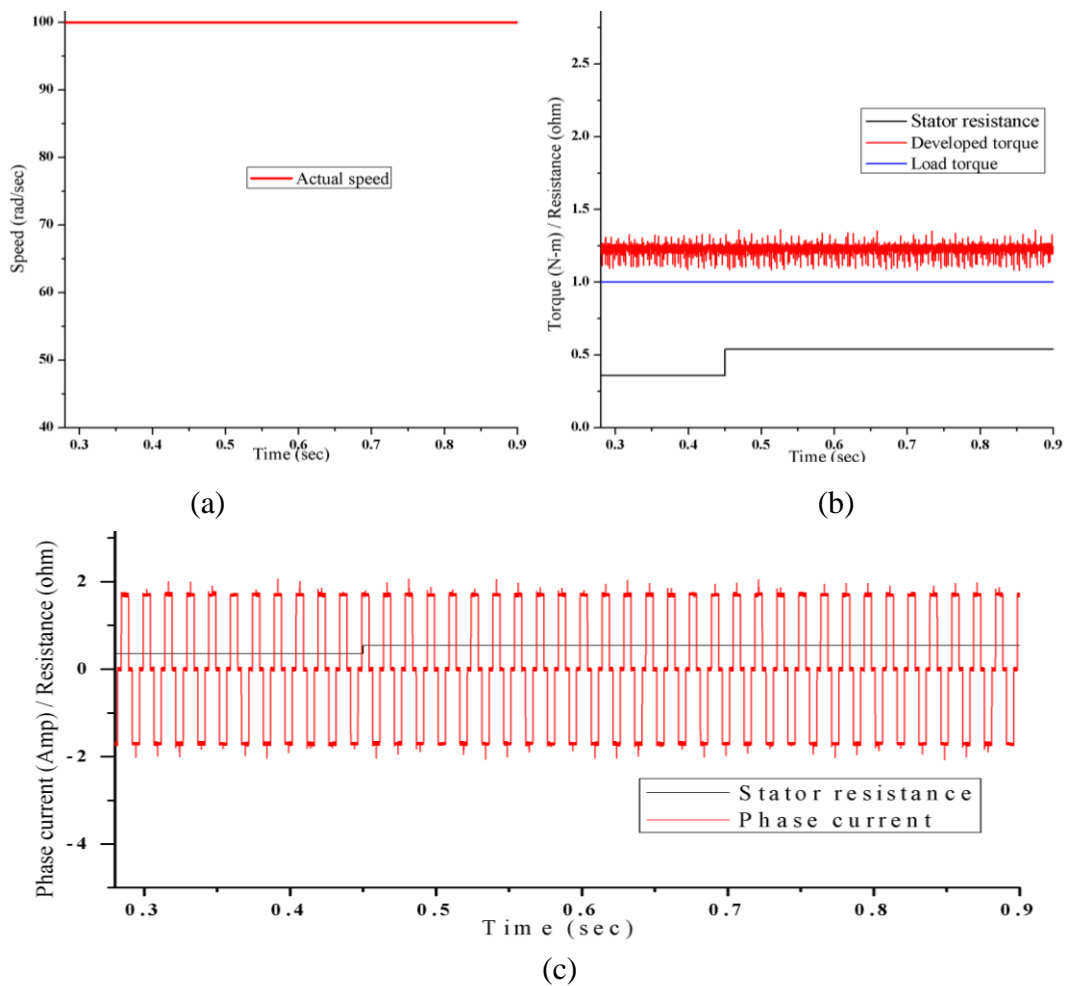


Fig.8.26: (a) Speed characteristic, (b) Torque characteristic and (c) Phase current with ANFIS based on Takagi- Sugeno Model

ANFIS controller based on Line Voltage Model was engaged to test drive performance. Fig.8.27 (a) and Fig.8.27 (b) show response of speed and torque which remain stable when stator resistance is raised to 50 % of rated value at 0.45 sec. It is also noticed that no changes occur in motor phase current as shown in Fig.8.27 (c).

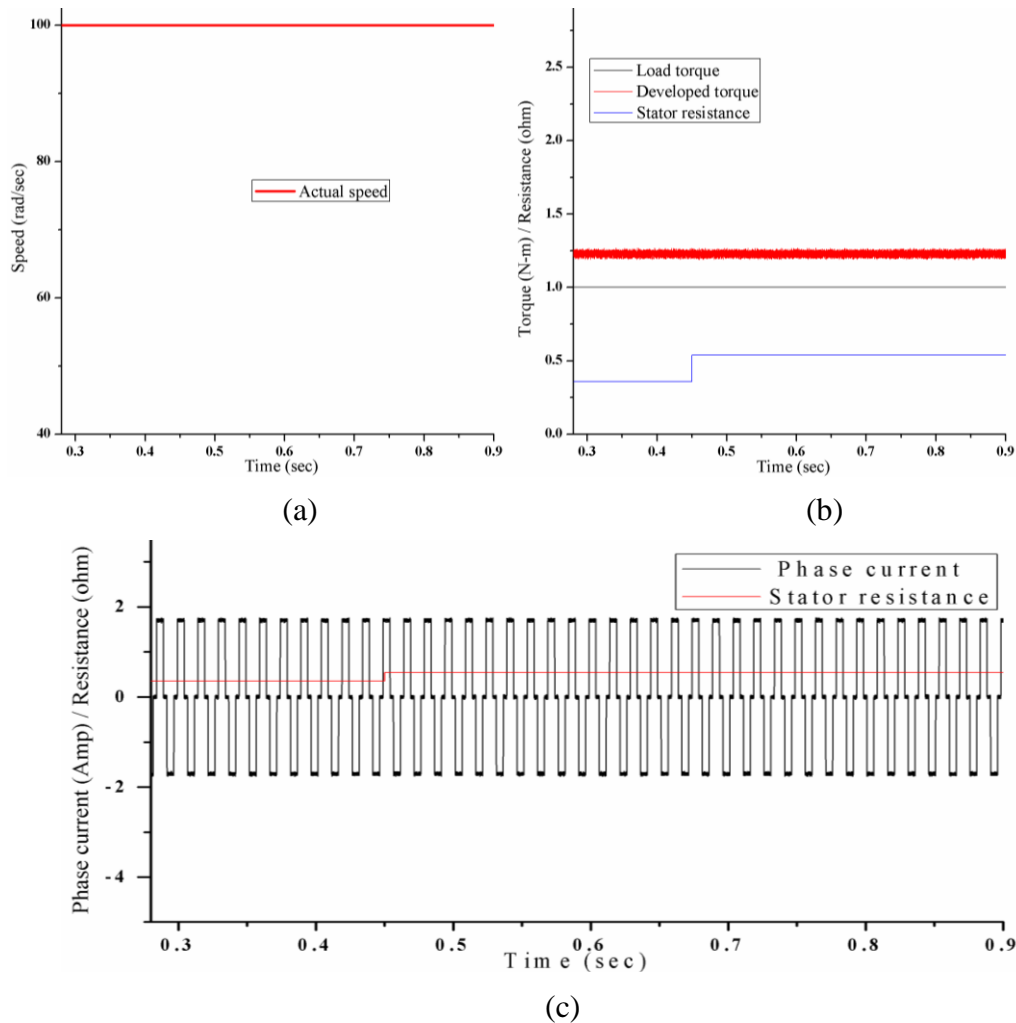


Fig.8.27: (a) Speed response, (b) Torque response and (c) Phase current with ANFIS based on Line Voltage Model

In this step, drive performance was trialed by WNN based controller. At 0.45 sec stator resistance was raised to 50% of its rated value. Fig.8.28 (a) and Fig.8.28 (b) express as responses of speed and torque. It is clear that motor speed and torque are controlled as well as having no impact on changing parameter. But some overshoots in speed at all operating conditions is observed. Phase current is controlled in well on parameter changing mode as shown in Fig.8.28 (c).

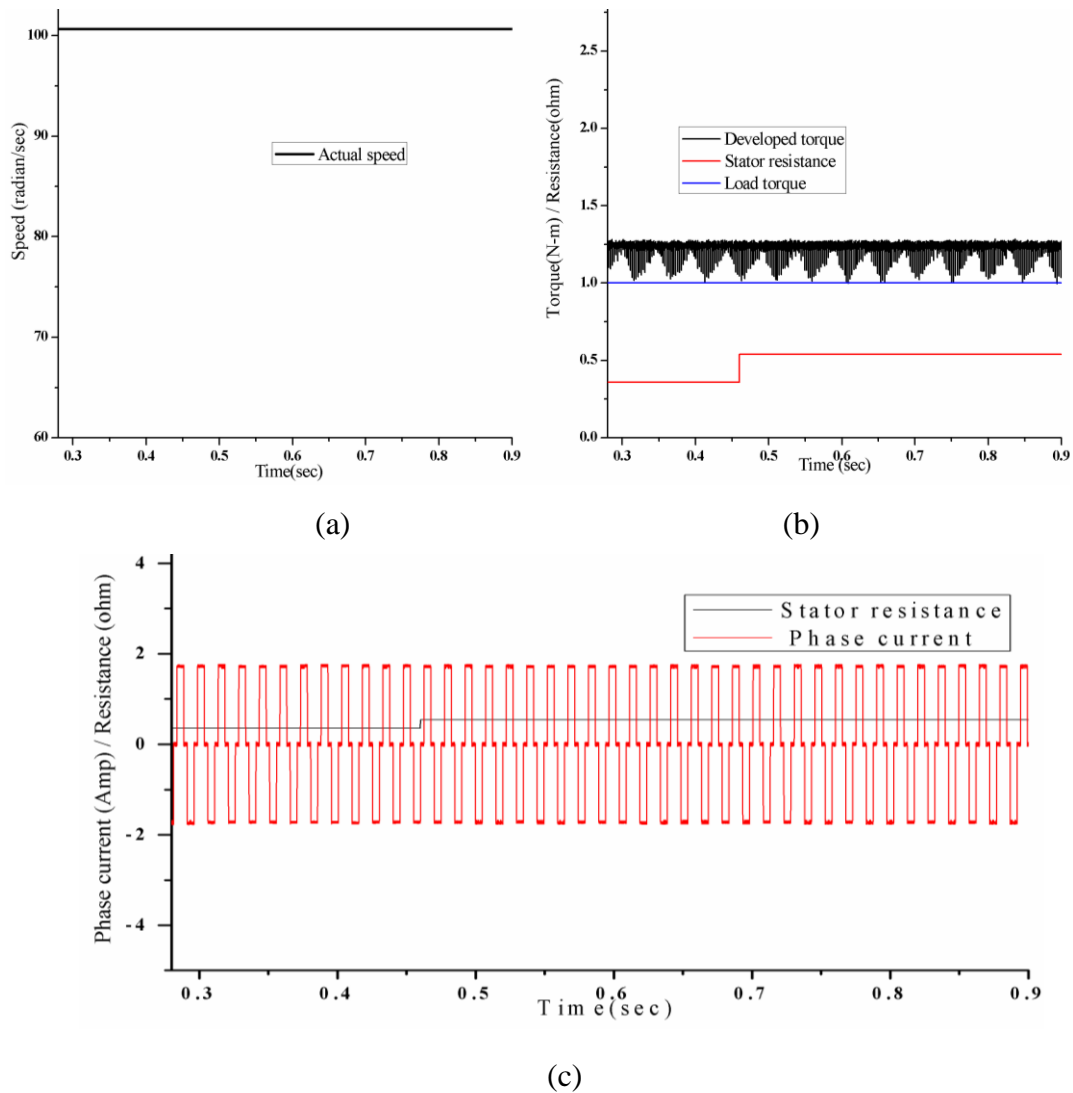


Fig.8.28: (a) Speed characteristic, (b) Torque characteristic and (c) Phase current with WNN based controller

8.6 Conclusion

In this study we have found that the drive system performs well with all the proposed controllers under different dynamic conditions. From the simulation results it is clear that some overshoot observed in motor speed with fixed PI and WNN based controller in all operating conditions indicating their weakness. Torque and phase current are controlled well with respect to demand torque with all proposed controllers. No impact is observed in all controllers under speed variation condition except fixed PI and WNN based controller. In this situation weights, consequent parameters and premise parameters of ANFIS based controller with RBF are updated precisely to adjust motor speed according user command. In the similar way weights of Single Neuron based Adaptive controller are also updated. Proportional, Integral and derivative gains of Single Neuron based Adaptive PID controller

are retuned to get desired performance but WNN based controller and Adaptive PID controller could not work under the speed decrement mode. Only undershoot is observed in the speed responses of WNN based controller, Single Neuron based Adaptive PID controller and PI controller under load torque changing mode. Finally, we have seen that all controllers with PMBLDC Motor drive work effectively without any performance degradation in the increment of stator resistance hence, the proposed controllers perform as insensitive controller with the variation of stator resistance.

CHAPTER IX

CONCLUSION AND FUTURE WORK

The Chapter at a glance

Conclusion	Section 9.1
Proposal for Future Work	Section 9.2

9.1 Conclusion

This dissertation emphasizes on the performance of PMBLDC Motor drive with different types of controllers based on artificial neural network. Speed control of PMBLDC motor is required frequently for controlling drives such as electric vehicles, copters, robotics, medical instrumentation, etc. The control of PMBLDC motors is difficult due to their nonlinear and multivariable nature and the industries still in need of superior controllers. To achieve desired performance from the motor a high performance controllers are needed. This study was conducted for implementing field oriented control of the PMBLDC Motor to get better dynamic performance. In this case the stator direct axis current was adjusted to zero and only quadrature axis current was used to generate useful torque. It was observed that all proposed controllers have worked effectively under field oriented control. The reference current input to the machine was sinusoidal or square wave. Better performance was observed with square wave reference current and it was used in this study. In these closed loops control system speed error was processed through proposed controllers to generate reference current according to demand torque.

The controllers used in the study were Single Neuron based Adaptive Controller, Single Neuron based Adaptive PID Controller, WNN based Controller, ANFIS based Controller with Radial Basis Function, ANFIS Controller based on Takagi- Sugeno Model and ANFIS Controller based on Line voltage Mathematical Model were proposed in this study to test drive performance. A conventional PI Controller with constant parameters was also designed and tuned by Ziegler-Nichol method. With this controller the starting duration from standstill condition to 100 rad. per sec (used throughout this study) was 0.31 sec with

sinusoidal reference current and it was very fast and as shown speed overshoot. It was seen that actual motor speed reaches the set speed 100 rad per sec with square wave reference current in 0.26 sec and is a fast response. But it could not work properly under dynamic condition such as overshoot in speed at starting and fall of speed due to sudden enhancement of load torque.

In this study a Single Neuron based Adaptive Controller was designed and applied to control speed of the PMSM Motor drive system. With square wave reference current and online tuning of parameters the motor starting time (0 to 100 rad/sec) is 0.26 sec. This controller worked effectively without any speed oscillation at starting and no speed fall due to load torque enhancement. The next controller used in the study is Single Neuron based Adaptive PID Controller. Here the controller parameters K_p , K_i and K_d were updated by ANN based training method and it has shown negligible speed fall due to sudden increment of load torque. The drive performance was almost similar to the Single Neuron based Adaptive Controller that uses weights to implement control action. The WNN based Controller was introduced in the control of the drive. Here the weights were selected on trial and error basis. The speed response was fast and required 0.26 sec to reach reference speed (100 rad/sec) but some overshoot are observed. Also speed falls due to sudden enhancement of load torque. ANFIS based controllers were used in the study. Both the ANFIS based Controllers with Radial Basis Function with on line tuning and based on Takagi- Sugeno Model with constant parameters were used to study the drive performance. The speed response is very fast in both the cases and is 0.26 sec. No speed overshoot or speed fall during load torque enhancement was observed. The Takagi- Sugeno Model based ANFIS controller with constant parameters was used in PMSM Motor control using the Line Voltage Model of the motor. Here also no speed overshoot or speed fall during load torque enhancement is observed.

It has been observed that the performance of PMSM motor drive is good with the proposed controllers under different dynamic conditions. It has also seen that small speed overshoot or undershoot was observed with fixed PI controller and WNN based controller under the all operating conditions. But other specify ere proposed controllers work effectively without speed overshoot and undershoot. In this case weights, consequent parameters and premise parameters of ANFIS based controller with RBF were updated

precisely to adjust motor speed according to user command. In the similar way weights of Single Neuron based Adaptive controller were also updated. Proportional, Integral and derivative gains of Single Neuron based Adaptive PID controller were retuned to get desired performance but WNN based controller and Adaptive PID controller could not work under the speed decrement mode. We have observed that all the proposed controllers with PMLDLC motor drive work effectively without any performance degradation in the increment of stator resistance. Finally, it was found that performance of ANFIS type controller, SNA Controller and SNAPID Controller were better than fixed PI and WNN based Controller and detail was given in Table 1.1.

Table 1.1

Name of Controller	Time to reach final Speed 100 rps at starting	When settling to final speed	During Speed change	Sudden load torque increment	Changing parameter	Tuning of Controller parameter
PI controller Constant parameter	0.26 sec	Speed overshoot	Speed overshoot and undershoot	Speed undershoot	No speed overshoot or undershoot	Off line tuning only
Single Neuron based Adaptive controller	0.26 sec	No speed over shoot or undershoot	No speed over shoot or undershoot	No speed over shoot or undershoot	No speed over shoot or undershoot	Online weight adjustment possible
Single Neuron based Adaptive PID controller	0.26 sec	No speed over shoot or undershoot	No speed over shoot or undershoot	Negligible Speed undershoot	No speed over shoot or undershoot	Online tuning & controller gains adjustment possible
ANFIS controller with RBF	0.26 sec	No speed over shoot or undershoot	No speed over shoot or undershoot	No speed over shoot or undershoot	No speed over shoot or undershoot	Online tuning & parameter adjustment possible
ANFIS controller based on T-S	0.26 sec	No speed over shoot or undershoot	No speed over shoot or undershoot	No speed over shoot or undershoot	No speed over shoot or undershoot	Off line tuning only
ANFIS controller based on Line Voltage Model	0.26 sec	No speed over shoot or undershoot	No speed over shoot or undershoot	No speed over shoot or undershoot	No speed over shoot or undershoot	Off line tuning only
ANFIS controller based on Line Voltage Model	0.26 sec	No speed over shoot or undershoot	No speed over shoot or undershoot	No speed over shoot or undershoot	No speed over shoot or undershoot	Off line tuning only

9.2 Proposal for Future Work

Permanent Magnet Brushless DC (PMBLDC) Motors are highly promising commutator-less motors. Speed response of this motor is very fast than other motor. To develop motor control model future research can be done on the following areas.

- i) A new controller may be designed based on Deep Learning theory for PMBLDC Motor.
- ii) A controller can be modeled based on genetic algorithm and back propagation neural network for the PMBLDC Motor
- iii) WNN based controller and Single Neuron based Adaptive PID can be modified on the speed decrement mode by adjusting values of different parameters with online tuning.
- iv) Sensorless control based on direct back emf detection method can be constructed with above proposed controllers.

REFERENCES

1. Yong Liu, Student Member, IEEE, Z. Q. Zhu, Senior Member, IEEE, and David Howe, "Direct Torque Control of Brushless DC Drives With Reduced Torque Ripple", IEEE Trans on Industry Appl, Vol. 41, NO. 2, Mar/Apr 2005, pp 599-606.
2. A Watanabe and S. Yuta, "Efficient Feed forward Current Control Method of Brushless DC Motor By Using Non-Complementary Switching in Driver Circuit", The 11th IEEE International Workshop on Advanced Motion Control March 21-24, 2010, Nagaoka, Japan pp.768-773.
3. S.Rambabu, "Modeling and Control of a Brushless DC Motor", M Tech Thesis, Department of Electrical Engineering National Institute of Technology Rourkela 2007.
4. Nasser Hashernnia and Behzad Asaei, "Comparative Study of Using Different Electric Motors in the Electric Vehicles", Proceedings of the 2008 International Conference on Electrical Machines, Paper ID-1257.

5. R. Giridhar Balakrishna, P. Yogananda Reddy, "Speed Control of Brushless DC Motor Using Microcontroller", *International Journal of Engineering Technology, Management and Applied Sciences*, vol. 3, Issue 6, ISSN 2349-4476, June 2015.
6. Hrushikesh Meher, "Performance Analysis of Interior Permanent Magnet Synchronous Motor (IPMSM) Drive System using different Speed Controllers", M Tech Thesis, Department of Electrical Engineering National Institute of Technology, Rourkela, India.
7. Igor Jakubička, Vladislav Bača, Peter Fuchs, Peter Drahoš, "Implementing Features of 32 bit DSP Microprocessor for BLDC Motor Control", *Proceeding of the 28th International Conference 2016 Cybernetics & Informatics (K&I)*, February 2-5, 2016, Levoca, slovakia, 978-1-5090-1834-5/16/\$31.00 2016 IEEE
8. S.Ravi, Dasari. Narasimha Rao, K.Mali.S.N.Krishna, Vitaliy Mezhyuev, "A Proposed GA Based PID Controller for Three Phases Brushless DC Motor", *Universal Journal of Control and Automation* 2(4): 69-76, 2014, DOI: 10.13189/ujca.2014.020401.
9. A. Tashakori, M. Ektesabi, and N. Hosseinzadeh, "Modeling of BLDC Motor with Ideal Back-EMF for Automotive Applications", *Proceedings of the World Congress on Engineering 2011 Vol. II, WCE 2011*, July 6 – 8, 2011, London, U.K.
10. Yadu Kiran¹, Dr.P.S.Puttaswamy, "Field Oriented Control of a Permanent Magnet Synchronous Motor using a DSP", *International Journal of Advanced Research in Electrical, Electronics and Instrumentation Engineering*, Vol.3, Issue 10, October 2014.
11. M.V. Ramesh, J. Amarnath, S. Kamakshaiah and M. Balakrishna, "Field Oriented Control for Space Vector Modulation Based Brushless DC Motor Drive", *International Journal of Advanced Research in Electrical, Electronics and Instrumentation Engineering*, vol.2, Issue 9, pp.4231-4238, September 2013.
12. Feng Liu, Hua Wang, Qingli Shi, Hengxian Wang, Mengyin Zhang and Hailong Zhao, "Comparison of an ANFIS and Fuzzy PID Control Model for Performance in Two-Axis Inertial Stabilized Platform" *IEEE ACCESS*, Vol.5,2017,PP- 12951-12962.
13. V. Lavanya and, P.Devendra, "Parameter Identification and Control of BLDC Motor", *International Journal of Industrial Electronics and Electrical Engineering*, ISSN: 2347-6982, Volume-3, Issue-8, August 2015.
14. P.Danusuya, K.Balamuruga and R.Mahalakshmi "Parameter Identification in BLDC Motor using Optimization Technique", *Journal of Applied Science and Engineering Methodologies* Volume 3, No.2, (2017): Page.465-470

15. N. Parhizkar, M. Shafiei, and M. Bahrami Kouhshahi, "Direct Torque Control of Brushless DC Motor Drives with Reduced Starting Current Using Fuzzy Logic Controller ", 2011 International Conference on Uncertainty Reasoning and Knowledge Engineering.
16. D.Thandava Krishna, P.Jyosna, "Improvement in the Performance of Brushless DC Motor Control by ANN", International Journal of Emerging Engineering Research and Technology Volume 3, Issue 6, June 2015, PP 96-102.
17. Tony Mathew, Caroline Ann Sam "Modeling and Closed Loop Control of BLDC Motor using a Single Current Sensor", International Journal of Advanced Research in Electrical, Electronics and Instrumentation Engineering, Vol. 2, Issue 6, June 2013.
18. K.Premkumar, Dr.B.V.Manikandan, " Adaptive fuzzy logic speed controller for Brushless DC motor", 2013 International Conference on Power, Energy and Control (ICPEC).
19. Jianwen Shao, "Direct Back EMF Detection Method for Sensorless Brushless DC (BLDC) Motor Drives", Virginia Polytechnic Institute and the State University, September, 2003 Blacksburg, Virginia.
20. Md. Belal Hossen and Bashudeb Chandra Ghosh, "Performance Analysis of a PMSBLDC Motor Drive based on ANFIS Controller and PI Controller", International Conference on Electrical, Computer and Communication Engineering (ECCE),7-9 February, 2019,978-1-5386-9111-3/19/\$31.00 ©2019 IEEE
21. Vinod KR Singh Patel and A.K. Pandey, "Modeling and Performance Analysis of PID Controlled BLDC Motor and Different Schemes of PWM Controlled BLDC Motor" The International Journal of Scientific and Research Publication, Vol.3, Issue 4, ISSN 2250-3153, April 2013.
22. Albert John Varghese¹, Rejo Roy², Prof. S. Thirunavukkarasu³, "Optimized Speed Control for BLDC Motor", International Conference on Engineering Technology and Science-(ICETS'14), page-1019-1030, Volume 3, Special Issue 1, February 2014.
23. Emil Klintberg, "Comparison of Control Approaches for Permanent Magnet Motors", Master of Science Thesis, Department of Energy and Environment, Division of Electric Power Engineering, Chalmers University of Technology, Sweden 2013
24. S.Arockia Edwin Xavier, "Brushless DC Motor Speed Control using Microcontroller", International Journal of Current Engineering and Scientific Research (IJCESR), ISSN (print): 2393-8374, (online): 2394-0697, Volume-2, Issue-2, page-182-188, 2015.

25. Laxmiprasanna Ch and Ramesh Palakeerthi, “BLDC Drive Control using Artificial Intelligence Technique”, *International Journal of Computer Applications* (0975 – 8887), Volume 118 – No. 4, page 5-9, May 2015.
26. Z.Q. Zhu, D. Howe, “Electrical machines and drives for electric, hybrid and fuel cell vehicles”, *Proceedings of IEEE.*, vol. 95 n. 4, April 2008, pp. 746 – 765.
27. Pushek Madaan, “Brushless DC motor-part 1: Construction and Operating Principles”, *EDN network*, Cypress Semiconductor - February 11, 2013.
28. Md. Arshaful Islam, M. Sc. Project Report “Design and analysis of Field Oriented Control of Permanent Magnet Brushless DC Motor”, *Khulna University of Engineering & Technology*, Khulna – 9203, Bangladesh.
29. C.Y. Chen, W.C. Chan, T.C. Ou, S.H. Yu and T.W. Liu, “Sliding Mode Speed Control of Brushless DC Motor Using Pulse-Width-Modulated Current Regulator”, 2009 *IEEE/ASME International Conference on Advanced Intelligent Mechatronics Suntec Convention and Exhibition Center Singapore*, July 14-17, 2009.
30. Bashudeb Chandra Ghosh and Md. Belal Hossen, “Wavelet Neural Network based Controller Performance Analysis of a PMBLDC Motor”, 2018 *International Conference on Advancement in Electrical, Electronic and Engineering*, Paper ID-136, 22-24 November 2018, *IEEE*, Gazipur, Bangladesh.
31. Hidayat, Sasonko P H Sarjiya and Suharyanto, “Performance Analysis of Hybrid PID-ANFIS for speed Control of Brushless DC Motor based on Identification Model System”, *International Journal of Computer and Information Technology*, vol.2, Issue 4, July 2013, pp 694-700.
32. W.D. Chang, J.J. Yan and J.L. Chen, “On-line PID Controller Design via a Single Auto-tuning Neuron” A report of Department of Computer and Communication, *Shu-Te University Kaohsiung 824*, Taiwan.
33. Bin Wang, Xi Wang and Yue Liu, “Single Neuron PID Control of a Turbofan Engine with Inlet Pressure Distortion *Advanced Materials Research*”, Online: 2013-08-30 ISSN: 1662-8985, Vols. 753-755, pp 1534-1538.
34. Bin Chen, Hong-zhen Yang and Li-wen Wang, “Single Neuron PID Control of Aircraft Deicing Fluids Rapid Heating System”, *Journal of Networks*, Vol.8, No.2, pp.405-408, February 2013.
35. Md. Belal Hossen and Bashudeb Chandra Gosh, “Performance Analysis of a Single Neuron based Adaptive Controller and PI Controller based PMBLDC Motor Drive”,

- International Journal of Advanced Research in Electrical, Electronics and Instrumentation Engineering ,page-3309-3321, Vol. 7, Issue 8, August 2018.
36. Mohammad Divband, “A Comparison of Particle Swarm Optimization and Gradient Descent in Training Wavelet Neural Network to Predict DGPS Corrections”, Proceedings of the World Congress on Engineering and Computer Science 2010 Vol.1, WCECS 2010, October 20-22, 2010, San Francisco, USA.
 37. J. Rivera Mejia, A J Leon-Rubio, E Arzabaia-Contreras, “PID based on a Single Artificial Neural Network Algorithm for Intelligent Sensors”, Journal of Applied Research and Technology, April 2012, pp.262-282
 38. Bilal Akin and Manish Bhardwaj, “Sensorless Trapezoidal Control of BLDC Motors”, Application Report Texas Instruments, July 2013.
 39. Ankita Dwivedi, R. K. Srivastava “Analysis of Dual Stator PM Brushless DC Motor”, IOSR Journal of Electrical and Electronics Engineering (IOSRJEEE), ISSN: 2278-1676 Volume 1, Issue 2 (May-June 2012), PP 51-56.
 40. Brian R Copeland, “The design of PID controllers using Ziegler Nichols Tuning”,2008.
 41. Noureen Talpur, Mohd Najib Mohd Salleh, Kashif Hussain “An investigation of membership functions on performance of ANFIS for solving classification problems”, International Research and Innovation Summit (IRIS 2017);doi:10.1088/1757-899X/226/1/012103.
 42. Ali Moltajaei Farid, S. Masoud Barakati, and Navid Seifipour, “Online ANFIS Controller Based on RBF Identification and PSO”, June 2013 DOI: 10.1109/ASCC.2013.6606232, 978-1-4673-5851-4/13/\$31.00 c 2013 IEEE.
 43. Navneet Walia, Harsukhpreet Sing, Anurag Sharm “ANFIS: Adaptive Neuro-Fuzzy Inference System- A Survey”, International Journal of Computer Applications (0975 – 8887) Volume 123 – No.13, August 2015.
 44. Peilin Liu, Wenhao Leng and Wei Fang “Training ANFIS Model with an Improved Quantum –Behaved Particle Swarm Optimization Algorithm”, Hindawi Publication Corporation Mathematical Problems in Engineering, Volume 20013, Article ID 595639, 10 pages.
 45. Andrej Krenker, Janez Bešter and Andrej Kos “Introduction to the Artificial Neural Networks”, Faculty of Electrical Engineering, University of Ljubljana, Slovenia, ISBN 978-953-307-243-2 Hard cover, 362 pages, Publisher In Tech Published online 11, April, 2011.

APPENDIX A

Parameter of the PMBLDC Motor

SL.No.	Specifications	Quantity
1	Number of poles	8
2	Rated Current	4 Amp
3	Rated Voltage	48 V
4	Rated Torque	1.45 N-m
5	Rated Sped	150 radian/sec
6	Initial Torque	1.0 N-m
7	Resistance per Phase	0.36
8	Self Inductance	2.1 mH
9	Mutual Inductance	1.5 mH
10	Torque Constant	0.40 V-s/rad
11	Damping Constant	0.002 N-m/rad/sec
12	Moment of Inertia	0.0048 kg-m ²
13	Flux Linkages Constant	0.105 V-s/rad

List of Publications

1. **Md. Belal Hossen** and Bashudeb Chandra Ghosh, "Performance Analysis of a PMBLDC Motor Drive based on ANFIS Controller and PI Controller", International Conference on Electrical, Computer and Communication Engineering (ECCE), 7-9 February, 2019, 978-1-5386-9111-3/19/\$31.00 ©2019 IEEE, Coxes Bazar, Bangladesh.
2. Bashudeb Chandra Ghosh and **Md. Belal Hossen** "Wavelet Neural Network based Controller Performance Analysis of a PMBLDC Motor", 2018 International Conference on Advancement in Electrical, Electronic and Engineering, Paper ID-136, 22-24 November 2018, 978-1-5386-8252-4/18/\$31.00©2018IEEE, Gazipur, Bangladesh.
3. **Md. Belal Hossen** and Bashudeb Chandra Ghosh, "Performance Analysis of a Single Neuron based Adaptive Controller and PI Controller based PMBLDC Motor Drive ", International Journal of Advanced Research in Electrical, Electronics and Instrumentation Engineering ,page-3309-3321, Vol. 7, Issue 8, August 2018.

4. Arshaful Islam, **Md. Belal Hossen**, Badal Banik and Bashudeb Chandra Ghosh, "Field Oriented Space Vector Pulse Width Modulation Control of Permanent Magnet Brushless DC Motor", 2017 IEE Region10 Humanitarian Technology Conference(R10-HTC) , PP322-327, Dhaka, Bangladesh.
5. Arshaful Islam, **Md. Belal Hossen**, Md. Soyaeb Hasan and Bashudeb Chandra Ghosh, "Field Oriented Rectangular Current Regulated PWM Control of Permanent Magnet Brushless DC Motor" 2017 4th International Conference on Advance in Electrical Engineering , PP352-357, Dhaka, Bangladesh